1521-009X/51/4/521–531$35.00
DRUG METABOLISM AND DISPOSITION
dx.doi.org/10.1124/dmd.122.001195
Drug Metab Dispos 51:521–531, April 2023

Biotransformation of Efavirenz and Proteomic Analysis of Cytochrome P450s and UDP-Glucuronosyltransferases in Mouse, Macaque, and Human Brain-Derived In Vitro Systems[S]

Abigail M. Wheeler, Benjamin C. Orsburn, and Namandjé N. Bumpus

Department of Pharmacology and Molecular Sciences, Johns Hopkins University School of Medicine, Baltimore, Maryland

Received November 1, 2022; accepted December 16, 2022

ABSTRACT

Antiretroviral drugs such as efavirenz (EFV) are essential to combat human immunodeficiency virus (HIV) infection in the brain, but little is known about how these drugs are metabolized locally. In this study, the cytochrome P450 (P450) and UDP-glucuronosyltransferase (UGT)-dependent metabolism of EFV was probed in brain microsomes from mice, cynomolgus macaques, and humans as well as primary neural cells from C57BL/6N mice. Utilizing ultra high performance liquid chromatography high-resolution mass spectrometry (uHPLC-HRMS), the formation of 8-hydroxyefavirenz (8-OHEFV) from EFV and the glucuronidation of P450-dependent metabolites 8-OHEFV and 8,14-dihydroxyefavirenz (8,14-diOHEFV) were observed in brain microsomes from all three species. The direct glucuronidation of EFV, however, was only detected in cynomolgus macaque brain microsomes. In primary neural cells treated with EFV, microglia were the only cell type to exhibit metabolism, forming 8-OHEFV only. In cells treated with the P450-dependent metabolites of EFV, glucuronidation was detected only in cortical neurons and astrocytes, revealing that certain aspects of EFV metabolism are cell type specific. Untargeted and targeted proteomics experiments were used to identify the P450s and UGTs present in brain microsomes. Eleven P450s and 11 UGTs were detected in human brain microsomes, whereas seven P450s and 14 UGTs were identified in mouse brain microsomes and 15 P450s and four UGTs, respectively, were observed in macaque brain microsomes. This was the first time many of these enzymes have been noted in brain microsomes at the protein level. This study indicates the potential for brain metabolism to contribute to pharmacological and toxicological outcomes of EFV in the brain.

SIGNIFICANCE STATEMENT

Metabolism in the brain is understudied, and the persistence of human immunodeficiency virus (HIV) infection in the brain warrants the evaluation of how antiretroviral drugs such as efavirenz are metabolized in the brain. Using brain microsomes, the metabolism of efavirenz by both cytochrome P450s (P450s) and UDP-glucuronosyltransferases (UGTs) is established. Additionally, proteomics of brain microsomes characterizes P450s and UGTs in the brain, many of which have not yet been noted in the literature at the protein level.

Introduction

Efavirenz (EFV) is a non-nucleoside reverse transcriptase inhibitor used in combination antiretroviral therapy (cART) to treat human immunodeficiency virus (HIV)-1. Up until 2018, EFV was one component of the first-line treatment (World Health Organization, 2018) and is still used in resource-limited settings. EFV is associated with neurologic adverse events such as dizziness, depression, impaired concentration, disordered sleep, and anxiety (Fumaz et al., 2002; Gutiérrez et al., 2005; Romão et al., 2011; Ma et al., 2016; Checa et al., 2020; Hakkers et al., 2020; van Rensburg et al., 2022). Higher plasma concentrations of EFV and its primary metabolite, 8-hydroxyefavirenz (8-OHEFV), have been linked to poorer neurocognitive performance and mood changes (Grilo et al., 2016; Hakkers et al., 2020). EFV has also been shown to be toxic to neurons in culture and as it induces mitochondrial disruption (Purnell and Fox, 2014; Funes et al., 2015; Ciavatta et al., 2017). Of note, its cytochrome P450 (P450)-dependent metabolite, 8-OHEFV, has been found to elicit an even greater neurotoxic effect, demonstrating decreased neuron survival at the same dose as well as increased calcium influx and dendritic spine morphology (Tovar-y-Romo et al., 2012). Despite the negative neurologic consequences and evidence of brain penetration by EFV (Avery et al., 2013b; Thompson et al., 2015; Srinivas et al., 2019; Seneviratne et al., 2020), little is known about EFV metabolism in the brain.

Although we have highly effective combination antiretroviral therapy (cART), the brain remains a particularly elusive haven for HIV-1 infection. Vulnerable to infection (Aljawai et al., 2014; Cenker et al., 2017), the brain's macrophages, microglia, are considered to be the primary reservoir of HIV in the brain (Ko et al., 2019). When infected by HIV-1, microglial cells release inflammatory cytokines (Walsh et al., 2014; Akiyama et al., 2020) and neurotoxic factors (van Marle et al., 2004; Eugenin et al.,

This work was funded by National Institutes of Health National Institute on Aging [Grant 5R01-AG064908] (to N.N.B.) and National Institute of General Medical Sciences [Grant 5R01-GM103853] (to N.N.B.) and [Grant T32-GM008763] (to A.M.W.).

No author has an actual or perceived conflict of interest with the contents of this article.

dx.doi.org/10.1124/dmd.122.001195.

[S] This article has supplemental material available at dmd.aspetjournals.org.

ABBREVIATIONS: cART, combination antiretroviral therapy; CNS, central nervous system; CSF, cerebrospinal fluid; 8, 14-diOHEFV, 8, 14-dihydroxyefavirenz; 8, 14-diOHEFV-G, 8, 14-dihydroxyefavirenz glucuronide; EFV, efavirenz; EFV-G, efavirenz glucuronide; HAND, HIV-associated neurocognitive disorder; HIV, human immunodeficiency virus; MS, mass spectrometry; m/z, mass-to-charge ratio; 8-OHEFV, 8-hydroxyefavirenz; 8-OHEFV-G, 8-hydroxyefavirenz glucuronide; P450, cytochrome P450; UDPGA, UDP glucuronic acid; UGT, UDP-glucuronosyltransferase; uHPLC-HRMS, ultrahigh performance liquid chromatography high-resolution mass spectrometry.

2007). These contribute to increased blood-brain barrier permeability to HIV (Gandhi et al., 2010; Xu et al., 2012; Chaganti et al., 2019), prolonged neuroinflammation (Chivero et al., 2017), and cell death (van Marle et al., 2004; Eugenin et al., 2007). Individuals who are considered virally suppressed in terms of plasma HIV-1 RNA levels can have elevated HIV-1 RNA levels in the cerebrospinal fluid (CSF), which was found to correlate with adverse neurologic symptoms such as ataxia and cognitive impairment (Peluso et al., 2012). HIV-1 in the central nervous system often leads to the development of HIV-associated neurocognitive disorder (HAND), which includes symptoms such as neurocognitive impairment and functional decline (Antinori et al., 2007). Although cART has reduced the severity of HAND symptoms since the pre-cART era, the fraction of people living with HIV who develop HAND remains at approximately 42% (Wang et al., 2020). This indicates that HIV infection is persistent in the brain and underlines the importance of understanding the disposition of antiretrovirals such as EFV in the brain.

The biotransformation of EFV in the liver occurs via cytochromes P450s (P450s) and UDP-glucuronosyltransferases (UGTs). In humans, CYP2B6 and CYP2A6 form hydroxylated metabolites of EFV whereas UGT2B7 can directly glucuronidate EFV, and a variety of different UGTs can glucuronidate the P450-dependent metabolites of EFV (Mutlib et al., 1999; Ward et al., 2003; Bae et al., 2011; Ji et al., 2012; Avery et al., 2013b). P450-dependent metabolites are also noted to be sulfated, but these metabolites only account for approximately 0.7% of the excreted compound in urine and are not analyzed here (Aouri et al., 2016). In the present study, we characterize the P450 and UGT metabolism of EFV in brain using brain microsomes from mice, cynomolgus macaques, and humans as well as primary neurons, astrocytes, and microglia from C57Bl6/N mice. We show that biotransformation of EFV can occur in the brain and is carried out in a cell type–specific manner. UGT expression in brain, both in human and model species, has been historically understudied. Previous work has primarily reported on the tissue distribution of UGT mRNA (Buckley and Klaassen, 2007; Court et al., 2012; Uno and Yamazaki, 2020b), but less is currently known regarding the protein expression of UGTs in brain tissue. Therefore, a targeted mass spectrometry-based proteomics approach was developed and employed to aid in the understanding of drug metabolism in the brain by identifying the P450s and UGTs present. Several P450s and 15, 6, and 11 UGTs were detected in brain microsomes of mice, cynomolgus macaques, and humans, respectively. This work strengthens our understanding of EFV metabolism by P450s and UGTs in the brain, which will be fundamental to the investigation of the toxicity and efficacy of EFV in the brain.

Materials and Methods

Microsomal Metabolism Assays. Mouse and cynomolgus macaque pooled whole brain and pooled liver microsomes and pooled human brain microsomes were purchased from BioIVT (Baltimore, MD). Microsome donor pools were as follows: mouse whole brain (836), cynomolgus macaque whole brain (three), human brain (three), mouse liver (478), and cynomolgus macaque liver (five). Mouse, cynomolgus macaque, and human pooled liver microsomes were purchased from XenoTech (Kansas City, KS). Microsome donor pools were as follows: mouse liver (1000), cynomolgus macaque liver (10), and human liver (50). For the P450 metabolism assays, microsomes used at a protein concentration of 0.5 mg/ml were combined with 10 μM rac EFV (Toronto Research Chemicals, Toronto, Ontario, Canada; Santa Cruz Biotechnology, Dallas, TX) and NADPH regenerating system (Corning, Corning, NY) in 80 mM potassium phosphate buffer (pH 7.4; Corning). Samples were prewarmed at 37°C for 5 minutes before initialization of reaction via the addition of microsomes. Incubations without NADPH or without substrate were used as negative controls. Reactions were incubated in a 37°C water bath with shaking for 30 minutes and quenched using equal volume ice-cold acetonitrile and stored on ice until centrifugation. For the UGT metabolism assays, brain microsomes used at a protein concentration of 0.5 mg/ml were combined with 10 μM EFV, rac 8-OHEFV (Toronto Research Chemicals), or rac 8,14-diOHEFV (Toronto Research Chemicals) and a UGT reaction mixture containing 25 mM UDP glucuronic acid (UDPGA), 40 mM $MgCl_2$, 250 mM Tris-HCl, and 0.125 mg/ml alamethicin (Corning). Samples were prewarmed at 37°C for 5 minutes before initialization of the reaction via the addition of microsomes. Incubations without UDPGA or substrate were used as negative controls. Reactions were incubated in a 37°C water bath with shaking for 30 minutes and quenched with equal volume ice-cold acetonitrile and stored on ice until centrifugation. Both P450 and UGT metabolism assay samples were centrifuged at 10,000 × g and 4°C for 5 minutes, and the supernatant was dried down in a vacufuge (Eppendorf, Hamburg, Germany). Samples were reconstituted to one-fifth the original reaction volume in 100% methanol (Optima LCMS grade; Fisher Scientific, Hampton, NH) and were separated using a HALO C18 2.7 μm, 2.1 × 100 mm column (Advanced Materials Technology, Wilmington, DE) on a Dionex 3000 ultrahigh performance liquid chromatography system (uHPLC) coupled with a Q Exactive Orbitrap mass spectrometer (Thermo Fisher, Pittsburg, PA). The column heater was maintained at 30°C, and the sample injection volume was 2 μl. Water with 0.1% formic acid and acetonitrile with 0.1% formic acid were used for mobile phases A and B, respectively, with a flow rate of 0.600 ml/min. From 0 to 0.5 minutes, the liquid chromatography (LC) gradient held at 25% before increasing to 85% from 0.5 to 3.5 minutes. Eighty-five percent B was held for 3.5–5.5 minutes and then decreased to 0% for 5.5–5.6 minutes. A gradient up to 25% B ran from 5.6 to 7.0 minutes and was then held for the last 0.5 minutes of the method. The Q Exactive acquired full mass spectrometry (MS) scans from 150 to 800 m/z (mass-to-charge ratio) at a resolution of 70,000 and in negative mode. The heated electrospray source ionization parameters were as follows: sheath gas flow rate = 70, auxiliary gas flow rate = 20, sweep gas flow rate = 3, spray voltage = 3.00 kV, capillary temperature = 390°C, S-lens RF level = 60.0, and auxiliary gas heater temperature = 500°C. Peak area values for efavirenz glucuronide (EFV-G) (m/z = 490.0522), 8-OHEFV (m/z = 330.0145), 8-hydroxyefavirenz glucuronide (8-OHEFV-G) (m/z = 506.0471), 8,14-dihydroxyefavirenz (8,14-diOHEFV) (m/z = 346.0099), and 8,14-diOHEFV glucuronide (8,14-diOHEFV-G) (m/z = 522.0420) were obtained in QualBrowser (Thermo Fisher) using a 5-ppm mass error tolerance.

EFV Metabolite Formation over Time for Human Liver and Brain Microsomes. Liver and brain microsomes from pooled human donors (0.5 mg/ml) were incubated at 37°C for 0, 5, 15, 30, 60, 90, 120, 150, and 240 minutes with 100 mM potassium phosphate buffer (pH 7.4; Corning), NADPH regenerating system (Corning), UGT reaction mixture (Corning), and 5 μM EFV (Toronto Research Chemicals). Samples were prewarmed at 37°C for 5 minutes before initialization of reaction via the addition of microsomes. At each incubation time point, an aliquot was removed from the reaction tube and quenched using ice-cold 100 nM EFV-d4 (Toronto Research Chemicals) in acetonitrile. Samples were stored on ice until they were centrifuged at 10,000 × g and 4°C for 5 minutes. The supernatant was dried in a vacufuge and reconstituted in 100% methanol. Ionized metabolites and internal standard EFV-d4 (m/z = 318.0452) were detected via the ultra high performance liquid chromatography high-resolution mass spectrometry (uHPLC-HRMS) method described above. Peak area values were obtained in QualBrowser (Thermo Fisher) using a 5-ppm mass error tolerance. Data visualization and analysis were carried out in GraphPad Prism (version 9.3.1).

Primary Neural Cell Metabolism Assays. All cells were maintained at 37°C and 5% CO_2. C57BL/6N cortical neurons, striatal neurons, and astrocytes were purchased from Lonza (Basel, Switzerland), and microglia were purchased from ScienCell (Carlsbad, CA). Neurons were plated at approximately 1.04×10^5 cells/cm^2 in vendor-recommended medium, and a medium exchange was performed after 2 hours. Astrocytes were plated at approximately 1.32×10^4 cells/cm^2 in vendor-recommended medium, and a medium exchange was performed after 6 hours. Microglia were plated at approximately 2.19×10^4 cells/cm^2 in vendor-recommended medium, and a media exchange was performed after 24 hours. After 3 days in culture, cells were treated with 10 μM EFV, 8-OHEFV, 8,14-diOHEFV, or 0.1% DMSO vehicle control for approximately 24 hours. Cells were pelleted, and culture media was removed, dried down, and resuspended in 100% methanol. Metabolite formation was detected using a Q Exactive Orbitrap as described above.

Proteomics Sample Preparation. Liver and brain microsomes from mice, cynomolgus macaques, and humans were prepared for proteomic analyses using S-Trap spin columns (S-Trap Micro, PN: C02-Micro-10; ProtiFi, Farmingdale, NY) according to the manufacturer's protocol, where peptides were generated via reduction, alkylation, acidification, and tryptic digestion. Peptides were then dried down,

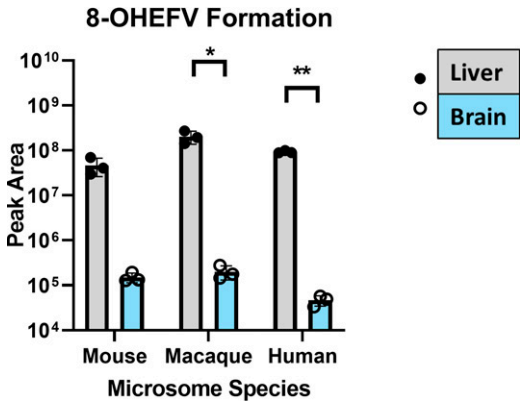

Fig. 1. P450-dependent metabolism of EFV occurs in brain microsomes but to a lesser extent than in liver microsomes. Brain and liver microsomes (0.5 mg/ml) were incubated with 10 μM EFV and NADPH cofactor for 30 minutes. The 8-OHEFV (m/z = 330.0145) metabolite was detected using uHPLC-HRMS. Formation of P450-dependent metabolites 7-OHEFV and 8,14-diOHEFV was not detected after incubation of EFV with brain microsomes from any species. Each data point represents an individual measurement from a microsomal metabolism assay. Assays were performed in triplicate. Statistical analysis of metabolite formation in liver vs. brain microsomes was performed using a two-tailed Welch's unequal variances *t* test. $*P < 0.05$, $**P < 0.01$.

reconstituted in water 0.1% formic acid, and quantified using a quantitative colorimetric assay (PN: 23275; Thermo Fisher) according to the manufacturer's protocol. To improve the depth of proteins identified for the targeted P450 and UGT methods, 100 μg of the brain microsome peptides were also separated into eight fractions using high pH reversed-phase chromatography (PN 84868; Thermo Fisher) according to the manufacturer's protocol.

Untargeted Proteomics. Peptides acquired from liver and brain microsomes (200 ng) were separated using a Waters HPLC nanoEase M/Z HSS T3, 100Å, 1.8 μm, 300 μm × 150 mm column and ACQUITY M Class ultra-performance liquid chromatographer (Waters, Milford, MA) before being injected onto a ZenoTOF 7600 mass spectrometer (SCIEX, Framingham, MA). Mobile phases A (water with 0.1% formic acid) and B (acetonitrile with 0.1% formic acid) flowed at 5 μl/min on the following 75-minute gradient: 3%–25% B from 0 to 38 minutes, 25%–50% B from 38 to 55 minutes, and 50%–80% B from 55 to 60 minutes, and then 80% B was held for 5 minutes before decreasing back to 3% B at 67 minutes, which was held for the remaining 8 minutes. Source parameters were as follows: ion source gas 1 = 20 psi, ion source gas 2 = 60 psi, curtain gas = 35, CAD gas = 7, source temperature = 200°C, and column temperature = 30°C. TOF MS parameters were as follows: acquisition range = 400–1250 Da, accumulation time = 0.1 seconds, declustering potential = 80 V, declustering spread = 0 V, collision energy = 10 V, and collision energy spread = 0 V. TOF MSMS parameters were as follows: acquisition range = 100–1800 Da, accumulation time = 0.02 seconds, declustering potential = 80 V, declustering spread = 0 V, collision energy = 12V, collision energy spread = 5 V, maximum number of candidate enzymes = 45, intensity threshold = 150 cps. Fragmentation was achieved using collision-induced dissociation, and former candidate ions were excluded for 12 seconds after one occurrence. SCIEX .wiff files were converted to .mgf files with MS Convert before data analysis was performed in Proteome Discoverer (version 2.4.0.305; Thermo Fisher) using SEQUEST HT for peptide spectral matching with a mass error tolerance of 25 ppm. Reference proteomes obtained from UniProt for mouse (*Mus musculus*, 10090), cynomolgus macaque (*Macaca fascicularis*, 9541), and human (*Homo sapiens*, 9606) were used for protein identification.

Targeted P450 and UGT Proteomics. Mouse, cynomolgus macaque, and human pooled liver microsomes were used to develop, validate, and optimize targeted methods for later analysis of brain microsomes. First, an untargeted proteomic analysis of the liver microsomes as described above was used to generate a list of detected peptides corresponding to P450 or UGT proteins that could be used for a targeted method. Untargeted proteomics data analysis was performed in Proteome Discoverer (version 2.4.0.305; Thermo Fisher) using SEQUEST HT for peptide spectral matching and the UniProt proteomes for mouse (*Mus musculus*, 10090), cynomolgus macaque (*Macaca fascicularis*, 9541), and human (*Homo sapiens*, 9606) were used for protein identification. Due to the relatively small number of reviewed proteins in UniProt/Swiss-Prot for cynomolgus macaque at the date of this study, an additional database was assembled from NCBI RefSeq by compiling all protein sequences available for species 9541 in NCBI Annotation Release 102 into a single fasta file. The acquired list of peptides from the untargeted proteomics was combined with the Skyline software-generated peptide prediction for 2+, 3+, and 4+ charged peptides (Skyline version 21.2.0.568; MacCoss Laboratory, University of Washington, Seattle, WA) based on protein sequences imported from UniProt (Geneva, Switzerland). A targeted proteomic analysis was performed using the same liquid chromatography (LC) gradient and MS parameters as above, first without and then with scheduled ionization based on peptide retention times. The lists of target peptides, the corresponding proteins, collision energies, and retention times can be found in Supplemental Tables 1–6. The TOF MSMS parameters for the targeted methods were as follows: acquisition range = 100–1800 Da, accumulation times = 25–80 milliseconds, declustering potential = 80 V, fragmentation = collision-induced dissociation, and collision energy varied with each individual peptide. After the target list was iteratively narrowed down to 100–200 peptides with quality peak shapes at high intensities in the liver microsomes, brain microsomes were analyzed for the presence of P450 or UGT metabolizing enzymes. Species-matched liver microsomes were run in tandem with the brain microsomes to validate findings. Targeted proteomic data analysis was performed in Skyline with the proteomes for mouse (*Mus musculus*, 10090), cynomolgus macaque (*Macaca fascicularis*, 9541), and human (*Homo sapiens*, 9606) narrowed down to just contain P450s and UGTs, ensuring consistent retention

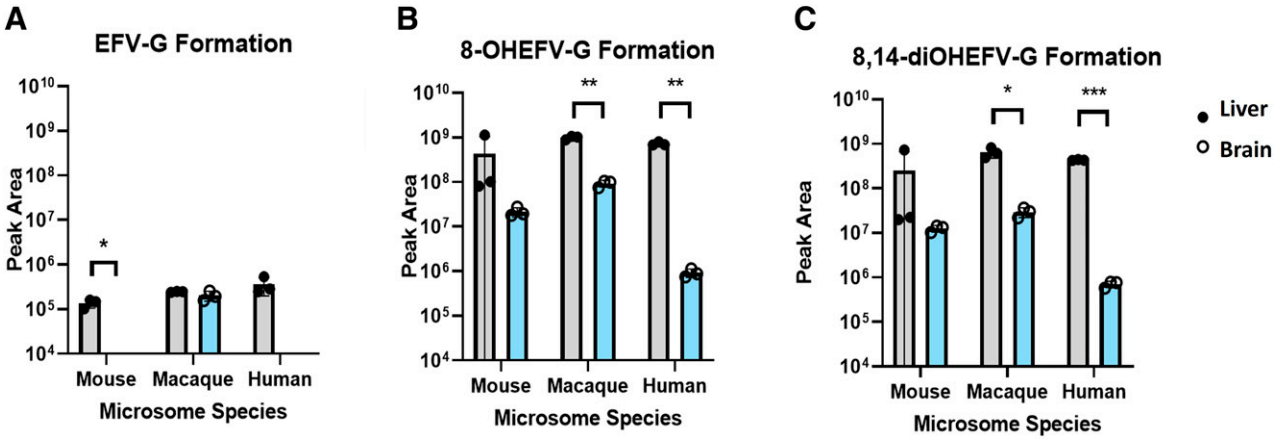

Fig. 2. Glucuronidation of EFV is species specific, and glucuronidation of P450-dependent metabolites of EFV occurs to a greater extent in liver microsomes than in brain microsomes. Brain and liver microsomes (0.5 mg/ml) were incubated with 10 μM substrate: (A) EFV, (B) 8-OHEFV, or (C) 8,14-diOHEFV, and UDPGA cofactor for 30 minutes. The metabolites EFV-G (m/z = 490.0522), 8-OHEFV-G (m/z = 506.0471), and 8,14-diOHEFV-G (m/z = 522.0420) were detected using uHPLC-HRMS. Each data point represents an individual measurement from a microsomal metabolism assay. Assays were performed in triplicate. Statistical analysis of metabolite formation in liver vs. brain microsomes was performed using a two-tailed Welch's unequal variances *t* test. $*P < 0.05$, $**P < 0.01$, $***P < 0.001$.

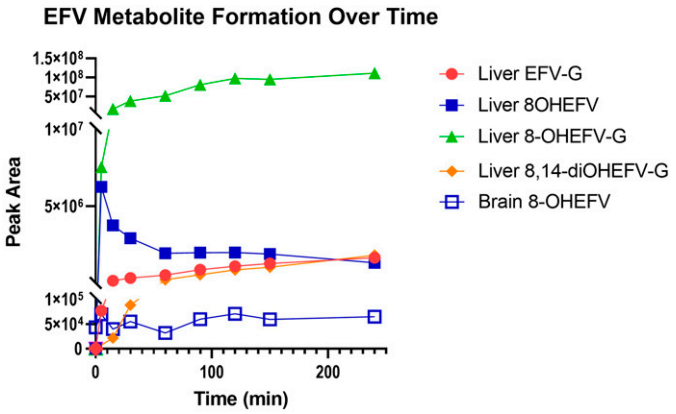

Fig. 3. EFV metabolite formation is greater after incubation with human liver microsomes than human brain microsomes across time points. Brain and liver microsomes (0.5 mg/ml) were incubated with 5 μM EFV, NADPH regenerating system, and a UGT reaction mixture (alamethicin and UDPGA cofactor) for 0, 5, 15, 30, 60, 90, 120, 150, and 240 minutes. The metabolites EFV-G (m/z = 490.0522), 8-OHEFV (m/z = 330.0145), 8-OHEFV glucuronide (8-OHEFV-G) (m/z = 506.0471), and 8,14-diOHEFV glucuronide (8,14-diOHEFV-G) (m/z = 522.0420) were detected using uHPLC-HRMS. Each data point is representative of a single measurement. Statistical analysis of total 8-OHEFV formation in liver vs. brain microsomes was performed using a two-tailed Welch's unequal variances *t* test: $P = 0.0033$.

times and fragment ion distribution between identifications made in the brain microsomes and those parameters established in the species-matched liver microsomes. All samples were run in technical duplicate or triplicate and if peptide was observed in more than one brain microsome fraction, the chromatograms from fraction with the highest peak intensity were used in the figures. All proteomic files and results were deposited at the MASSIVE public repository and can be accessed at ftp://massive.ucsd.edu/MSV000090576/.

Statistical Analysis. Data visualization and statistical analysis was carried out in GraphPad Prism (version 9.3.1; San Diego, CA). A two-tailed Welch's *t* test was used to determine significant differences in metabolite formation between liver microsomes and brain microsomes, where $*P < 0.05$ and $**P < 0.01$.

Results

Brain Microsomes Demonstrate Both P450 and UGT Activity toward EFV and Its P450-Dependent Metabolites, 8-OHEFV and 8,14-diOHEFV. To characterize metabolic activity toward EFV in the brain, we employed microsomal assays utilizing pooled brain microsomes from mice, cynomolgus macaques, and humans. Brain and species-matched liver microsomes were incubated with EFV or one of its P450-dependent

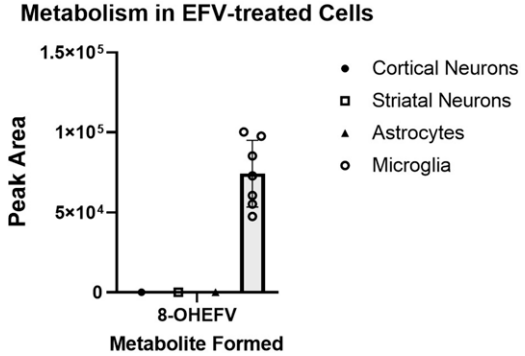

Fig. 4. P450-dependent metabolism occurs in microglial cells from C57BL/6N mice. Cortical and striatal neurons, astrocytes, and microglia from C57BL/6N mice were incubated for 24 hours with 10 μM EFV. Culture media was analyzed for metabolite formation using uHPLC-HRMS. Microglia were the only cell type tested to exhibit EFV biotransformation to 8-OHEFV. No other metabolites were observed for any of the cell types. Each data point is representative of a measurement from a single culture well. Cells were plated and treated in duplicate.

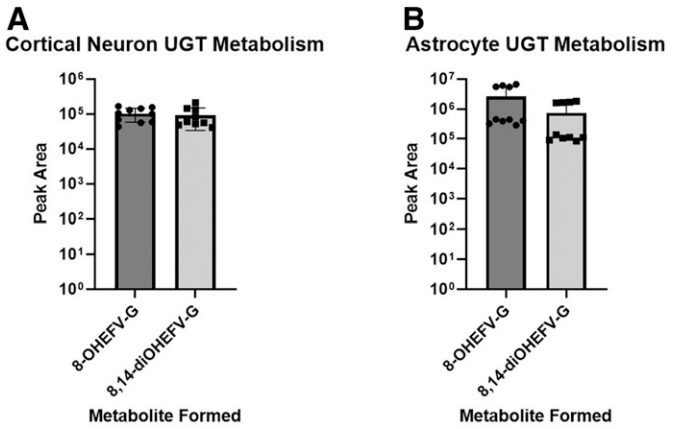

Fig. 5. Glucuronidation of EFV P450-dependent metabolites occurs in cortical neurons and astrocytes from C57BL/6 mice. Cortical and striatal neurons, astrocytes, and microglia from C57BL/6 mice were incubated for 24 hours with 10 μM 8-OHEFV or 8,14-diOHEFV. Culture media was analyzed for metabolite formation using uHPLC-HRMS. Glucuronidation of both P450-dependent metabolites was detected in the cortical neurons and astrocytes. Each data point is representative of a measurement from a single culture well. Cells were plated and treated in duplicate.

metabolites, 8-OHEFV or 8,14-diOHEFV. Incubation of EFV with the brain microsomes from all three species tested resulted in the formation of 8-OHEFV from EFV (Fig. 1). For each species, the formation of 8-OHEFV in the brain microsomes was less than that observed in the liver microsomes, with this difference being statistically significant for the cynomolgus macaque and human microsomes, whereas $P = 0.0586$ for the mouse microsomes. The formation of other previously reported P450-dependent EFV metabolites such as 7-OHEFV and 8,14-diOHEFV was not noted in the brain microsomes of any species tested. Metabolic assays to evaluate UGT activity toward EFV in the brain microsomes were also performed, using EFV or one of its P450-dependent metabolites as a substrate. We found the direct glucuronidation of EFV by brain microsomes to be species specific, where only the macaque brain microsomes formed EFV-G (Fig. 2A). We detected the glucuronidation of both 8-OHEFV and 8,14-diOHEFV in brain microsomes from all three species but again to a lesser extent than what we noted in the liver (Fig. 2,

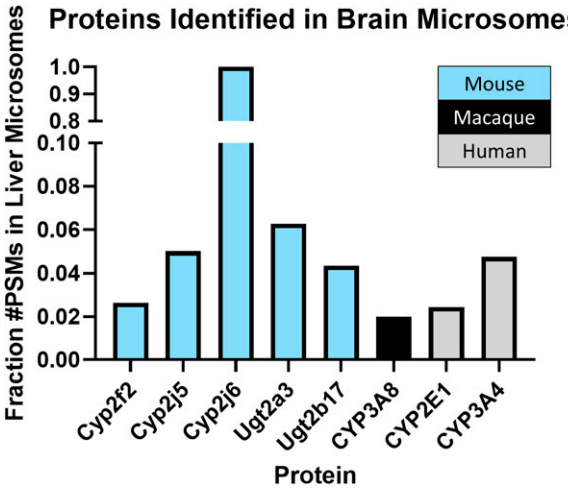

Fig. 6. Proteins detected in the brain microsomes exhibited a fraction of the peptide spectral matches identified for the same proteins in the liver microsomes. Untargeted proteomics comparing liver vs. brain microsomes from mouse, cynomolgus macaque, and human revealed the presence of several drug metabolizing enzymes, each with a single peptide spectral match. These matches were only a fraction of the peptide spectral matches observed in the liver microsomes for all proteins except for Cyp2j6 in the mouse microsomes.

TABLE 1

Summary of P450s and UGTs detected in brain microsomes

Mouse P450s	1a1, 2c39, 2d10, 2d11, 2d26, 4a10, 7b1
Macaque P450s	1A1, 1A2, 1B1, 2E1, 2F1, 2F12, 2R1, 2U1, 2W1, 4F12, 11B2 20A1, 21A2, 27A1, 27C1
Human P450s	1A2, 2A6, 2B6, 2C9, 2E1, 2J2, 3A4, 4A11, 4F3, 4F11, 4F12, 20A1
Mouse UGTs	1a1, 1a2, 1a5, 1a7, 1a8, 1a9, 1a10, 2a1, 2a2, 2a3, 2b17, 2b34, 2b35, 3a1
Macaque UGTs	1A9, 1A10, 2B9, 2B20
Human UGTs	1A1, 1A4, 1A5, 1A6, 1A8, 2A1, 2A2, 2B4, 2B7, 2B17, 2B28

B and C). The differences between liver and brain microsome formation of 8-OHEFV-G and 8,14diOHEFV-G were statistically significant in the macaque and human samples. The formation of EFV metabolites in human liver and brain microsomes was then evaluated using a time course experiment. The microsomal incubations, consisting of nine timepoints over 4 hours, contained both NADPH and UDPGA cofactors to examine P450 and UGT activity concurrently. In the human brain microsomes, only 8-OHEFV was formed at a detectable level, and the peak areas observed for this metabolite were two orders of magnitude lower than the 8-OHEFV formed in the human liver microsomes. (Fig. 3). In the human liver microsomes, we observe the formation of 8-OHEFV, 8-OHEFV-G, EFV-G, and 8,14-diOHEFV-G. Additionally, the 8-OHEFV in the liver microsomes was glucuronidated at each time point investigated, where 8-OHEFV-G was the metabolite formed in the highest abundance from 15 to 240 minutes.

Metabolism of EFV Is Cell Type Specific. Because microsomal assays do not capture the cell type heterogeneity of the brain, EFV metabolism was studied in primary cortical and striatal neurons, astrocytes, and microglia from C57BL/6N mice. After incubation of EFV with individual cultures of each of the above-mentioned primary cell types, culture media was analyzed for the formation of EFV metabolites. The microglial cells were the only cell type where biotransformation of EFV was detected, with 8-OHEFV present in the culture medium (Fig. 4). The 8-OHEFV metabolite was the only metabolite observed. The primary cortical neurons, striatal neurons, or astrocytes did not exhibit any metabolic activity toward EFV. When synthetic P450-dependent metabolites 8-OHEFV or 8,14-diOHEFV were used as substrates, glucuronidation of both P450-dependent metabolites was detected in the cortical neurons (Fig. 5A) and astrocytes (Fig. 5B). No other P450-, UGT-, or sulfotransferase-dependent metabolites were observed.

Untargeted Proteomics Confirmed Higher Abundance of P450s and UGTs in the Liver Microsomes Compared with the Brain Microsomes. A global untargeted proteomics experiment was first used to determine the expression of P450s and UGTs in liver microsomes versus brain microsomes isolated from mouse, cynomolgus macaque, or human tissue. Relative comparisons were achieved by using the number of peptide spectral matches identified for each protein, a label-free, semiquantitative way to measure protein abundance (Lundgren et al., 2010). In the mouse brain microsomes, a single unique peptide spectral match was found for Cyp2f2, Cyp2j5, Cyp2j6, Ugt2a3, and Ugt2b17. For all but Cyp2j6, these matches were only a fraction of those observed in liver microsomes (Fig. 6). Due to high sequence homology between these enzymes, additional nonunique peptide spectral matches were found for Cyp2d10, Cyp2d11, and Cyp2d26, where a single peptide corresponding to all three proteins was observed. UGTs 1a1, 1a2, 1a6, and 1a9 also shared a single peptide spectral match. Conversely, multiple peptides corresponding to each of these proteins were revealed in the mouse liver microsomes. In the microsomes from cynomolgus macaque, one unique peptide matching CYP3A8 was identified in the brain microsomes compared with 58 peptide spectral matches for CYP3A8 in the liver microsomes. In the human brain microsomes, CYP2E1 and CYP3A4 each showed a single

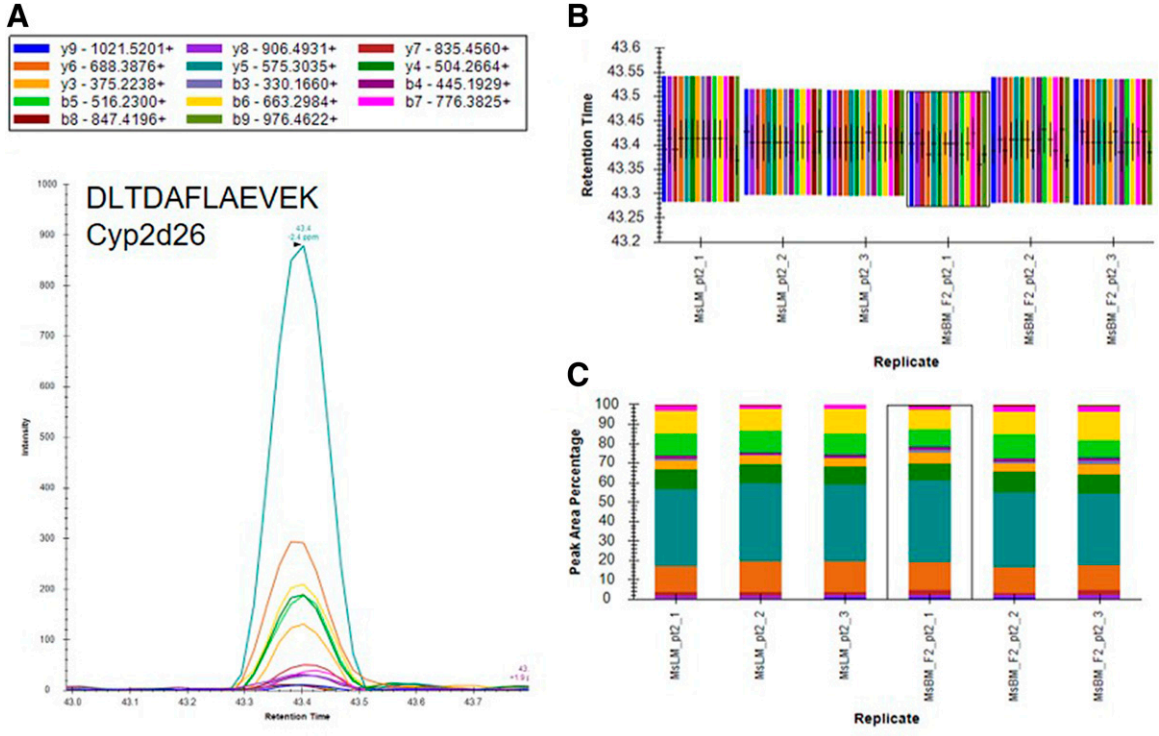

Fig. 7. Identification of Cyp2d26 in mouse brain microsomes using a targeted proteomics approach. Mouse brain microsomes were digested and resulting peptides were fractionated before using targeted proteomics to show the presence of Cyp2d26 (A). Samples were run in triplicate and peptide identifications were validated by comparing retention time (B) and peak area percentage of fragment ions (C) between mouse brain microsomes (MsBM) and mouse liver microsomes (MsLM). Peptide identifications for Cyp1a1, Cyp2c39, Cyp2d10, Cy2d11, Cyp4a10, and Cyp7b1 are illustrated in Supplemental Fig. 1.

unique peptide spectral match compared with 41 and 21 unique peptide matches in the liver microsomes, respectively (Fig. 6). A nonunique peptide corresponding to UGT1A1, UGT1A3, UGT1A4, UGT1A5, UGT1A6, UGT1A7, UGT1A8, UGT1A9, or UGT1A10 was also noted in the human brain microsomes.

Targeted Proteomics Identified Several P450s and UGTs in Brain Microsomes. Based on the results of our microsomal assays indicating the presence of UGTs in the macaque and human brain microsomes and the lack of identification of these enzymes in our untargeted proteomics results, we sought a method to identify the low abundance proteins of interest in the brain microsome samples. It is well established that targeted proteomic methods have a lower limit of detection than global analysis techniques (Domon and Aebersold, 2010). A recent advance in targeted mass spectrometry allows the simultaneous generation of multiple fragment ions from a peptide that can be identified with high resolution and high mass accuracy. To develop targeted proteomics methods, we created a target list of unique peptides to be used in the identification of P450s and UGTs in mouse, cynomolgus macaque, and human brain microsomes. To be considered an identification, each unique peptide had a mass error ≤5 ppm, a minimum of three fragment ions with intensities at least three times above the noise, and an acceptable peak shape. Only proteins from which quality peptides could be reliably detected in the liver microsomes were targeted in these experiments. Using the target lists, scheduled ionization, and these criteria, we identified peptides from several different P450s and UGTs (Table 1). In the mouse brain microsomes, 10 peptides corresponding to seven different P450s—1a1, 2c39, 2d10, 2d11, 2d26, 4a10, and 7b1 (Fig. 7; Supplemental Fig. 1; Supplemental Table 7)—and 25 peptides matching 15 UGTs—1a1, 1a2, 1a5, 1a7, 1a8, 1a9, 1a10, 2a1, 2a2, 2a3, 2b17, 2b34, 2b35, and 3a1 (Fig. 8; Supplemental Fig. 2; Supplemental Table 7)—were observed. In the cynomolgus macaque brain microsomes, 18 unique peptides corresponding to 15 P450s—1A1, 1A2, 1B1, 2C18, 2E1, 2F1, 2F12, 2R1, 2U1, 2W1, 11B2, 20A1, 21A2, 27A1, and 27C1 (Fig. 9; Supplemental Fig. 3; Supplemental Table 8)—and four peptides matching four UGTs—1A9, 1A10, 2B9, and 2B20—were detected (Fig. 10; Supplemental Fig. 4; Supplemental Table 8). In the human brain microsomes, 15 peptides matching 11 different P450s—1A2, 2A6, 2B6, 2D6, 2E1, 2J2, 3A4, 4A11, 4F3, 4F12, and 20A1 (Fig. 11; Supplemental Fig. 5; Supplemental Table 9)—and 14 peptides matching 11 different UGTs—1A1, 1A4, 1A5, 1A6, 1A8, 2A1, 2A2, 2B4, 2B7, 2B17, and 2B28—were observed (Fig. 12; Supplemental Fig. 6; Supplemental Table 9).

Discussion

This work aimed to deepen the understanding of drug metabolism in the brain, specifically for EFV. Our in vitro studies indicate that the brain can metabolize EFV and glucuronidate its P450-dependent metabolites. Moreover, we identified species differences in the direct glucuronidation of EFV, where brain microsomes from cynomolgus macaques formed EFV-G but the other brain microsomes did not. We also uncovered cell type–specific metabolism of EFV in mouse neural cells. Microglia metabolized EFV to 8-OHEFV, whereas cortical neurons and astrocytes glucuronidated both 8-OHEFV and 8,14-diOHEFV. This evidence indicates that local biotransformation of EFV and its P450-dependent metabolites can occur in brain and that this metabolism can vary by cell type and species. EFV metabolism in the brain could have consequences in both the sphere of drug efficacy and neurotoxicity.

Clinically, EFV is associated with a range of neurologic adverse events, with symptoms such as dizziness, depression, impaired concentration, disordered sleep, and anxiety occurring in up to 70% of patients (Fumaz et al., 2002; Gutiérrez et al., 2005; Checa et al., 2020). Although these

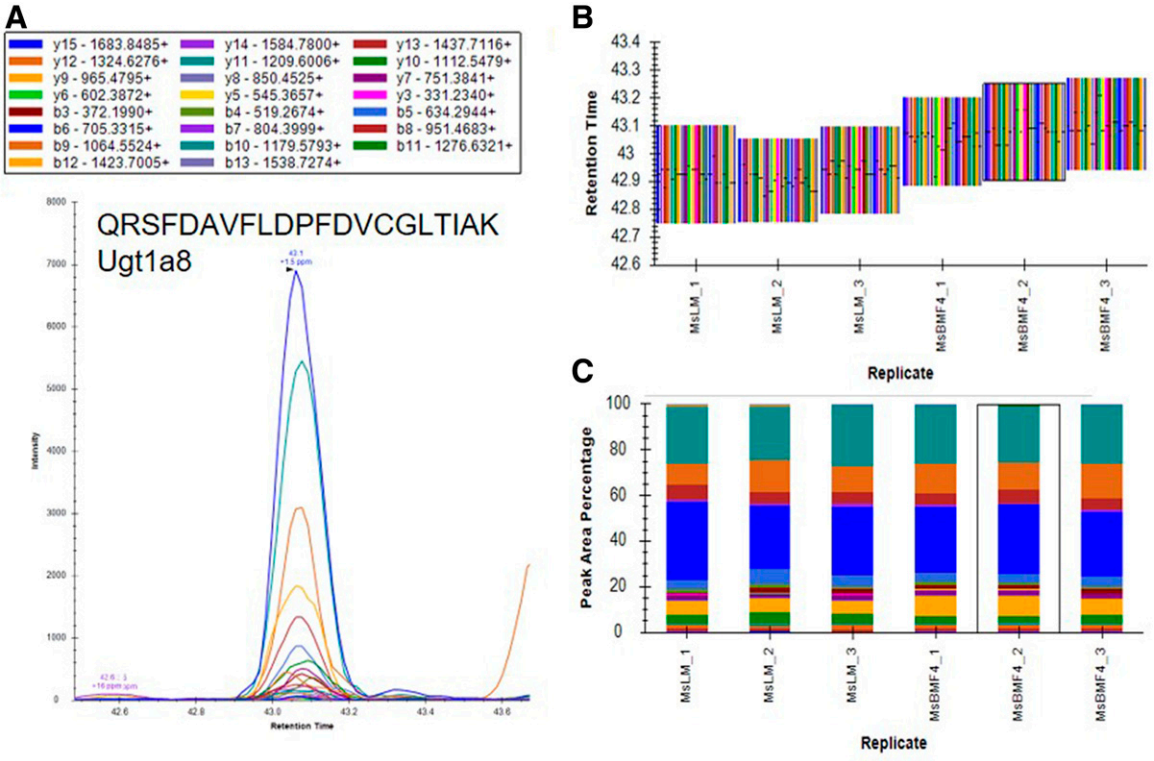

Fig. 8. Identification of Ugt1a8 in mouse brain microsomes using a targeted proteomics approach. Mouse brain microsomes were digested and resulting peptides were fractionated before using targeted proteomics to show the presence of Ugt1a8 (A). Samples were run in triplicate and peptide identifications were validated by comparing retention time (B) and peak area percentage of fragment ions (C) between mouse brain microsomes (MsBM) and mouse liver microsomes (MsLM). Peptide identifications for Ugt1a1, Ugt1a2, Ugt1a5, Ugt1a7, Ugt1a9, Ugt1a10, Ugt2a1, Ugt2a2, Ugt2a3, Ugt2b1, Ugt2b17, Ugt2b34, Ugt2b35, and Ugt3a1 are illustrated in Supplemental Fig. 2.

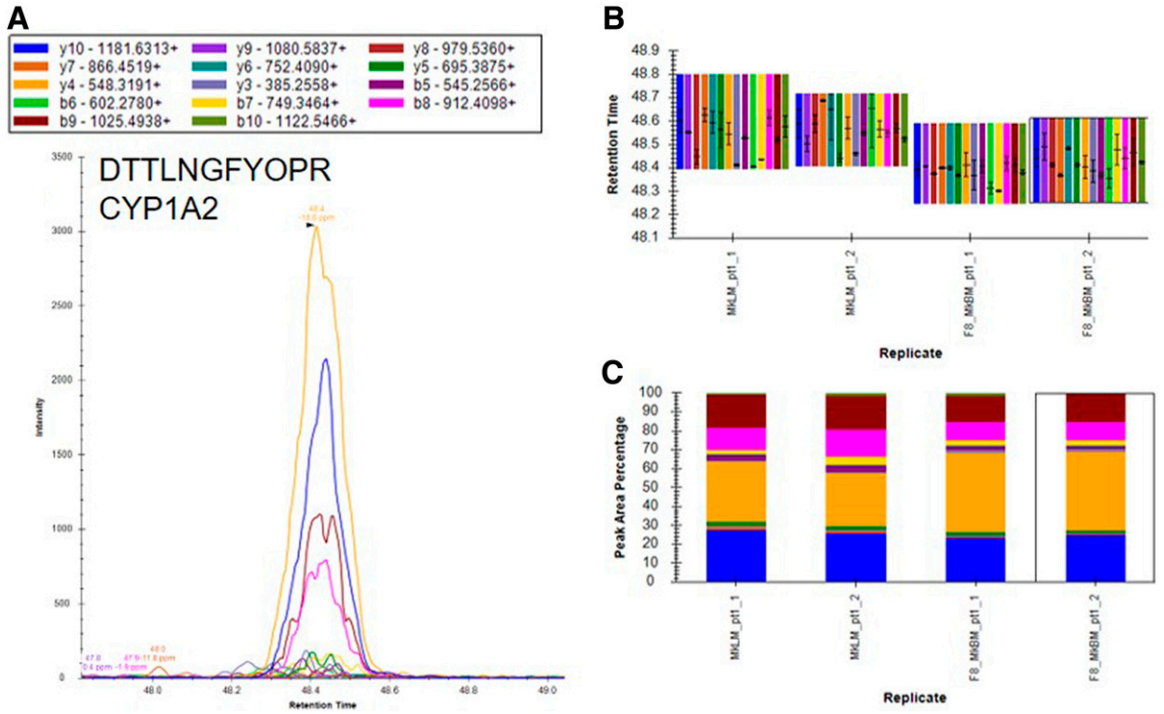

Fig. 9. Identification of CYP1A2 in cynomolgus macaque brain microsomes using a targeted proteomics approach. Cynomolgus macaque brain microsomes were digested and resulting peptides were fractionated before using targeted proteomics to show the presence of CYP1A2 (A). Samples were run in duplicate and peptide identifications were validated by comparing retention time (B) and peak area percentage of fragment ions (C) between macaque brain microsomes (MkBM) and macaque liver microsomes (MkLM). Peptide identifications for CYP1A1, CYP1B1, CYP2E1, CYP2F1, CYP2R1, CYP2U1, CYP2W1, CYP4F12, CYP4F22, CYP11B2, CYP20A1, CYP21A2, CYP27A1, and CYP27C1 are illustrated in Supplemental Fig. 3.

symptoms often subside over time, central nervous system (CNS) adverse events lead to regimen interruption and lower quality of life (Fumaz et al., 2002; Gutiérrez et al., 2005; Hawkins et al., 2005; Vera et al., 2019). Both EFV and 8-OHEFV reach the CSF at approximately 10 ng/ml and 3 ng/ml, respectively. (Tashima et al., 1999; Best et al., 2011; Avery et al., 2013a,b). Though EFV is 99.5% protein bound, similar unbound drug concentrations

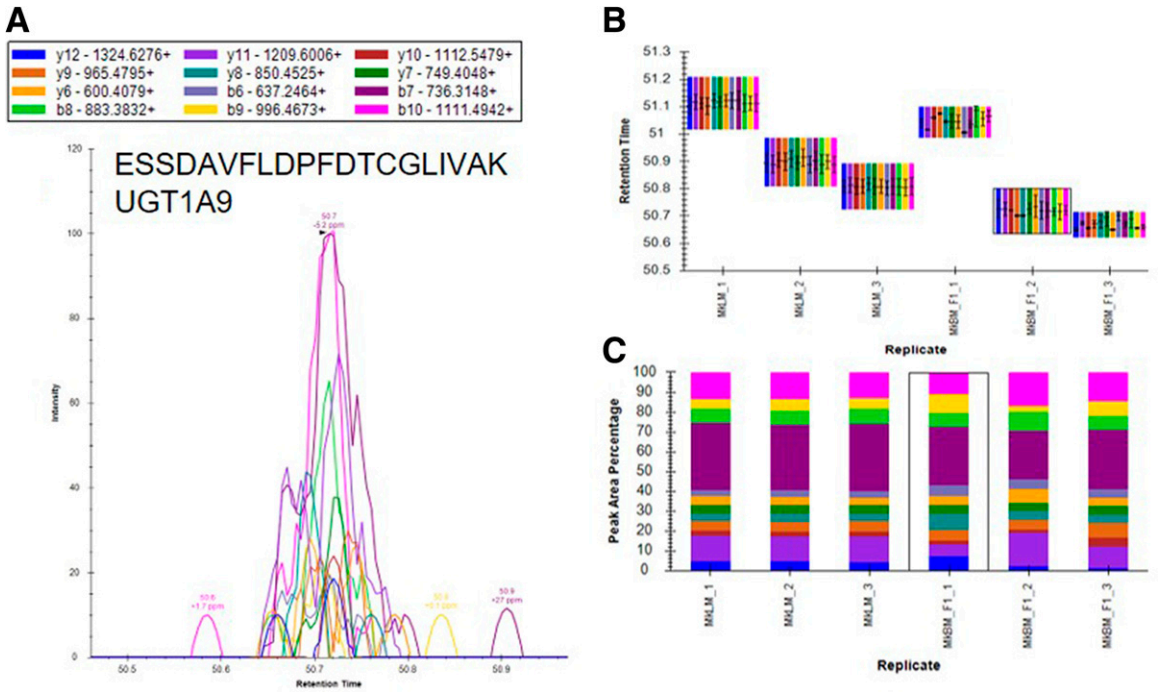

Fig. 10. Identification of UGT1A9 in cynomolgus macaque brain microsomes using a targeted proteomics approach. Cynomolgus macaque brain microsomes were digested and resulting peptides were fractionated before using targeted proteomics to show the presence of UGT1A9 (A). Samples were run in triplicate and peptide identifications were validated by comparing retention time (B) and peak area percentage of fragment ions (C) between macaque brain microsomes (MkBM) and macaque liver microsomes (MkLM). Peptide identifications for UGT1A10, UGT2B9, and UGT2B20 are illustrated in Supplemental Fig. 4.

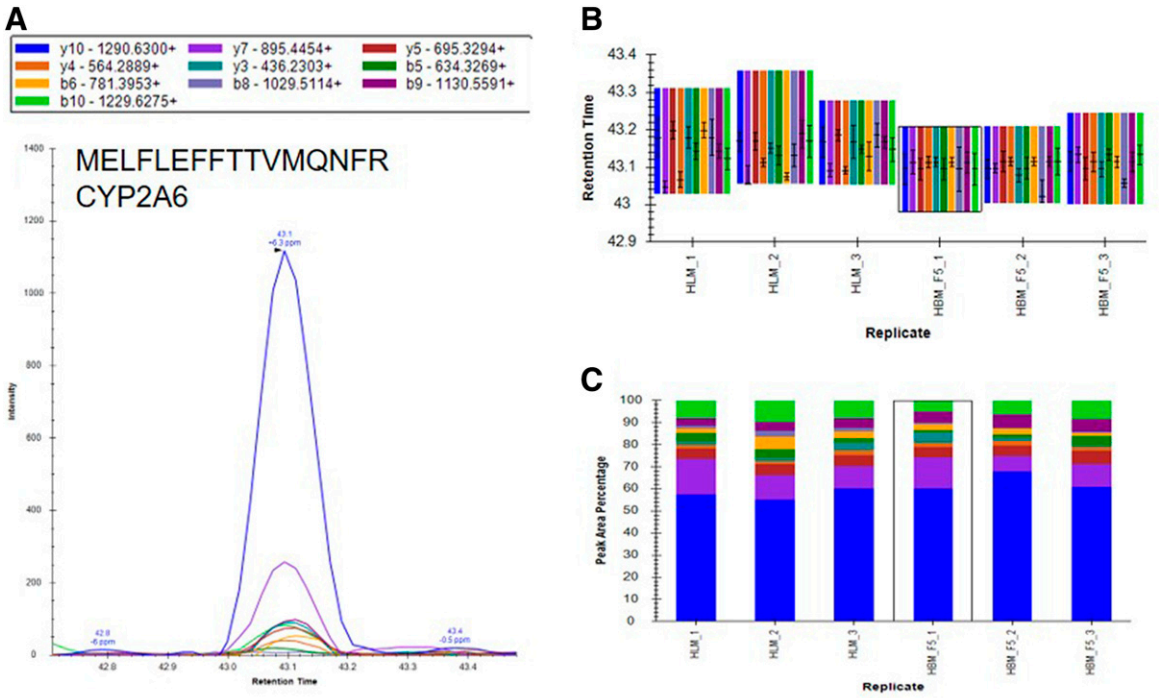

Fig. 11. Identification of CYP2A6 inhuman brain microsomes using a targeted proteomics approach. Human brain microsomes were digested and resulting peptides were fractionated before using targeted proteomics to show the presence of CYP2A6 (A). Samples were run in duplicate or triplicate and peptide identifications were validated by comparing retention time (B) and peak area percentage of fragment ions (C) between human brain microsomes (HBM) and human liver microsomes (HLM). Peptide identifications for CYP1A2, CYP2B6, CYP2D6, CYP2E1, CYP2J2, CYP3A4, CYP4A11, CYP4F3, CYP4F12, and CYP20A1 are illustrated in Supplemental Fig. 5.

between plasma and CSF suggests unbound efavirenz can passively enter the CNS (Best et al., 2011; Avery et al., 2013a). Although EFV has been noted to induce P-glycoprotein, it is not a substrate of the transporter (Dirson et al., 2006; Chan et al., 2013). EFV is found in the CSF at concentrations above the IC_{95} for wild-type HIV-1 (Tashima et al., 1999; Best et al., 2011; Calcagno et al., 2015), contradicting the notion that the ongoing prevalence of HAND is a result of poor antiretroviral penetration into the CNS. Additionally, the 8-OHEFV concentrations found in human CSF are similar to the dose that induced in vitro toxicity in rat hippocampal neurons (Tovar-y-Romo et al., 2012; Avery et al., 2013b). However, phase 2 metabolites, 8-OHEFV-G and 8-OHEFV-sulfate, were noted at even higher concentrations: 15–56 ng/ml and 0–29 ng/ml, respectively (Aouri et al., 2016; Nightingale et al., 2016). Nightingale et al. (2016) note that these higher concentrations could be a result of local metabolism, as the percentage of free EFV is not significantly greater in the CSF than it is in the plasma. The slow metabolizing CYP2B6 (G516T) T/T genotype is associated with higher plasma and CSF concentrations of EFV (Haas et al., 2004; Nightingale et al., 2016) as well as late onset efavirenz neurotoxicity

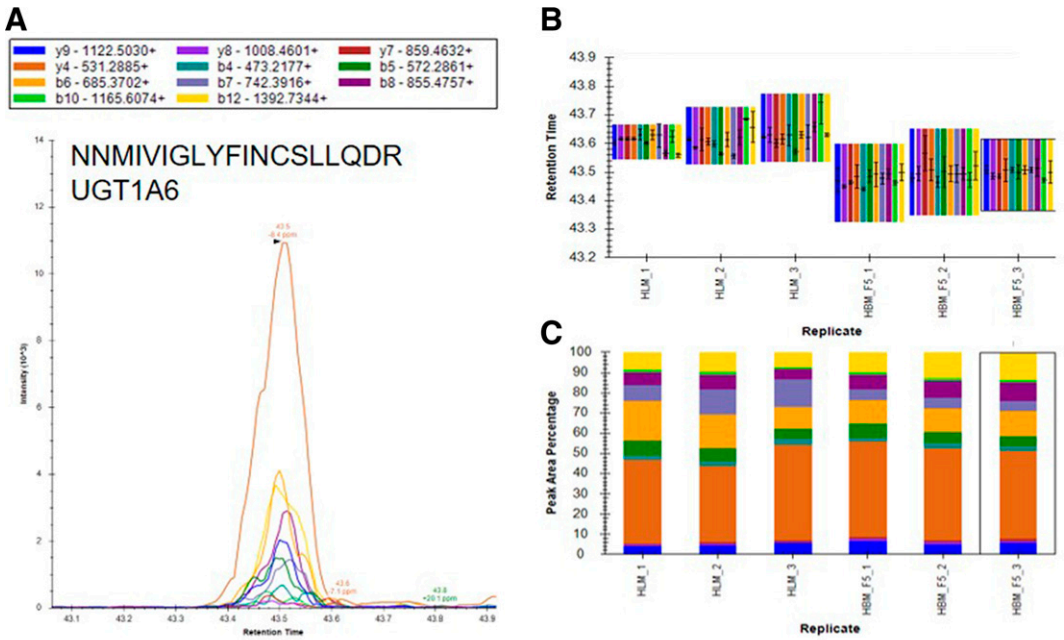

Fig. 12. Identification of UGT1A6 in human brain microsomes using a targeted proteomics approach. Human brain microsomes were digested and resulting peptides were fractionated before using a targeted proteomics approach to show the presence of UGT1A6 (A). Samples were run in duplicate or triplicate and peptide identifications were validated by comparing retention time (B) and peak area percentage of fragment ions (C) between human brain microsomes (HBM) and human liver microsomes (HLM). Peptide identifications for UGT1A1, UGT1A4, UGT1A5, UGT1A6, UGT1A8, UGT2A1, UGT2A2, UGT2B4, UGT2B7, UGT2B17, and UGT2B28 are illustrated in Supplemental Fig. 6.

syndrome (van Rensburg et al., 2022). Further, in silico modeling indicates that measurements of EFV in the CSF likely underrepresent the EFV penetration into the brain (Curley et al., 2016). These predictions were confirmed in a study that analyzed the postmortem brain tissue of patients taking EFV and noted an average tissue concentration of 35.9 ng/ml EFV compared with 15.9 ng/ml in the CSF (Aouri et al., 2016; Ferrara et al., 2020). Local brain metabolism of EFV, particularly glucuronidation, could be advantageous in terms of neurotoxicity but detrimental to efficacy at the site of infection. Several studies have examined drug-metabolizing enzymes in the brain, but few have measured these drug-metabolizing enzymes at the protein level. Using a proteomics approach, we sought to identify the P450s and UGTs present in brain microsomes.

The mRNA transcripts of several P450s have been reported in the human brain, with 1B1, 2D6, 2E1, 2J2, and 46A1 being the most abundant (Dutheil et al., 2009). CYP2D6 metabolizes endogenous substances like dopamine and serotonin as well as a number of different drugs that target the CNS such as opioids, neuroleptics, antidepressants, selective serotonin reuptake inhibitors, and antiemetics (Hiroi et al., 1998; Yu et al., 2003; Wang et al., 2009; Bromek et al., 2011; Haduch et al., 2015). Furthermore, lower levels of CYP2D6 in the brain have been associated with Parkinson's disease (Mann et al., 2012). CYP2E1 is known to both metabolize and be induced by ethanol in the brain (Zimatkin et al., 2006; Zhong et al., 2012; Ferguson et al., 2013). In the brain, CYP2B6 has been implicated in nicotine metabolism (Garcia et al., 2015), and nicotine has been shown to induce CYP2B6 expression (Miksys et al., 2003; Lee et al., 2006; Ferguson et al., 2013). CYP2B6 is also known to metabolize the antidepressant and smoking cessation aid bupropion (Hesse et al., 2000), which has been observed, along with its metabolites, in brain tissue (Suckow et al., 1986). CYP46A1 catalyzes cholesterol 24-hydroxylation and is important in regulating cholesterol homeostasis in the brain, whereas dysregulation has been linked to neurodegeneration (Djelti et al., 2015). EFV is known to be a CYP46A1 activator at low doses and has been explored for the treatment of Alzheimer's disease (Petrov et al., 2019; Mast et al., 2020). Lastly, human brain microsomes have also been noted to exhibit P450 activity by CYP3A4, CYP2D6, or CYP2C19 through the demethylation of the antidepressant amitriptyline (Voirol et al., 2000).

Using targeted P450 proteomics, we identified a number of P450s in mouse, cynomolgus macaque, and human brain microsomes. Several studies have shown the presence of P450s, either at the mRNA or protein level, in murine brain (Stapleton et al., 1995; Choudhary et al., 2005; Renaud et al., 2011; Hersman and Bumpus, 2014; Stamou et al., 2014; Yamaori et al., 2017). Our identification of Cyp1a1, Cyp2c39, Cyp2d10, Cyp2d26, Cyp4a10, and Cyp7b1 coincides with these studies (Supplemental Table 10). Detection of CYP1A1 and CYP2E1 in macaque brain microsomes was commensurate with a previous mRNA-based study (Uno and Yamazaki, 2020b), whereas the remaining 13 P450s that we identified in macaque brain microsomes (P450s 1A2, 1B1, 2C18, 2F1, 2F12, 2R1, 2U1, 11B2, 20A1, 21A2, 27A1, and 27C1) have not been previously noted in the brain (Supplemental Table 11). P450s in the human brain have also been previously reported (McFadyen et al., 1998; Yun et al., 1998; Gervot et al., 1999; Upadhya et al., 2000; Miksys et al., 2002; Stark et al., 2008; Booth Depaz et al., 2015), including CYP1A2, CYP2B6, CYP2C9 CYP2E1, CYP3A4, and CYP20A1, which were identified in the present study using targeted proteomics (Supplemental Table 12). We additionally identified peptides corresponding to CYP2A6, CYP2J2, CYP4A11, CYP4F3, and CYP4F12.

Less is known about UGTs in the brain compared with P450s. However, UGTs have been shown to be involved in the metabolism of both endogenous substrates, such as dopamine and serotonin, and xenobiotics, such as morphine, in the brain (Wahlström et al., 1988; Uutela et al., 2009; Ouzzine et al., 2014). We identified 14 different UGTs in the mouse brain microsomes, 12 of which have been detected at the mRNA level in previous studies (Buckley and Klaassen, 2007; Heydel et al., 2010; Uchihashi et al., 2013), whereas the other two UGTs (Ugt1a9 and Ugt2b17) have not been previously reported in murine brain (Supplemental Table 10). The mRNA expression of UGTs 1A1, 1A9, 1A10, 2B9, 2B18, 2B19, 2B23, 3A2, and 8A1 has been reported in cynomolgus macaque brain tissue (Uno and Yamazaki, 2020a,b), of which we observed UGT1A9, UGT1A10, and UGT2B9 protein in macaque brain microsomes (Supplemental Table 11). We also identified UGT2B20, and to our knowledge, UGT protein and/or activity have yet to be reported in cynomolgus macaque brain. Lastly, the mRNA transcript of UGTs 1A1, 1A3, 1A4, 1A5, 1A6, 1A7, 1A10, 2A1, 2B7, and 2B17 have been previously identified in human brain tissue (Jedlitschky et al., 1999; King et al., 1999; Ohno and Nakajin, 2009; Court et al., 2012) and UGT1A4 protein has been reported as well (Ghosh et al., 2010), corresponding with our study (Supplemental Table 12). Using the targeted proteomics method that we developed, UGTs 1A8, 2A1, 2A2, 2B4, and 2B28 were also identified. These results are consistent with our microsomal metabolism data, as UGT1A1 and UGT1A8 have each been reported to carry out the glucuronidation of the P450-dependent metabolites of EFV (Bae et al., 2011).

In summary, the in vitro metabolism of EFV observed in this study and the identification of P450 and UGT protein in the brain microsomes of mice, cynomolgus macaques, and humans lend novel insight into the local metabolism of the EFV, which would have implications for combatting HIV in the brain. Biotransformation of EFV in the brain would reduce active drug concentration while potentially modulating neurotoxicity. The presence of drug-metabolizing enzymes in the brain at the protein level has not been previously well established, but the targeted methods used can be applied to probing low-abundance P450s and UGTs in other tissues, contributing to research regarding tissue-specific pharmaceuticals or toxicity. The proteomic data presented in this study represent a fundamental asset in understanding and predicting P450 and UGT metabolism of any drug that crosses the blood-brain barrier and can guide future activity-based studies.

Authorship Contributions

Participated in research design: Wheeler, Orsburn, Bumpus.

Conducted experiments: Wheeler.

Performed data analysis: Wheeler, Orsburn.

Wrote or contributed to the writing of the manuscript: Wheeler, Orsburn, Bumpus.

References

Akiyama H, Jalloh S, Park S, Lei M, Mostoslavsky G, and Gummuluru S (2020) Expression of HIV-1 intron-containing RNA in microglia induces inflammatory responses. *J Virol* **95**:e01385–20.

Aljawai Y, Richards MH, Seaton MS, Narasipura SD, and Al-Harthi L (2014) β-Catenin/TCF-4 signaling regulates susceptibility of macrophages and resistance of monocytes to HIV-1 productive infection. *Curr HIV Res* **12**:164–173.

Antinori A, Arendt G, Becker JT, Brew BJ, Byrd DA, Cherner M, Clifford DB, Cinque P, Epstein LG, Goodkin K, et al. (2007) Updated research nosology for HIV-associated neurocognitive disorders. *Neurology* **69**:1789–1799.

Aouri M, Barcelo C, Ternon B, Cavassini M, Anagnostopoulos A, Yerly S, Hugues H, Vernazza P, Günthard HF, Buclin T, et al.; Swiss HIV Cohort Study (2016) In vivo profiling and distribution of known and novel phase I and phase II metabolites of efavirenz in plasma, urine, and cerebrospinal fluid. *Drug Metab Dispos* **44**:151–161.

Avery LB, Sacktor N, McArthur JC, and Hendrix CW (2013a) Protein-free efavirenz concentrations in cerebrospinal fluid and blood plasma are equivalent: applying the law of mass action to predict protein-free drug concentration. *Antimicrob Agents Chemother* **57**:1409–1414.

Avery LB, VanAusdall JL, Hendrix CW, and Bumpus NN (2013b) Compartmentalization and antiviral effect of efavirenz metabolites in blood plasma, seminal plasma, and cerebrospinal fluid. *Drug Metab Dispos* **41**:422–429.

Bae SK, Jeong YJ, Lee C, and Liu KH (2011) Identification of human UGT isoforms responsible for glucuronidation of efavirenz and its three hydroxy metabolites. *Xenobiotica* **41**:437–444.

Best BM, Koopmans PP, Letendre SL, Capparelli EV, Rossi SS, Clifford DB, Collier AC, Gelman BB, Mbeo G, McCutchan JA, et al.; CHARTER Group (2011) Efavirenz concentrations in CSF exceed IC50 for wild-type HIV. *J Antimicrob Chemother* **66**:354–357.

Booth Depaz IM, Toselli F, Wilce PA, and Gillam EM (2015) Differential expression of cytochrome P450 enzymes from the CYP2C subfamily in the human brain. *Drug Metab Dispos* **43**:353–357.
Bromek E, Haduch A, Gołembiowska K, and Daniel WA (2011) Cytochrome P450 mediates dopamine formation in the brain in vivo. *J Neurochem* **118**:806–815.
Buckley DB and Klaassen CD (2007) Tissue- and gender-specific mRNA expression of UDP-glucuronosyltransferases (UGTs) in mice. *Drug Metab Dispos* **35**:121–127.
Calcagno A, Simiele M, Alberione MC, Bracchi M, Marinaro L, Ecclesia S, Di Perri G, D'Avolio A, and Bonora S (2015) Cerebrospinal fluid inhibitory quotients of antiretroviral drugs in HIV-infected patients are associated with compartmental viral control. *Clin Infect Dis* **60**:311–317.
Cenker JJ, Stultz RD, and McDonald D (2017) Brain microglial cells are highly susceptible to HIV-1 infection and spread. *AIDS Res Hum Retroviruses* **33**:1155–1165.
Chaganti J, Marripudi K, Staub LP, Rae CD, Gates TM, Moffat KJ, and Brew BJ (2019) Imaging correlates of the blood-brain barrier disruption in HIV-associated neurocognitive disorder and therapeutic implications. *AIDS* **33**:1843–1852.
Chan GN, Patel R, Cummins CL, and Bendayan R (2013) Induction of P-glycoprotein by antiretroviral drugs in human brain microvessel endothelial cells. *Antimicrob Agents Chemother* **57**:4481–4488.
Checa A, Castillo A, Camacho M, Tapia W, Hernandez I, and Teran E (2020) Depression is associated with efavirenz-containing treatments in newly antiretroviral therapy initiated HIV patients in Ecuador. *AIDS Res Ther* **17**:47.
Chivero ET, Guo ML, Periyasamy P, Liao K, Callen SE, and Buch S (2017) HIV-1 Tat primes and activates microglial NLRP3 inflammasome-mediated neuroinflammation. *J Neurosci* **37**:3599–3609.
Choudhary D, Jansson I, Stoilov I, Sarfarazi M, and Schenkman JB (2005) Expression patterns of mouse and human CYP orthologs (families 1-4) during development and in different adult tissues. *Arch Biochem Biophys* **436**:50–61.
Ciavatta VT, Bichler EK, Speigel IA, Elder CC, Teng SL, Tyor WR, and García PS (2017) In vitro and ex vivo neurotoxic effects of efavirenz are greater than those of other common antiretrovirals. *Neurochem Res* **42**:3220–3232.
Court MH, Zhang X, Ding X, Yee KK, Hesse LM, and Finel M (2012) Quantitative distribution of mRNAs encoding the 19 human UDP-glucuronosyltransferase enzymes in 26 adult and 3 fetal tissues. *Xenobiotica* **42**:266–277.
Curley P, Rajoli RK, Moss DM, Liptrott NJ, Letendre S, Owen A, and Siccardi M (2016) Efavirenz is predicted to accumulate in brain tissue: an in silico, in vitro, and in vivo investigation. *Antimicrob Agents Chemother* **61**:e01841–16.
Dirson G, Fernandez C, Hindlet P, Roux F, German-Fattal M, Gimenez F, and Farinotti R (2006) Efavirenz does not interact with the ABCB1 transporter at the blood-brain barrier. *Pharm Res* **23**: 1525–1532.
Djelti F, Braudeau J, Hudry E, Dhenain M, Varin J, Bièche I, Marquer C, Chali F, Ayciriex S, Auzeil N, et al. (2015) CYP46A1 inhibition, brain cholesterol accumulation and neurodegeneration pave the way for Alzheimer's disease. *Brain* **138**:2383–2398.
Domon B and Aebersold R (2010) Options and considerations when selecting a quantitative proteomics strategy. *Nat Biotechnol* **28**:710–721.
Dutheil F, Dauchy S, Diry M, Sazdovitch V, Cloarec O, Mellottée L, Bièche I, Ingelman-Sundberg M, Flinois JP, de Waziers I, et al. (2009) Xenobiotic-metabolizing enzymes and transporters in the normal human brain: regional and cellular mapping as a basis for putative roles in cerebral function. *Drug Metab Dispos* **37**:1528–1538.
Eugenin EA, King JE, Nath A, Calderon TM, Zukin RS, Bennett MV, and Berman JW (2007) HIV-tat induces formation of an LRP-PSD-95- NMDAR-nNOS complex that promotes apoptosis in neurons and astrocytes. *Proc Natl Acad Sci USA* **104**:3438–3443.
Ferguson CS, Miksys S, Palmour RM, and Tyndale RF (2013) Ethanol self-administration and nicotine treatment induce brain levels of CYP2B6 and CYP2E1 in African green monkeys. *Neuropharmacology* **72**:74–81.
Ferrara M, Bumpus NN, Ma Q, Ellis RJ, Soontornniyomkij V, Fields JA, Bharti A, Achim CL, Moore DJ, and Letendre SL (2020) Antiretroviral drug concentrations in brain tissue of adult decedents. *AIDS* **34**:1907–1914.
Fumaz CR, Tuldrà A, Ferrer MJ, Paredes R, Bonjoch A, Jou T, Negredo E, Romeu J, Sirera G, Tural C, et al. (2002) Quality of life, emotional status, and adherence of HIV-1-infected patients treated with efavirenz versus protease inhibitor-containing regimens. *J Acquir Immune Defic Syndr* **29**:244–253.
Funes HA, Blas-Garcia A, Esplugues JV, and Apostolova N (2015) Efavirenz alters mitochondrial respiratory function in cultured neuron and glial cell lines. *J Antimicrob Chemother* **70**:2249–2254.
Gandhi N, Saiyed ZM, Napuri J, Samikkannu T, Reddy PV, Agudelo M, Khatavkar P, Saxena SK, and Nair MP (2010) Interactive role of human immunodeficiency virus type 1 (HIV-1) clade-specific Tat protein and cocaine in blood-brain barrier dysfunction: implications for HIV-1-associated neurocognitive disorder. *J Neurovirol* **16**:294–305.
Garcia KL, Coen K, Miksys S, Lê AD, and Tyndale RF (2015) Effect of brain CYP2B inhibition on brain nicotine levels and nicotine self-administration. *Neuropsychopharmacology* **40**:1910–1918.
Gervot L, Rochat B, Gautier JC, Bohnenstengel F, Kroemer H, de Berardinis V, Martin H, Beaune P, and de Waziers I (1999) Human CYP2B6: expression, inducibility and catalytic activities. *Pharmacogenetics* **9**:295–306.
Ghosh C, Gonzalez-Martinez J, Hossain M, Cucullo L, Fazio V, Janigro D, and Marchi N (2010) Pattern of P450 expression at the human blood-brain barrier: roles of epileptic condition and laminar flow. *Epilepsia* **51**:1408–1417.
Grilo NM, Correia MJ, Sequeira C, Harjivan SG, Caixas U, Diogo LN, Marques MM, Monteiro EC, Antunes AM, and Pereira SA (2016) Efavirenz biotransformation as an up-stream event of mood changes in HIV-infected patients. *Toxicol Lett* **260**:28–35.
Gutiérrez F, Navarro A, Padilla S, Antón R, Masiá M, Borrás J, and Martín-Hidalgo A (2005) Prediction of neuropsychiatric adverse events associated with long-term efavirenz therapy, using plasma drug level monitoring. *Clin Infect Dis* **41**:1648–1653.
Haas DW, Ribaudo HJ, Kim RB, Tierney C, Wilkinson GR, Gulick RM, Clifford DB, Hulgan T, Marzolini C, and Acosta EP (2004) Pharmacogenetics of efavirenz and central nervous system side effects: an Adult AIDS Clinical Trials Group study. *AIDS* **18**:2391–2400.
Haduch A, Bromek E, Kot M, Kamińska K, Gołembiowska K, and Daniel WA (2015) The cytochrome P450 2D-mediated formation of serotonin from 5-methoxytryptamine in the brain in vivo: a microdialysis study. *J Neurochem* **133**:83–92.
Hakkers CS, Hermans AM, van Maarseveen EM, Teunissen CE, Verberk IMW, Arends JE, and Hoepelman AIM (2020) High efavirenz levels but not neurofilament light plasma levels are associated with poor neurocognitive functioning in asymptomatic HIV patients. *J Neurovirol* **26**:572–580.
Hawkins T, Geist C, Young B, Giblin A, Mercier RC, Thornton K, and Haubrich R (2005) Comparison of neuropsychiatric side effects in an observational cohort of efavirenz- and protease inhibitor-treated patients. *HIV Clin Trials* **6**:187–196.
Hersman EM and Bumpus NN (2014) A targeted proteomics approach for profiling murine cytochrome P450 expression. *J Pharmacol Exp Ther* **349**:221–228.
Hesse LM, Venkatakrishnan K, Court MH, von Moltke LL, Duan SX, Shader RI, and Greenblatt DJ (2000) CYP2B6 mediates the in vitro hydroxylation of bupropion: potential drug interactions with other antidepressants. *Drug Metab Dispos* **28**:1176–1183.
Heydel JM, Holsztynska EJ, Legendre A, Thiebaud N, Artur Y, and Le Bon AM (2010) UDP-glucuronosyltransferases (UGTs) in neuro-olfactory tissues: expression, regulation, and function. *Drug Metab Rev* **42**:74–97.
Hiroi T, Imaoka S, and Funae Y (1998) Dopamine formation from tyramine by CYP2D6. *Biochem Biophys Res Commun* **249**:838–843.
Jedlitschky G, Cassidy AJ, Sales M, Pratt N, and Burchell B (1999) Cloning and characterization of a novel human olfactory UDP-glucuronosyltransferase. *Biochem J* **340**:837–843.
Ji HY, Lee H, Lim SR, Kim JH, and Lee HS (2012) Effect of efavirenz on UDP-glucuronosyltransferase 1A1, 1A4, 1A6, and 1A9 activities in human liver microsomes. *Molecules* **17**:851–860.
King CD, Rios GR, Assouline JA, and Tephly TR (1999) Expression of UDP-glucuronosyltransferases (UGTs) 2B7 and 1A6 in the human brain and identification of 5-hydroxytryptamine as a substrate. *Arch Biochem Biophys* **365**:156–162.
Ko A, Kang G, Hattler JB, Galadima HI, Zhang J, Li Q, and Kim W-K (2019) Macrophages but not astrocytes harbor HIV DNA in the brains of HIV-1-infected aviremic individuals on suppressive antiretroviral therapy. *J Neuroimmune Pharmacol* **14**:110–119.
Lee AM, Miksys S, Palmour R, and Tyndale RF (2006) CYP2B6 is expressed in African green monkey brain and is induced by chronic nicotine treatment. *Neuropharmacology* **50**:441–450.
Lundgren DH, Hwang SI, Wu L, and Han DK (2010) Role of spectral counting in quantitative proteomics. *Expert Rev Proteomics* **7**:39–53.
Ma Q, Vaida F, Wong J, Sanders CA, Kao YT, Croteau D, Clifford DB, Collier AC, Gelman BB, Marra CM, et al.; CHARTER Group (2016) Long-term efavirenz use is associated with worse neurocognitive functioning in HIV-infected patients. *J Neurovirol* **22**:170–178.
Mann A, Miksys SL, Gaedigk A, Kish SJ, Mash DC, and Tyndale RF (2012) The neuroprotective enzyme CYP2D6 increases in the brain with age and is lower in Parkinson's disease patients. *Neurobiol Aging* **33**:2160–2171.
Mast N, Verwilst P, Wilkey CJ, Guengerich FP, and Pikuleva IA (2020) In vitro activation of cytochrome P450 46A1 (CYP46A1) by efavirenz-related compounds. *J Med Chem* **63**:6477–6488.
McFadyen MCE, Melvin WT, and Murray GI (1998) Regional distribution of individual forms of cytochrome P450 mRNA in normal adult human brain. *Biochem Pharmacol* **55**:825–830.
Miksys S, Lerman C, Shields PG, Mash DC, and Tyndale RF (2003) Smoking, alcoholism and genetic polymorphisms alter CYP2B6 levels in human brain. *Neuropharmacology* **45**:122–132.
Miksys S, Rao Y, Hoffmann E, Mash DC, and Tyndale RF (2002) Regional and cellular expression of CYP2D6 in human brain: higher levels in alcoholics. *J Neurochem* **82**:1376–1387.
Mutlib AE, Chen H, Nemeth GA, Markwalder JA, Seitz SP, Gan LS, and Christ DD (1999) Identification and characterization of efavirenz metabolites by liquid chromatography/mass spectrometry and high field NMR: species differences in the metabolism of efavirenz. *Drug Metab Dispos* **27**:1319–1333.
Nightingale S, Chau TT, Fisher M, Nelson M, Winston A, Else L, Carr DF, Taylor S, Ustianowski A, Back D, et al. (2016) Efavirenz and metabolites in cerebrospinal fluid: relationship with CYP2B6 c.516G→T genotype and perturbed blood-brain barrier due to tuberculous meningitis. *Antimicrob Agents Chemother* **60**:4511–4518.
Ohno S and Nakajin S (2009) Determination of mRNA expression of human UDP-glucuronosyltransferases and application for localization in various human tissues by real-time reverse transcriptase-polymerase chain reaction. *Drug Metab Dispos* **37**:32–40.
Ouzzine M, Gulberti S, Ramalanjaona N, Magdalou J, and Fournel-Gigleux S (2014) The UDP-glucuronosyltransferases of the blood-brain barrier: their role in drug metabolism and detoxication. *Front Cell Neurosci* **8**:349.
Peluso MJ, Ferretti F, Peterson J, Lee E, Fuchs D, Boschini A, Gisslén M, Angoff N, Price RW, Cinque P, et al. (2012) Cerebrospinal fluid HIV escape associated with progressive neurologic dysfunction in patients on antiretroviral therapy with well controlled plasma viral load. *AIDS* **26**:1765–1774.
Petrov AM, Lam M, Mast N, Moon J, Li Y, Maxfield E, and Pikuleva IA (2019) CYP46A1 activation by efavirenz leads to behavioral improvement without significant changes in amyloid plaque load in the brain of 5XFAD mice. *Neurotherapeutics* **16**:710–724.
Purnell PR and Fox HS (2014) Efavirenz induces neuronal autophagy and mitochondrial alterations. *J Pharmacol Exp Ther* **351**:250–258.
Renaud HJ, Cui JY, Khan M, and Klaassen CD (2011) Tissue distribution and gender-divergent expression of 78 cytochrome P450 mRNAs in mice. *Toxicol Sci* **124**:261–277.
Romão PR, Lemos JC, Moreira J, de Chaves G, Moretti M, Castro AA, Andrade VM, Boeck CR, Quevedo J, and Gavioli EC (2011) Anti-HIV drugs nevirapine and efavirenz affect anxiety-related behavior and cognitive performance in mice. *Neurotox Res* **19**:73–80.
Seneviratne HK, Hamlin AN, Heck CJS, and Bumpus NN (2020) Spatial distribution profiles of emtricitabine, tenofovir, efavirenz, and rilpivirine in murine tissues following *in vivo* dosing correlate with their safety profiles in humans. *ACS Pharmacol Transl Sci* **3**:655–665.
Srinivas N, Joseph SB, Robertson K, Kincer LP, Menezes P, Adamson L, Schauer AP, Blake KH, White N, Sykes C, et al. (2019) Predicting efavirenz concentrations in the brain tissue of HIV-infected individuals and exploring their relationship to neurocognitive impairment. *Clin Transl Sci* **12**:302–311.
Stamou M, Wu X, Kania-Korwel I, Lehmler HJ, and Lein PJ (2014) Cytochrome p450 mRNA expression in the rodent brain: species-, sex-, and region-dependent differences. *Drug Metab Dispos* **42**:239–244.
Stapleton G, Steel M, Richardson M, Mason JO, Rose KA, Morris RG, and Lathe R (1995) A novel cytochrome P450 expressed primarily in brain. *J Biol Chem* **270**:29739–29745.
Stark K, Wu ZL, Bartleson CJ, and Guengerich FP (2008) mRNA distribution and heterologous expression of orphan cytochrome P450 20A1. *Drug Metab Dispos* **36**:1930–1937.
Suckow RF, Smith TM, Perumal AS, and Cooper TB (1986) Pharmacokinetics of bupropion and metabolites in plasma and brain of rats, mice, and guinea pigs. *Drug Metab Dispos* **14**:692–697.
Tashima KT, Caliendo AM, Ahmad M, Gormley JM, Fiske WD, Brennan JM, and Flanigan TP (1999) Cerebrospinal fluid human immunodeficiency virus type 1 (HIV-1) suppression and efavirenz drug concentrations in HIV-1-infected patients receiving combination therapy. *J Infect Dis* **180**:862–864.
Thompson CG, Bokhart MT, Sykes C, Adamson L, Fedoriw Y, Luciw PA, Muddiman DC, Kashuba AD, and Rosen EP (2015) Mass spectrometry imaging reveals heterogeneous efavirenz distribution within putative HIV reservoirs. *Antimicrob Agents Chemother* **59**:2944–2948.

Tovar-y-Romo LB, Bumpus NN, Pomerantz D, Avery LB, Sacktor N, McArthur JC, and Haughey NJ (2012) Dendritic spine injury induced by the 8-hydroxy metabolite of efavirenz. *J Pharmacol Exp Ther* **343**:696–703.

Uchihashi S, Nishikawa M, Sakaki T, and Ikushiro S (2013) Comparison of serotonin glucuronidation activity of UDP-glucuronosyltransferase 1a6a (Ugt1a6a) and Ugt1a6b: evidence for the preferential expression of Ugt1a6a in the mouse brain. *Drug Metab Pharmacokinet* **28**:260–264.

Uno Y and Yamazaki H (2020a) Molecular characterization of UDP-glucuronosyltransferases 3A and 8A in cynomolgus macaques. *Drug Metab Pharmacokinet* **35**:397–400.

Uno Y and Yamazaki H (2020b) mRNA levels of drug-metabolizing enzymes in 11 brain regions of cynomolgus macaques. *Drug Metab Pharmacokinet* **35**:248–252.

Upadhya SC, Tirumalai PS, Boyd MR, Mori T, and Ravindranath V (2000) Cytochrome P4502E (CYP2E) in brain: constitutive expression, induction by ethanol and localization by fluorescence in situ hybridization. *Arch Biochem Biophys* **373**:23–34.

Uutela P, Reinilä R, Harju K, Piepponen P, Ketola RA, and Kostiainen R (2009) Analysis of intact glucuronides and sulfates of serotonin, dopamine, and their phase I metabolites in rat brain microdialysates by liquid chromatography-tandem mass spectrometry. *Anal Chem* **81**:8417–8425.

van Marle G, Henry S, Todoruk T, Sullivan A, Silva C, Rourke SB, Holden J, McArthur JC, Gill MJ, and Power C (2004) Human immunodeficiency virus type 1 Nef protein mediates neural cell death: a neurotoxic role for IP-10. *Virology* **329**:302–318.

van Rensburg R, Nightingale S, Brey N, Albertyn CH, Kellermann TA, Taljaard JJ, Esterhuizen TM, Sinxadi PZ, and Decloedt EH (2022) Pharmacogenetics of the late-onset efavirenz neurotoxicity syndrome (LENS). *Clin Infect Dis* **75**:399–405.

Vera JH, Bracchi M, Alagaratnam J, Lwanga J, Fox J, Winston A, Boffito M, and Nelson M (2019) Improved central nervous system symptoms in people with HIV without objective neuropsychiatric complaints switching from efavirenz to rilpivirine containing cART. *Brain Sci* **9**:195.

Voirol P, Jonzier-Perey M, Porchet F, Reymond MJ, Janzer RC, Bouras C, Strobel HW, Kosel M, Eap CB, and Baumann P (2000) Cytochrome P-450 activities in human and rat brain microsomes. *Brain Res* **855**:235–243.

Wahlström A, Winblad B, Bixo M, and Rane A (1988) Human brain metabolism of morphine and naloxone. *Pain* **35**:121–127.

Walsh JG, Reinke SN, Mamik MK, McKenzie BA, Maingat F, Branton WG, Broadhurst DI, and Power C (2014) Rapid inflammasome activation in microglia contributes to brain disease in HIV/AIDS. *Retrovirology* **11**:35.

Wang B, Yang LP, Zhang XZ, Huang SQ, Bartlam M, and Zhou SF (2009) New insights into the structural characteristics and functional relevance of the human cytochrome P450 2D6 enzyme. *Drug Metab Rev* **41**:573–643.

Wang Y, Liu M, Lu Q, Farrell M, Lappin JM, Shi J, Lu L, and Bao Y (2020) Global prevalence and burden of HIV-associated neurocognitive disorder: a meta-analysis. *Neurology* **95**:e2610–e2621.

Ward BA, Gorski JC, Jones DR, Hall SD, Flockhart DA, and Desta Z (2003) The cytochrome P450 2B6 (CYP2B6) is the main catalyst of efavirenz primary and secondary metabolism: implication for HIV/AIDS therapy and utility of efavirenz as a substrate marker of CYP2B6 catalytic activity. *J Pharmacol Exp Ther* **306**:287–300.

World Health Organization (2018) *Updated Recommendations on First-Line and Second-Line Antiretroviral Regimens and Post-Exposure Prophylaxis and Recommendations on Early Infant Diagnosis of HIV: Interim Guidelines. Supplement to the 2016 Consolidated Guidelines on the Use of Antiretroviral Drugs for Treating and Preventing HIV Infection*, World Health Organization, Geneva, Switzerland.

Xu R, Feng X, Xie X, Zhang J, Wu D, and Xu L (2012) HIV-1 Tat protein increases the permeability of brain endothelial cells by both inhibiting ccluding expression and cleaving ccluding via matrix metalloproteinase-9. *Brain Res* **1436**:13–19.

Yamaori S, Jiang R, Maeda C, Ogawa R, Okazaki H, Aramaki H, and Watanabe K (2017) Expression levels of 39 Cyp mRNAs in the mouse brain and neuroblastoma cell lines, C-1300N18 and NB2a – strong expression of Cyp1b1. *Fundam Toxicol Sci* **4**:195–200 DOI: 10.2131/fts.4.195.

Yu AM, Idle JR, Byrd LG, Krausz KW, Küpfer A, and Gonzalez FJ (2003) Regeneration of serotonin from 5-methoxytryptamine by polymorphic human CYP2D6. *Pharmacogenetics* **13**:173–181.

Yun CH, Park HJ, Kim SJ, and Kim HK (1998) Identification of cytochrome P450 1A1 in human brain. *Biochem Biophys Res Commun* **243**:808–810.

Zhong Y, Dong G, Luo H, Cao J, Wang C, Wu J, Feng YQ, and Yue J (2012) Induction of brain CYP2E1 by chronic ethanol treatment and related oxidative stress in hippocampus, cerebellum, and brainstem. *Toxicology* **302**:275–284.

Zimatkin SM, Pronko SP, Vasiliou V, Gonzalez FJ, and Deitrich RA (2006) Enzymatic mechanisms of ethanol oxidation in the brain. *Alcohol Clin Exp Res* **30**:1500–1505.

Address correspondence to: Dr. Namandjé N. Bumpus, Department of Pharmacology and Molecular Sciences, Johns Hopkins University School of Medicine, Physiology 312, 725 North Wolfe Street, Baltimore, MD 21205-2105. E-mail: nbumpus1@jhmi.edu; or Benjamin C. Orsburn, Department of Pharmacology and Molecular Sciences, Johns Hopkins University School of Medicine, Physiology 312, 725 North Wolfe Street, Baltimore, MD 21205-2105. E-mail: borsbur1@jhmi.edu

Biotransformation of efavirenz and proteomic analysis of P450s and UGTs in mouse, macaque, and human brain-derived *in vitro* systems

Abigail M. Wheeler, Benjamin C. Orsburn, and Namandjé N. Bumpus

Drug Metabolism and Disposition

DMD-AR-2022-001195R1

Supplemental Figure 1. Identification of 7 different P450s in the mouse brain microsomes using a targeted proteomics approach. Mouse brain microsomes (MsBM) were digested and resulting peptides were fractionated before using targeted proteomics to show the presence of Cyp1a1 (A), Cyp2c39 (B), Cyp2d10 (C-D), Cyp2d11 (E), Cyp2d26 (F), Cyp4a10 (G), and Cyp7b1 (H-J). Protein identifications were made using chromatograms (left) and confirmation of consistent retention times and fragment ions (right) with mouse liver microsomes (MsLM). Samples were analyzed in technical duplicate or triplicate. Some retention time shifts were observed in A-B, but MsLM and MsBM retention times are consistent within each replicate.

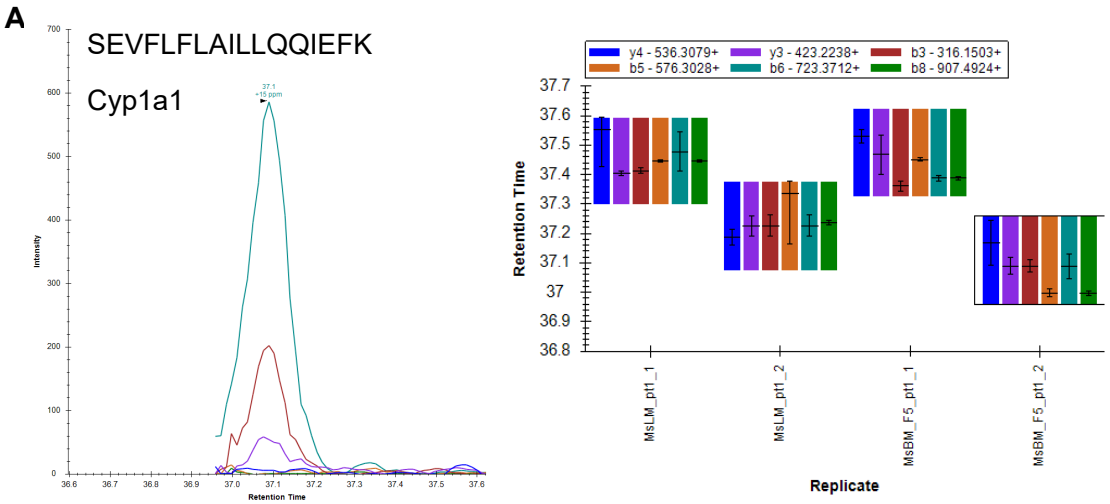

B

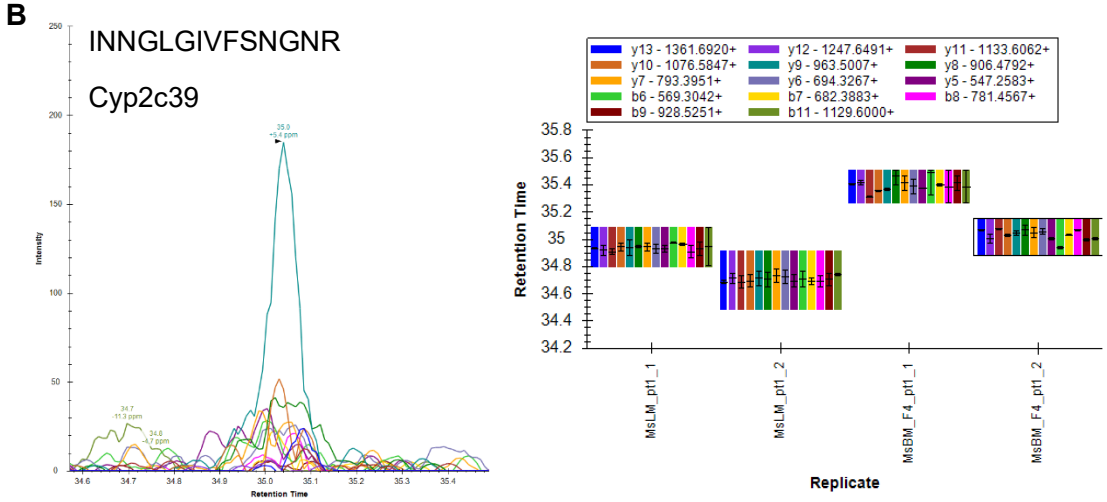
INNGLGIVFSNGNR
Cyp2c39
Intensity
Retention Time
y13 - 1361.6920+
y12 - 1247.6491+
y11 - 1133.6062+
y10 - 1076.5847+
y9 - 963.5007+
y8 - 906.4792+
y7 - 793.3951+
y6 - 694.3267+
y5 - 547.2583+
b6 - 569.3042+
b7 - 682.3883+
b8 - 781.4567+
b9 - 928.5251+
b11 - 1129.6000+
Retention Time
MsLM_pt1_1
MsLM_pt1_2
MsBM_F4_pt1_1
MsBM_F4_pt1_2
Replicate

C

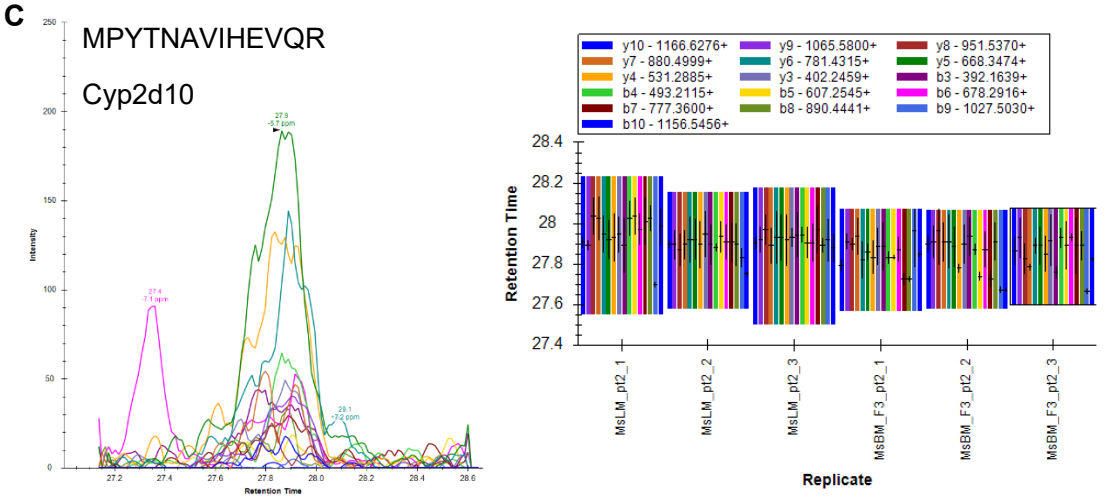
MPYTNAVIHEVQR
Cyp2d10
Intensity
Retention Time
y10 - 1166.6276+
y9 - 1065.5800+
y8 - 951.5370+
y7 - 880.4999+
y6 - 781.4315+
y5 - 668.3474+
y4 - 531.2885+
y3 - 402.2459+
b3 - 392.1639+
b4 - 493.2115+
b5 - 607.2545+
b6 - 678.2916+
b7 - 777.3600+
b8 - 890.4441+
b9 - 1027.5030+
b10 - 1156.5456+
Retention Time
MsLM_pt2_1
MsLM_pt2_2
MsLM_pt2_3
MsBM_F3_pt2_1
MsBM_F3_pt2_2
MsBM_F3_pt2_3
Replicate

D

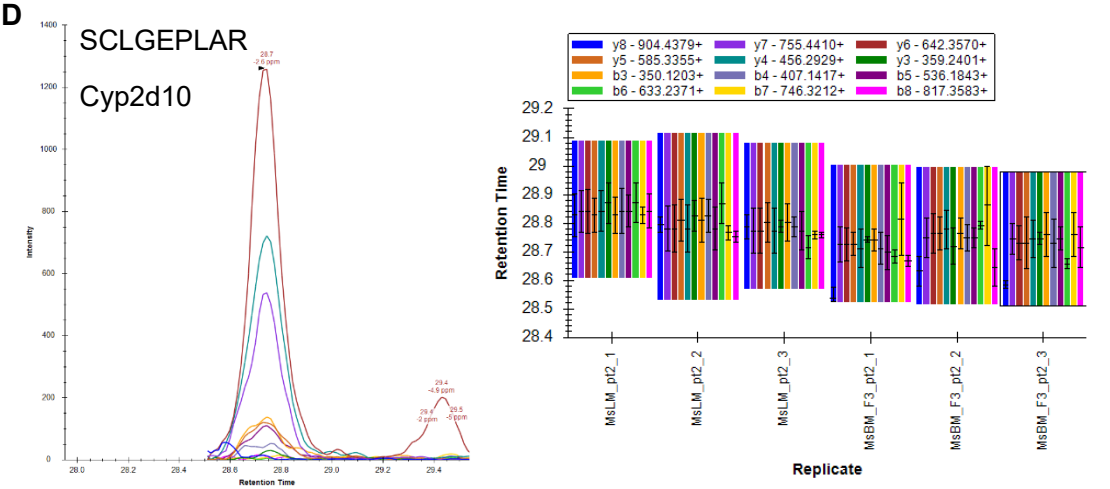
SCLGEPLAR
Cyp2d10
Intensity
Retention Time
y8 - 904.4379+
y7 - 755.4410+
y6 - 642.3570+
y5 - 585.3355+
y4 - 456.2929+
y3 - 359.2401+
b3 - 350.1203+
b4 - 407.1417+
b5 - 536.1843+
b6 - 633.2371+
b7 - 746.3212+
b8 - 817.3583+
Retention Time
MsLM_pt2_1
MsLM_pt2_2
MsLM_pt2_3
MsBM_F3_pt2_1
MsBM_F3_pt2_2
MsBM_F3_pt2_3
Replicate

E

GNPESSFNDENLR

Cyp2d11

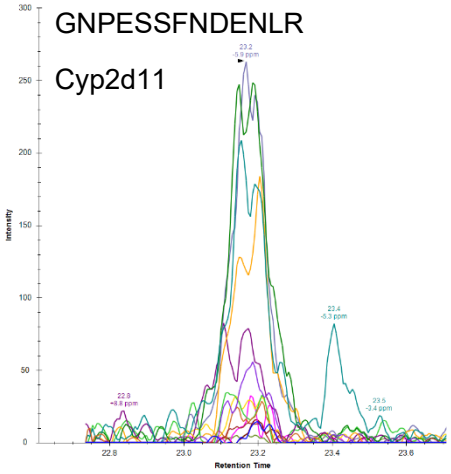

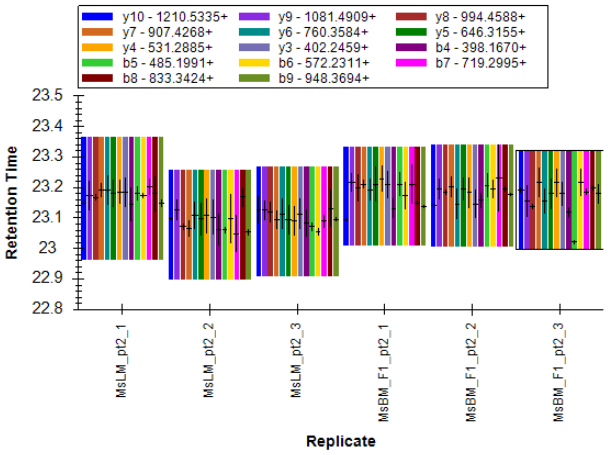

F

DLTDAFLAEVEK

Cyp2d26

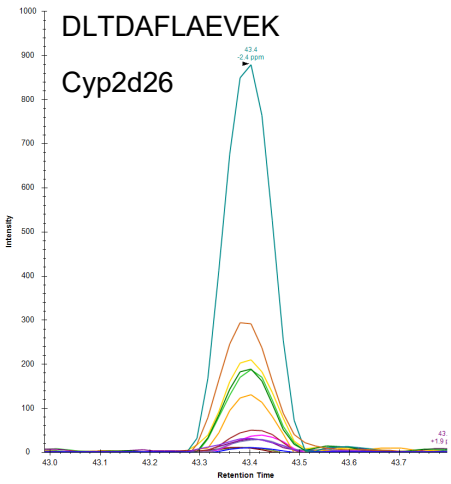

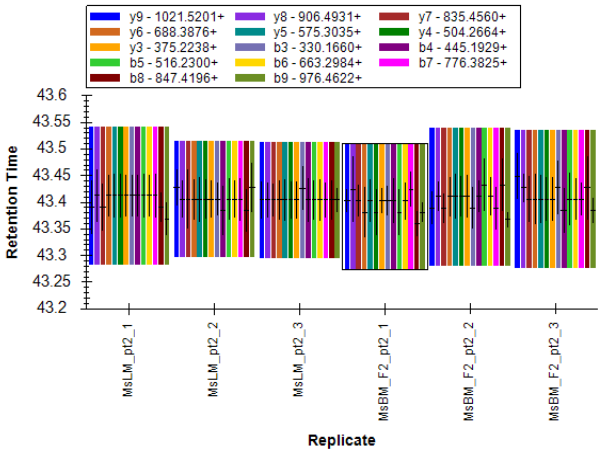

G

TYLQAIGDLNNLFHSR

Cyp4a10

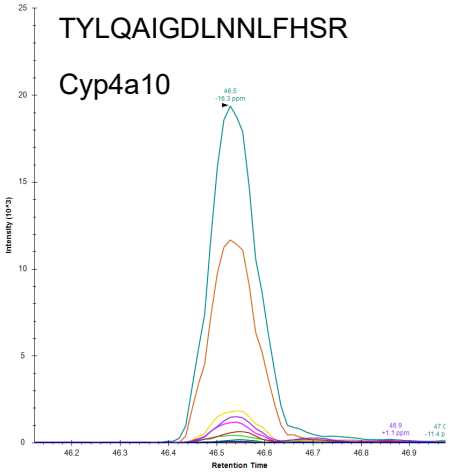

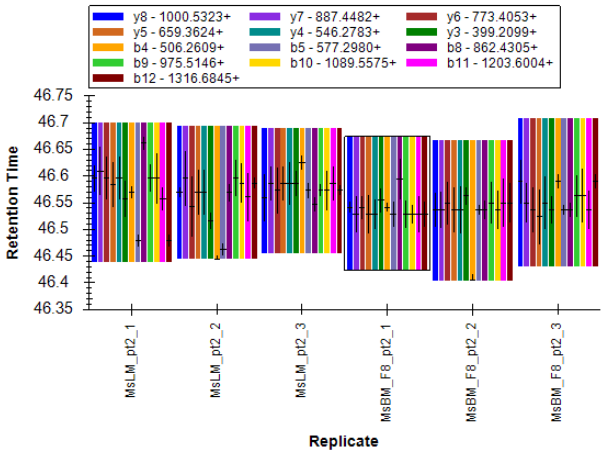

H

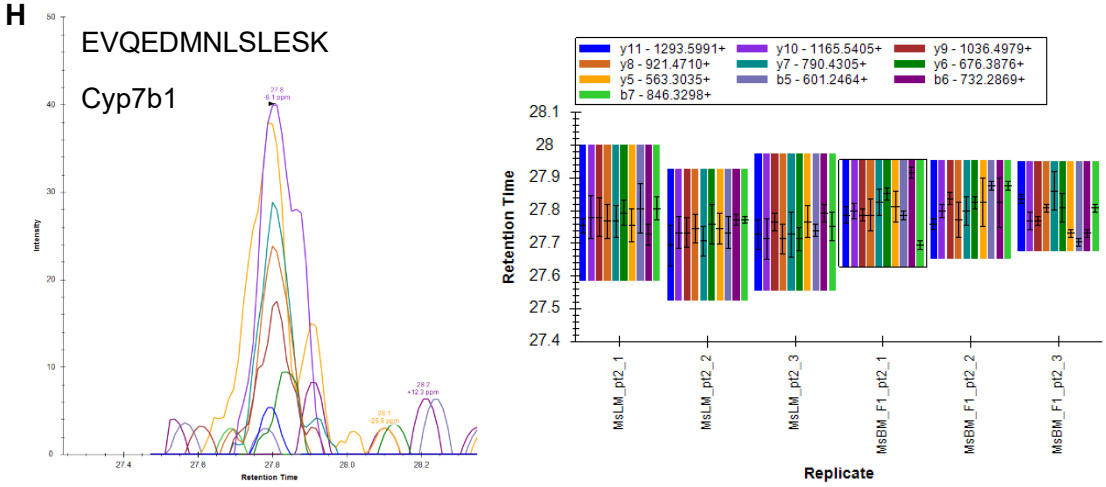
EVQEDMNLSLESK
Cyp7b1
Intensity
Retention Time
y11 - 1293.5991+
y10 - 1165.5405+
y9 - 1036.4979+
y8 - 921.4710+
y7 - 790.4305+
y6 - 676.3876+
y5 - 563.3035+
b5 - 601.2464+
b6 - 732.2869+
b7 - 846.3298+
Retention Time
MsLM_pt2_1
MsLM_pt2_2
MsLM_pt2_3
MsBM_F1_pt2_1
MsBM_F1_pt2_2
MsBM_F1_pt2_3
Replicate

I

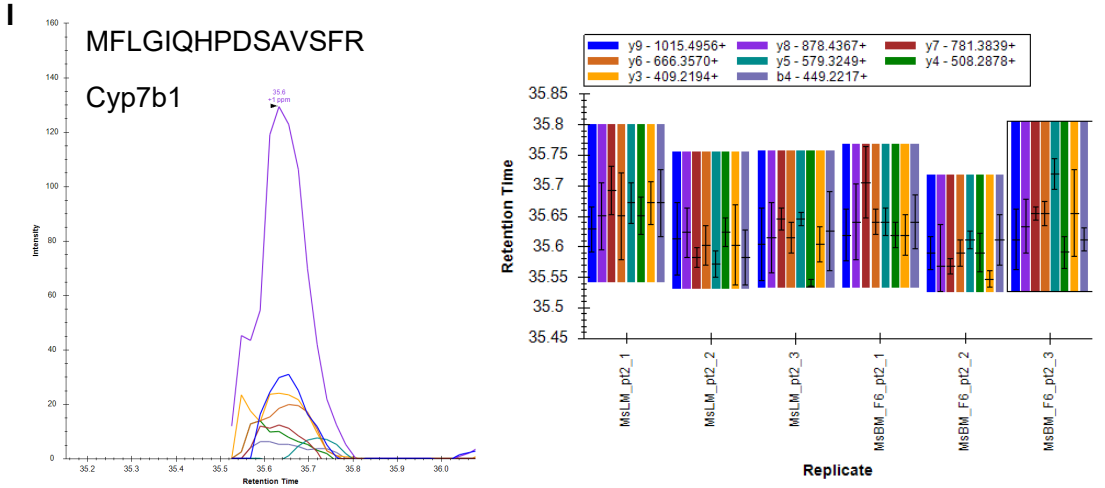
MFLGIQHPDSAVSFR
Cyp7b1
Intensity
Retention Time
y9 - 1015.4956+
y8 - 878.4367+
y7 - 781.3839+
y6 - 666.3570+
y5 - 579.3249+
y4 - 508.2878+
y3 - 409.2194+
b4 - 449.2217+
Retention Time
MsLM_pt2_1
MsLM_pt2_2
MsLM_pt2_3
MsBM_F6_pt2_1
MsBM_F6_pt2_2
MsBM_F6_pt2_3
Replicate

J

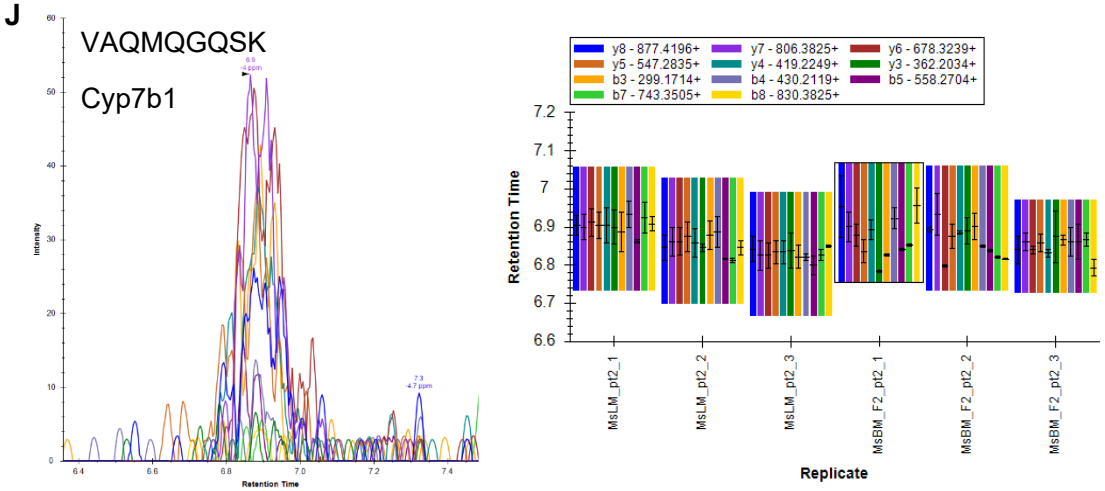
VAQMQGQSK
Cyp7b1
Intensity
Retention Time
y8 - 877.4196+
y7 - 806.3825+
y6 - 678.3239+
y5 - 547.2835+
y4 - 419.2249+
y3 - 362.2034+
b3 - 299.1714+
b4 - 430.2119+
b5 - 558.2704+
b7 - 743.3505+
b8 - 830.3825+
Retention Time
MsLM_pt2_1
MsLM_pt2_2
MsLM_pt2_3
MsBM_F2_pt2_1
MsBM_F2_pt2_2
MsBM_F2_pt2_3
Replicate

Biotransformation of efavirenz and proteomic analysis of P450s and UGTs in mouse, macaque, and human brain-derived *in vitro* systems

Abigail M. Wheeler, Benjamin C. Orsburn, and Namandjé N. Bumpus

Drug Metabolism and Disposition

DMD-AR-2022-001195R1

Supplemental Figure 2. Identification of 14 UGTs in the mouse brain microsomes using a targeted proteomics approach. Mouse brain microsomes (MsBM) were digested and resulting peptides were fractionated before using targeted proteomics to show the presence of Ugt1a1 (A-B), Ugt1a2 (C-D), Ugt1a5 (E), Ugt1a7 (F-H), Ugt1a8 (I), Ugt1a9 (J), Ugt1a10 (K), Ugt2a1 (L-Q), Ugt2a2 (R), Ugt2a3 (S), Ugt2b17 (T), Ugt2b34 (U-V), Ugt2b35 (W), and Ugt3a1 (X). Colored lines in each chromatogram are representative of unique fragment ions. Protein identifications were made using chromatograms (left) and confirmation of consistent retention times and fragment ions (right) with mouse liver microsomes (MsLM). Samples were analyzed in technical triplicate.

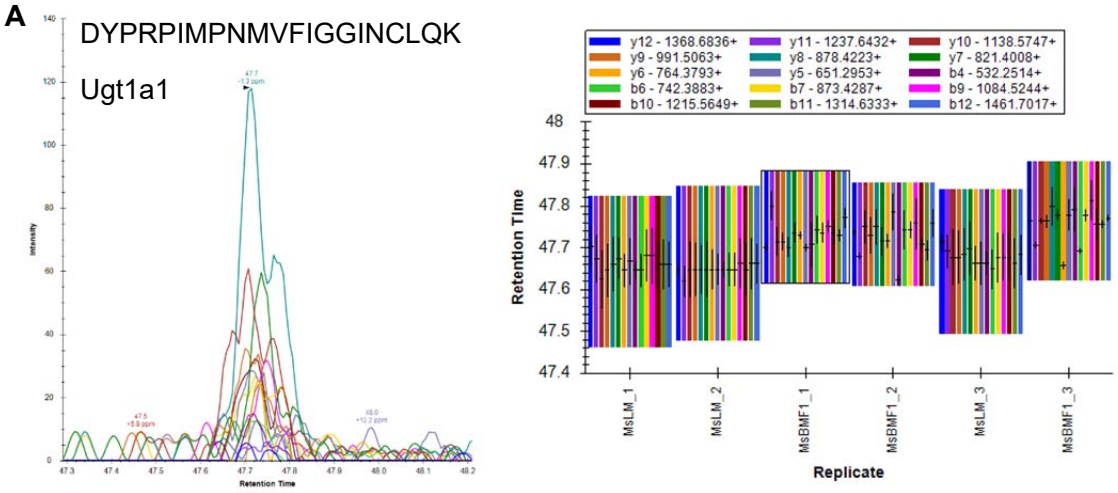

B

EVTVQDLLSPASIWLMR

Ugt1a1

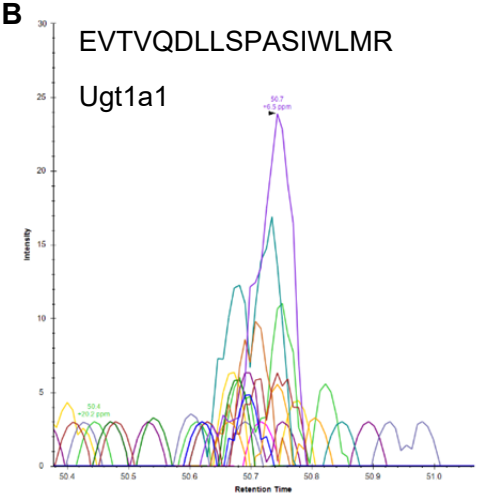

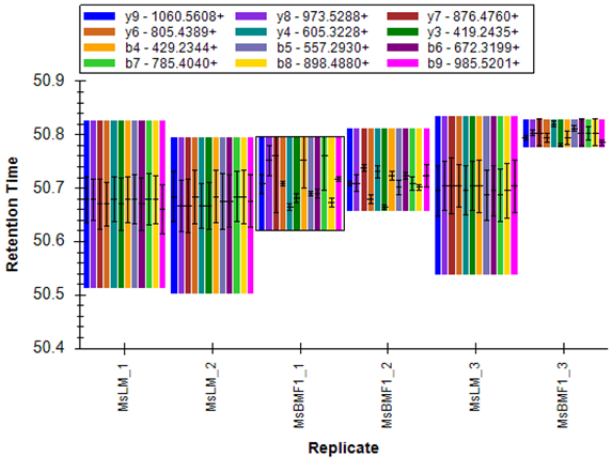

C

EEYQQEILSDIEK

Ugt1a2

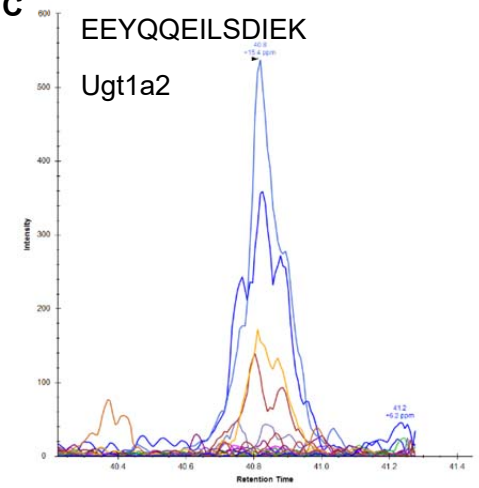

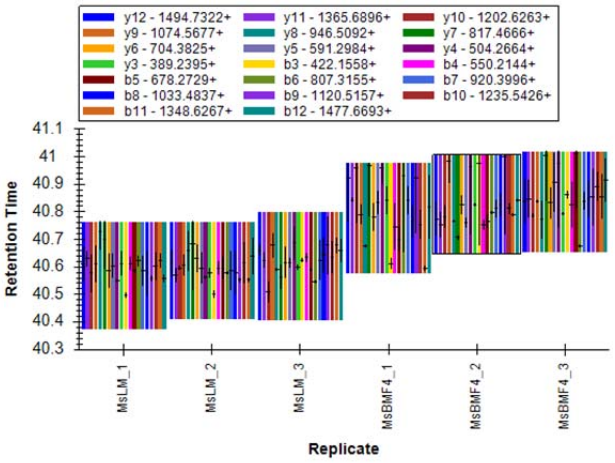

D

ELHARGHQTVVLASEVTVHIK

Ugt1a2

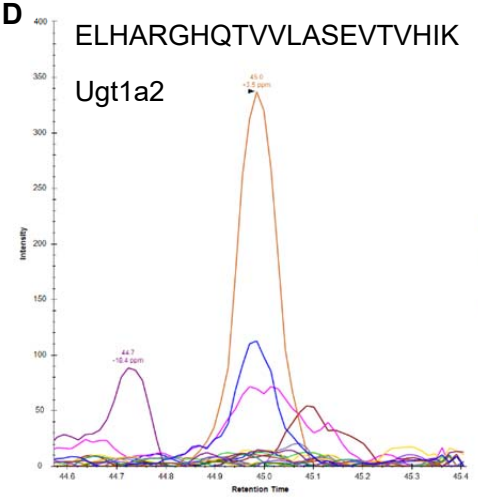

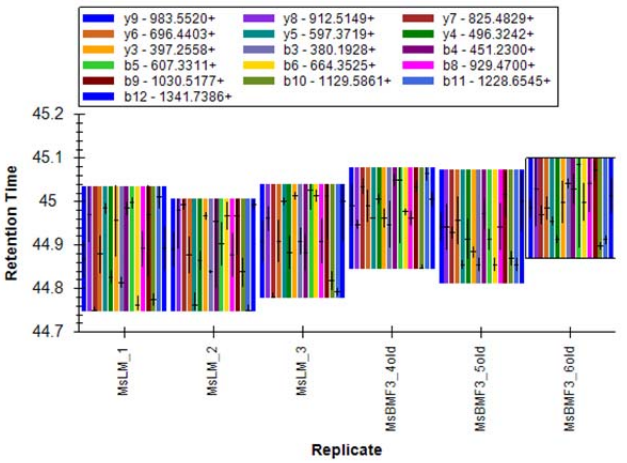

E

IKEEDFFTFK

Ugt1a5

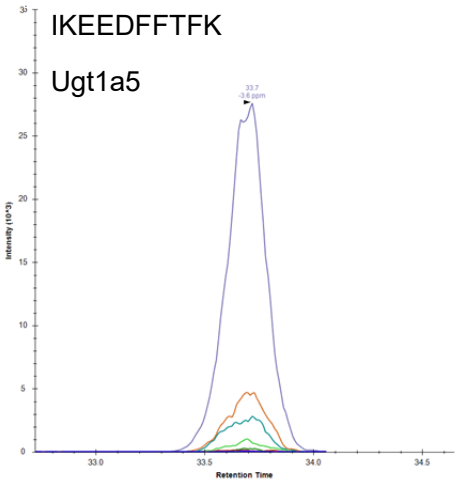

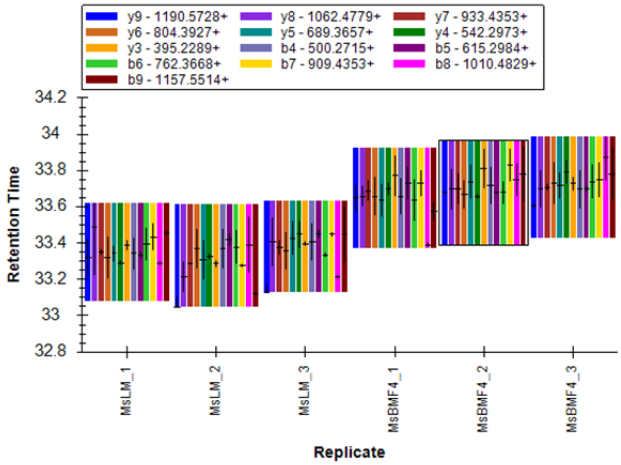

F

EFKIFIDAQWK

Ugt1a7

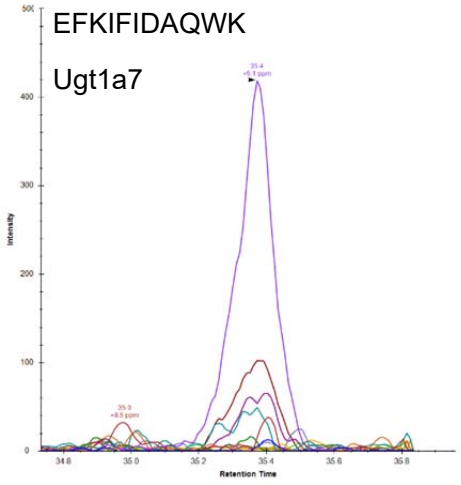

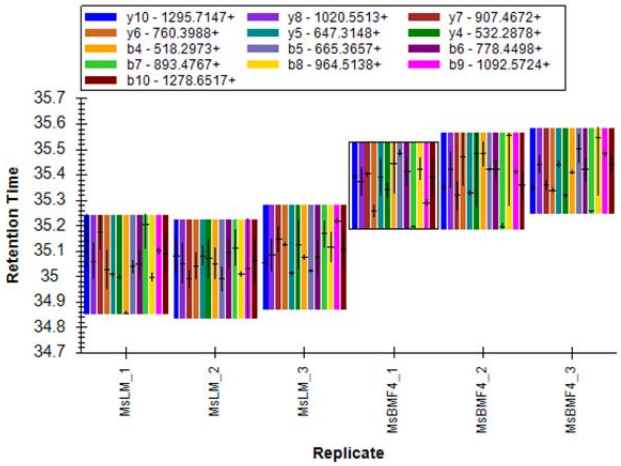

G

SQQEGGILPLLDSPAK

Ugt1a7

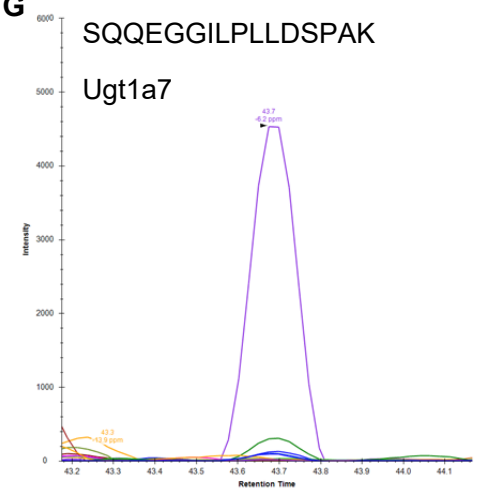

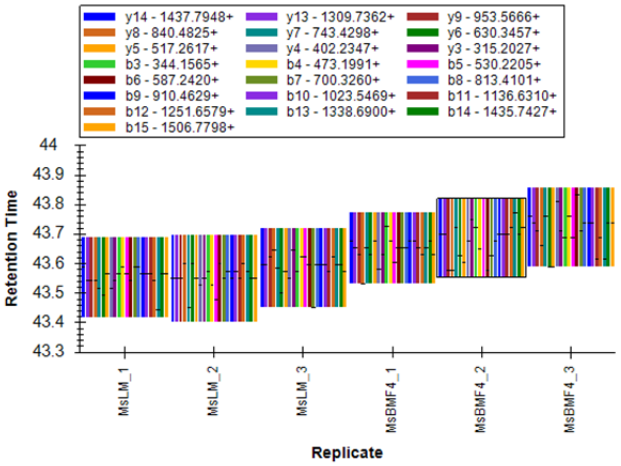

H

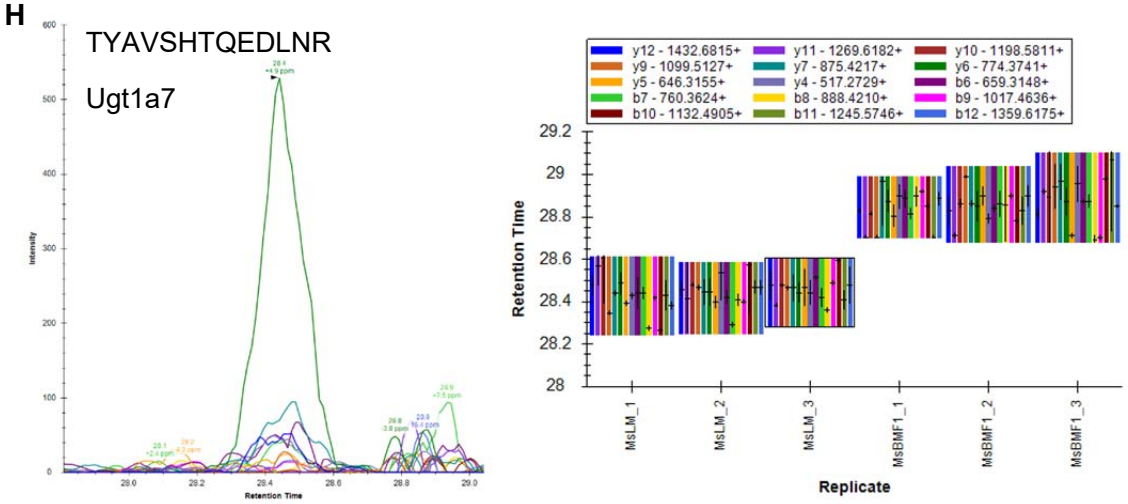
TYAVSHTQEDLNR
Ugt1a7
Intensity
Retention Time
y12 - 1432.6815+
y11 - 1269.6182+
y10 - 1198.5811+
y9 - 1099.5127+
y7 - 875.4217+
y6 - 774.3741+
y5 - 646.3155+
y4 - 517.2729+
b6 - 659.3148+
b7 - 760.3624+
b8 - 888.4210+
b9 - 1017.4636+
b10 - 1132.4905+
b11 - 1245.5746+
b12 - 1359.6175+
Retention Time
MsLM_1
MsLM_2
MsLM_3
MsBMF1_1
MsBMF1_2
MsBMF1_3
Replicate

I

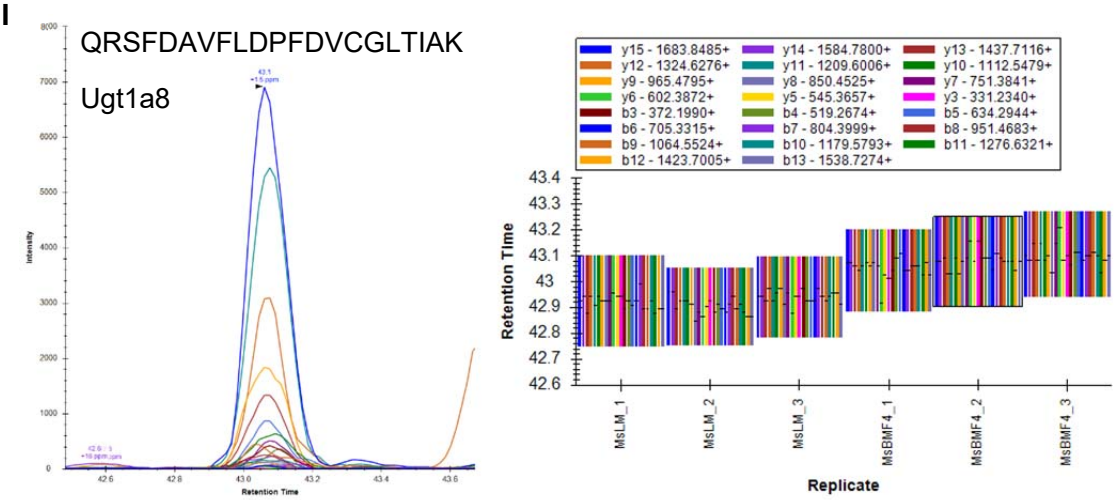
QRSFDAVFLDPFDVCGLTIAK
Ugt1a8
Intensity
Retention Time
y15 - 1683.8485+
y14 - 1584.7800+
y13 - 1437.7116+
y12 - 1324.6276+
y11 - 1209.6006+
y10 - 1112.5479+
y9 - 965.4795+
y8 - 850.4525+
y7 - 751.3841+
y6 - 602.3872+
y5 - 545.3657+
y3 - 331.2340+
b3 - 372.1990+
b4 - 519.2674+
b5 - 634.2944+
b6 - 705.3315+
b7 - 804.3999+
b8 - 951.4683+
b9 - 1064.5524+
b10 - 1179.5793+
b11 - 1276.6321+
b12 - 1423.7005+
b13 - 1538.7274+
Retention Time
MsLM_1
MsLM_2
MsLM_3
MsBMF4_1
MsBMF4_2
MsBMF4_3
Replicate

J

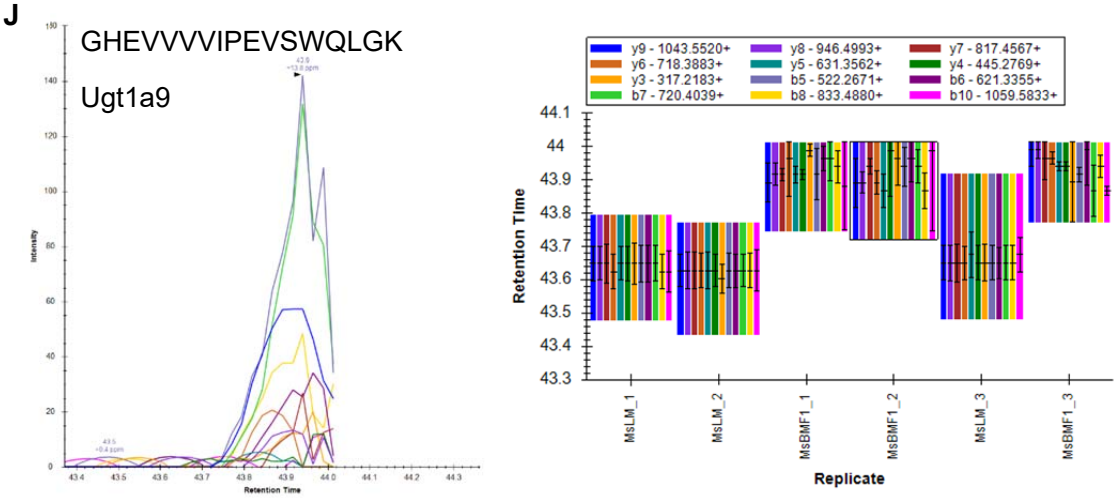
GHEVVVVIPEVSWQLGK
Ugt1a9
Intensity
Retention Time
y9 - 1043.5520+
y8 - 946.4993+
y7 - 817.4567+
y6 - 718.3883+
y5 - 631.3562+
y4 - 445.2769+
y3 - 317.2183+
b5 - 522.2671+
b6 - 621.3355+
b7 - 720.4039+
b8 - 833.4880+
b10 - 1059.5833+
Retention Time
MsLM_1
MsLM_2
MsBMF1_1
MsBMF1_2
MsLM_3
MsBMF1_3
Replicate

K

TYSVSHTLEDLDR

Ugt1a10

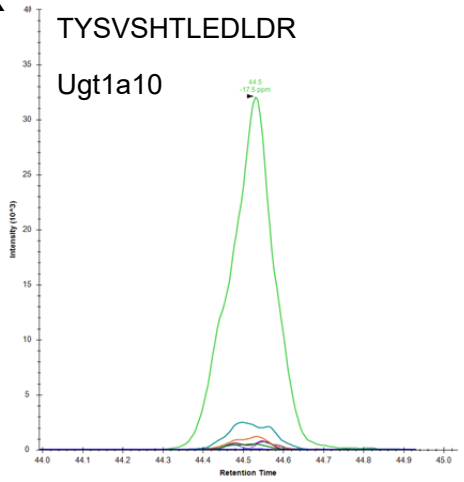

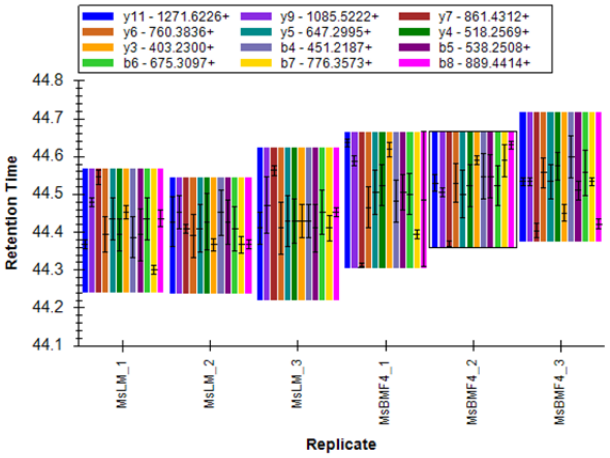

L

ALGRPTTLCETMGK

Ugt2a1

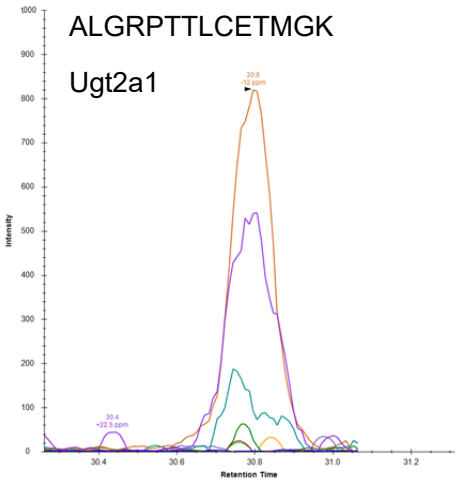

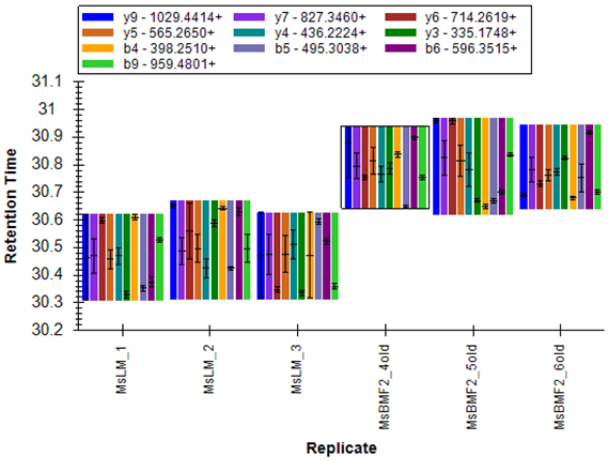

M

EKIESVIK

Ugt2a1

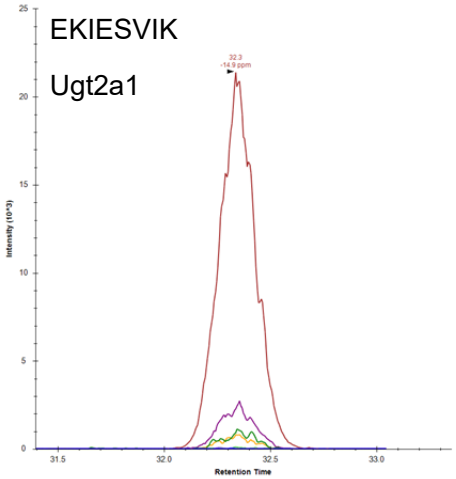

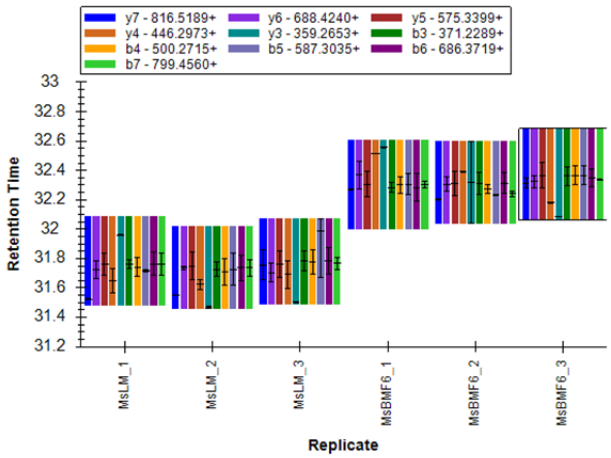

N

EMAKVIEEFHLVSR

Ugt2a1

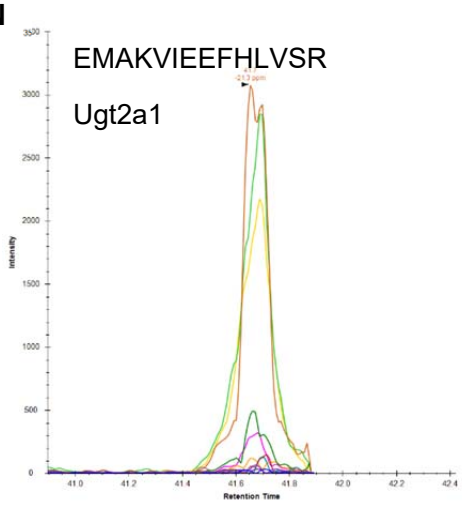

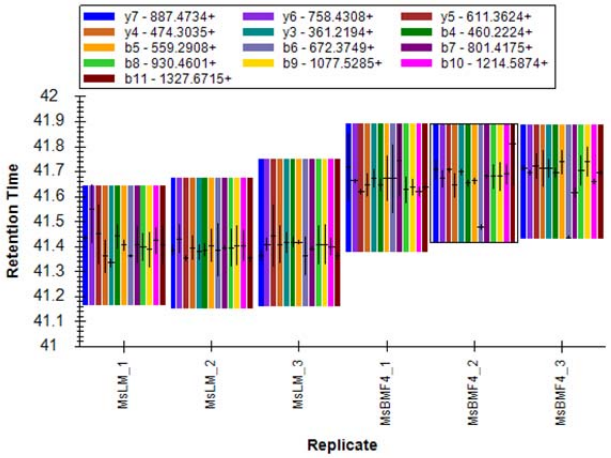

O

FSPASTVEK

Ugt2a1

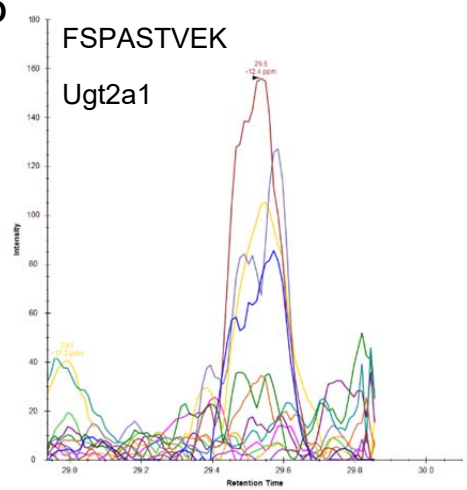

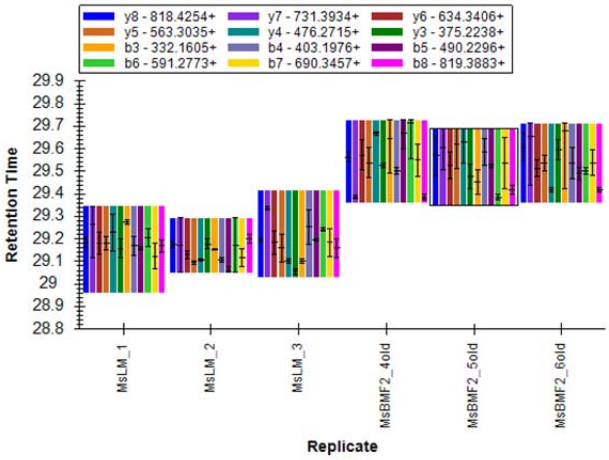

P

GICDGLVK

Ugt2a1

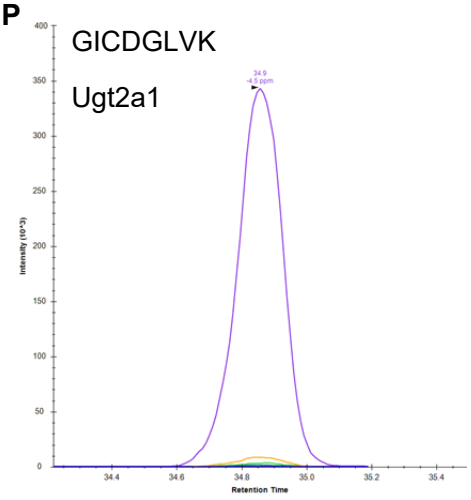

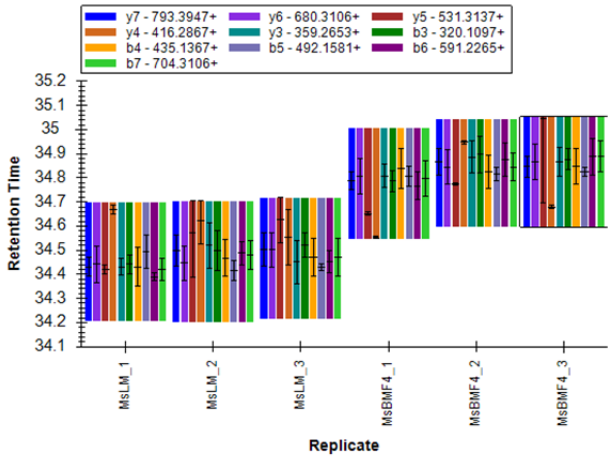

Q

LGIPFIYSLR

Ugt2a1

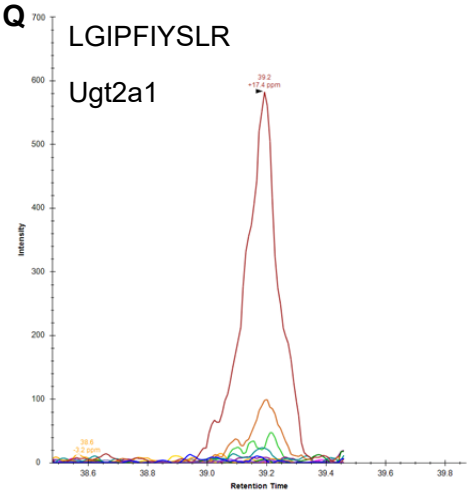

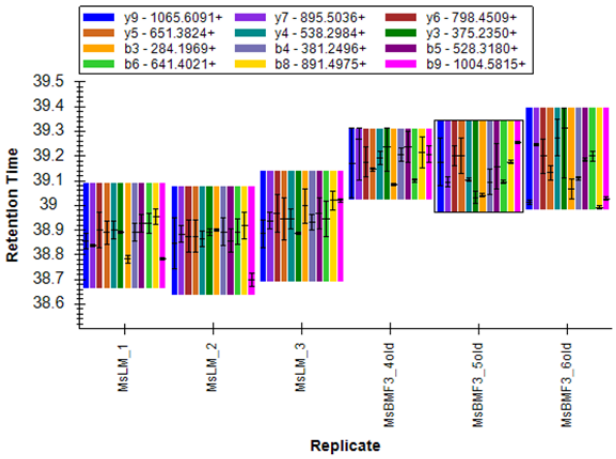

S

VSISTMTSTDLLSAVR

Ugt2a3

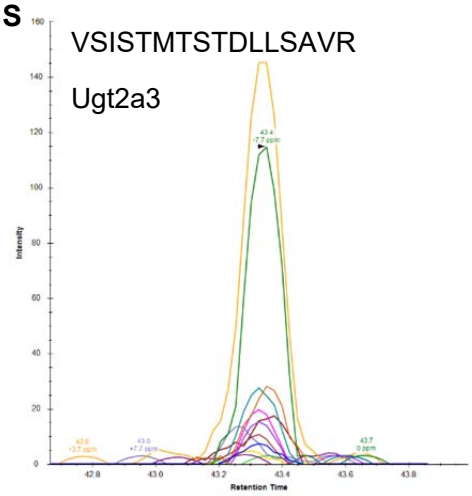

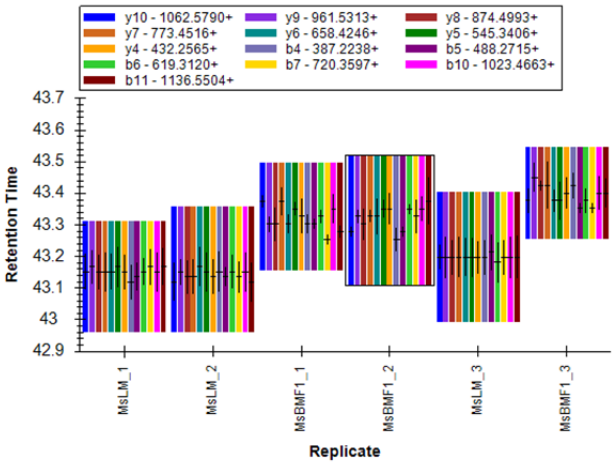

R

IPAPISYVPAALSELTDQMSFGER

Ugt2a2

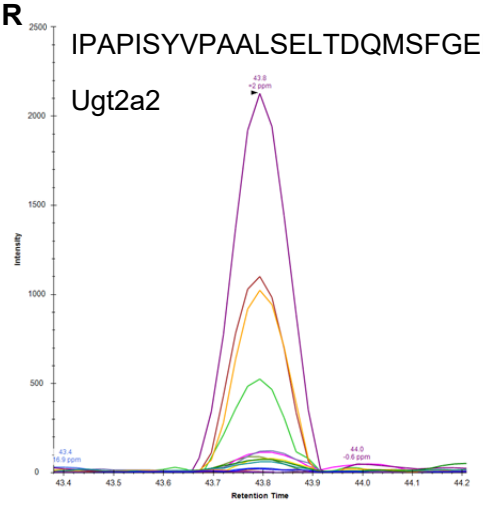

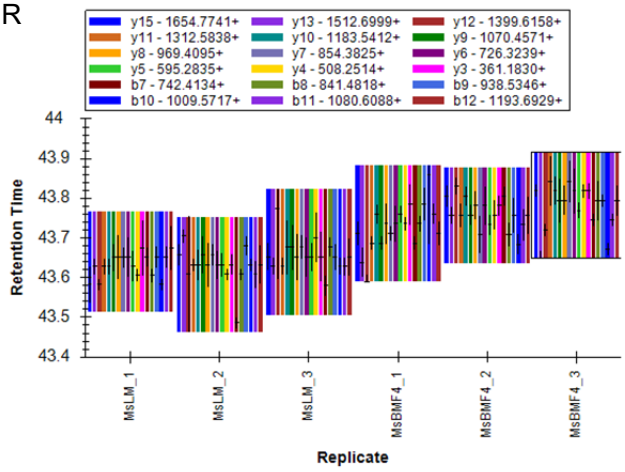

T

SDVLNALEEVIENPFYK

Ugt2b17

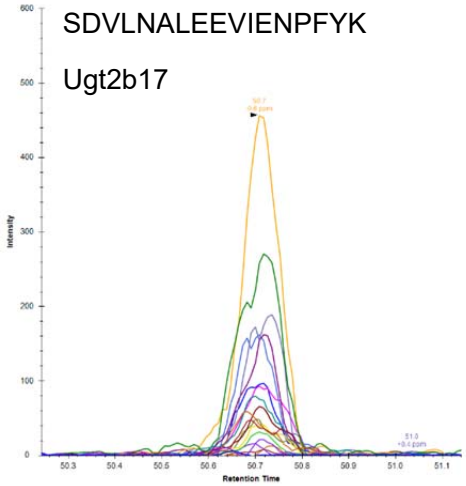

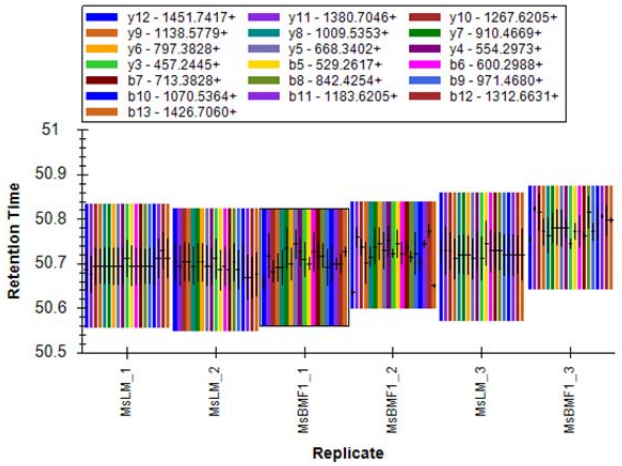

U

LDFLTMSSTDHLTALK

Ugt2b34

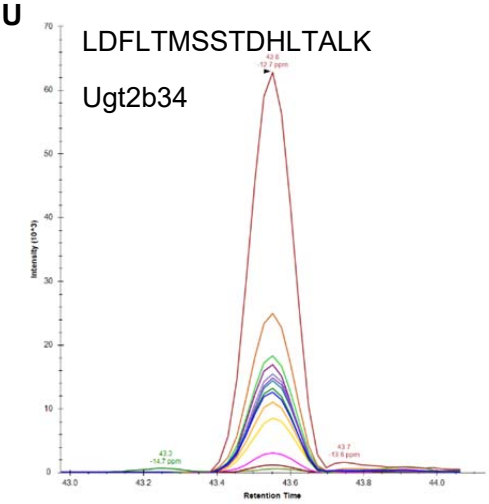

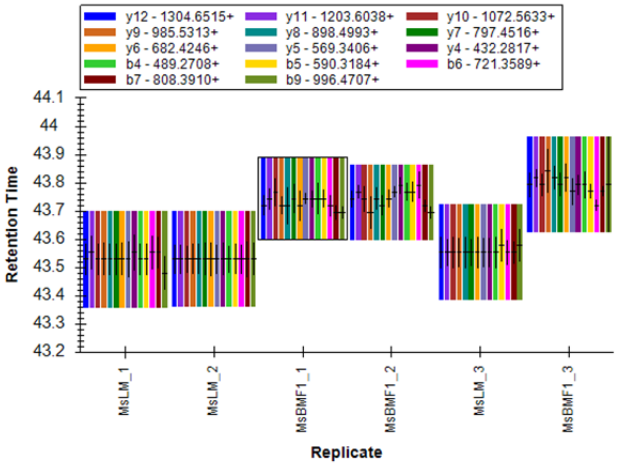

V

SRFDVILADPFIPCGDLLAEVLK

Ugt2b34

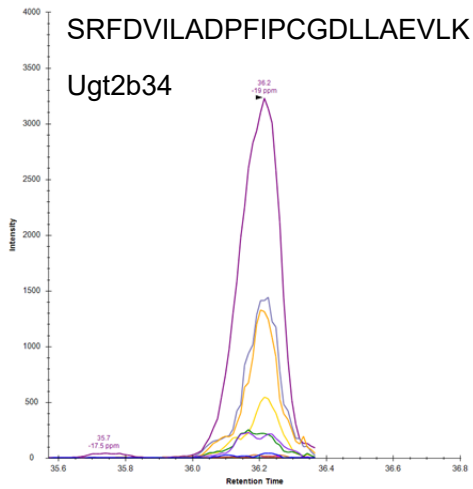

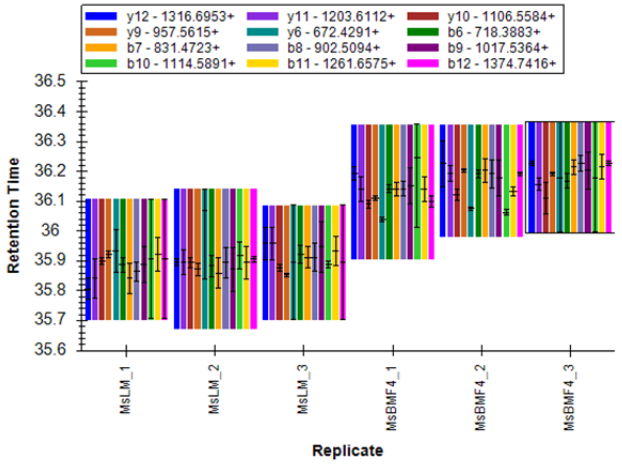

W

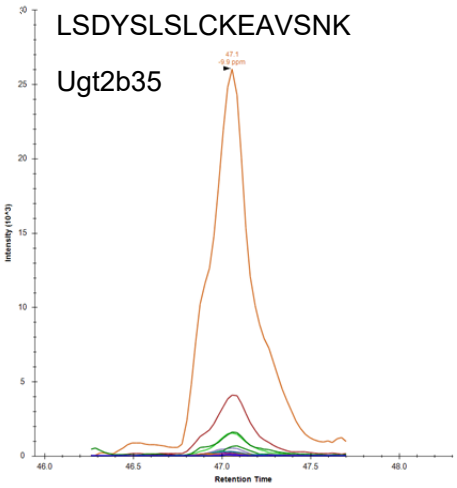
LSDYSLSLCKEAVSNK
Ugt2b35
Intensity (10^3)
Retention Time

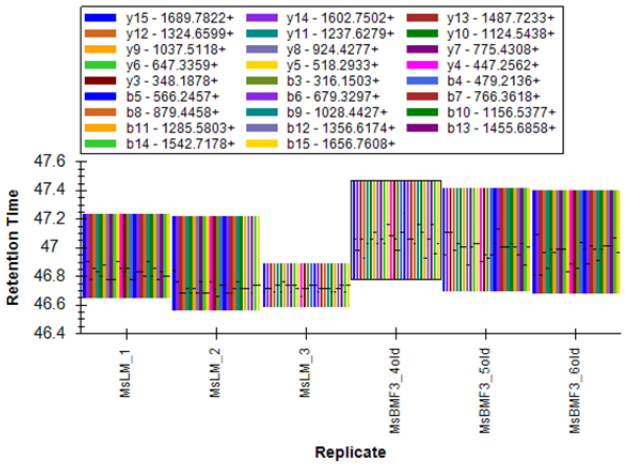
y15 - 1689.7822+
y14 - 1602.7502+
y13 - 1487.7233+
y12 - 1324.6599+
y11 - 1237.6279+
y10 - 1124.5438+
y9 - 1037.5118+
y8 - 924.4277+
y7 - 775.4308+
y6 - 647.3359+
y5 - 518.2933+
y4 - 447.2562+
y3 - 348.1878+
b3 - 316.1503+
b4 - 479.2136+
b5 - 566.2457+
b6 - 679.3297+
b7 - 766.3618+
b8 - 879.4458+
b9 - 1028.4427+
b10 - 1156.5377+
b11 - 1285.5803+
b12 - 1356.6174+
b13 - 1455.6858+
b14 - 1542.7178+
b15 - 1656.7608+
Retention Time
MsLM_1
MsLM_2
MsLM_3
MsBMF3_4old
MsBMF3_5old
MsBMF3_6old
Replicate

X

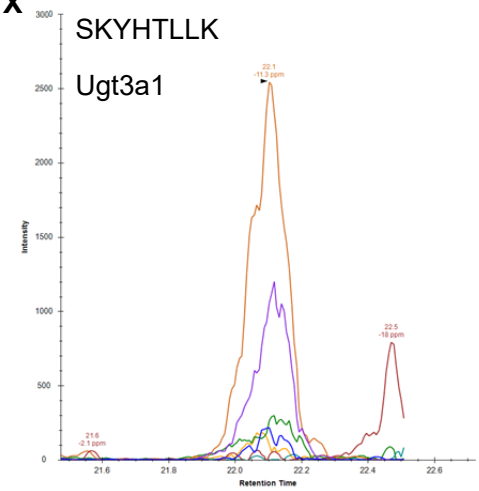
SKYHTLLK
Ugt3a1
Intensity
Retention Time

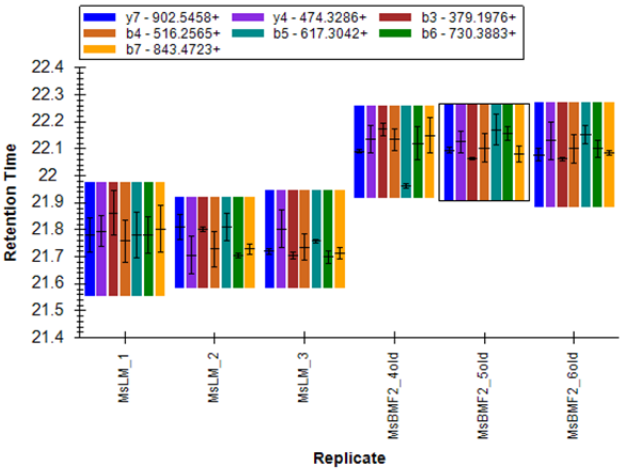
y7 - 902.5458+
y4 - 474.3286+
b3 - 379.1976+
b4 - 516.2565+
b5 - 617.3042+
b6 - 730.3883+
b7 - 843.4723+
Retention Time
MsLM_1
MsLM_2
MsLM_3
MsBMF2_4old
MsBMF2_5old
MsBMF2_6old
Replicate

Biotransformation of efavirenz and proteomic analysis of P450s and UGTs in mouse, macaque, and human brain-derived *in vitro* systems

Abigail M. Wheeler, Benjamin C. Orsburn, and Namandjé N. Bumpus

Drug Metabolism and Disposition

DMD-AR-2022-001195R1

Supplemental Figure 3. Identification of 15 P450s in the cynomolgus macaque brain microsomes using a targeted proteomics approach. Cynomolgus macaque brain microsomes (MkBM) were digested and resulting peptides were fractionated before using targeted proteomics to show the presence of CYP1A1 (A), CYP1A2 (B-C), CYP1B1 (D), CYP2E1 (E), CYP2F1 (F), CYP2R1 (G), CYP2U1 (H), CYP2W1 (I), CYP4F12 (J), CYP4F22 (K), CYP11B2 (L), CYP20A1 (M-O), CYP21A2 (P), CYP27A1 (Q), and CYP27C1 (R). Protein identifications were made using chromatograms (left) and confirmation of consistent retention times and fragment ions (right) with cynomolgus macaque liver microsomes (MkLM). Samples were analyzed in technical duplicates.

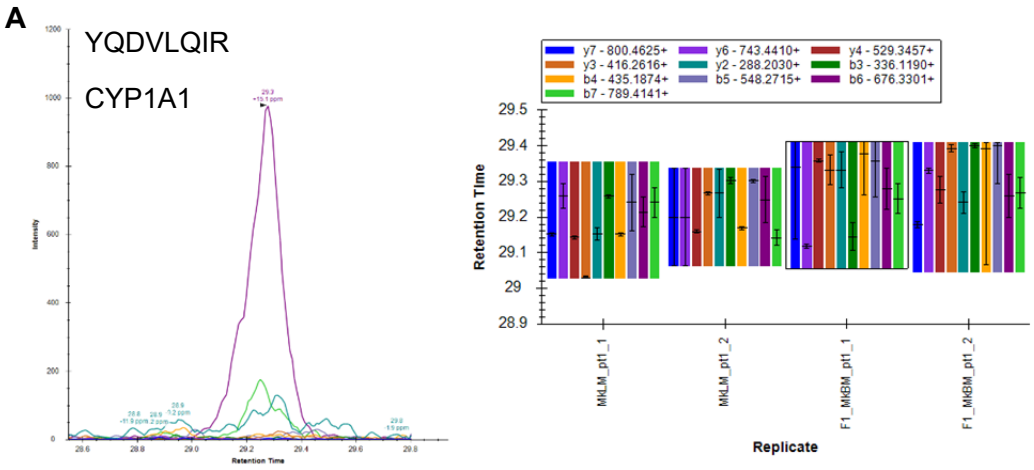

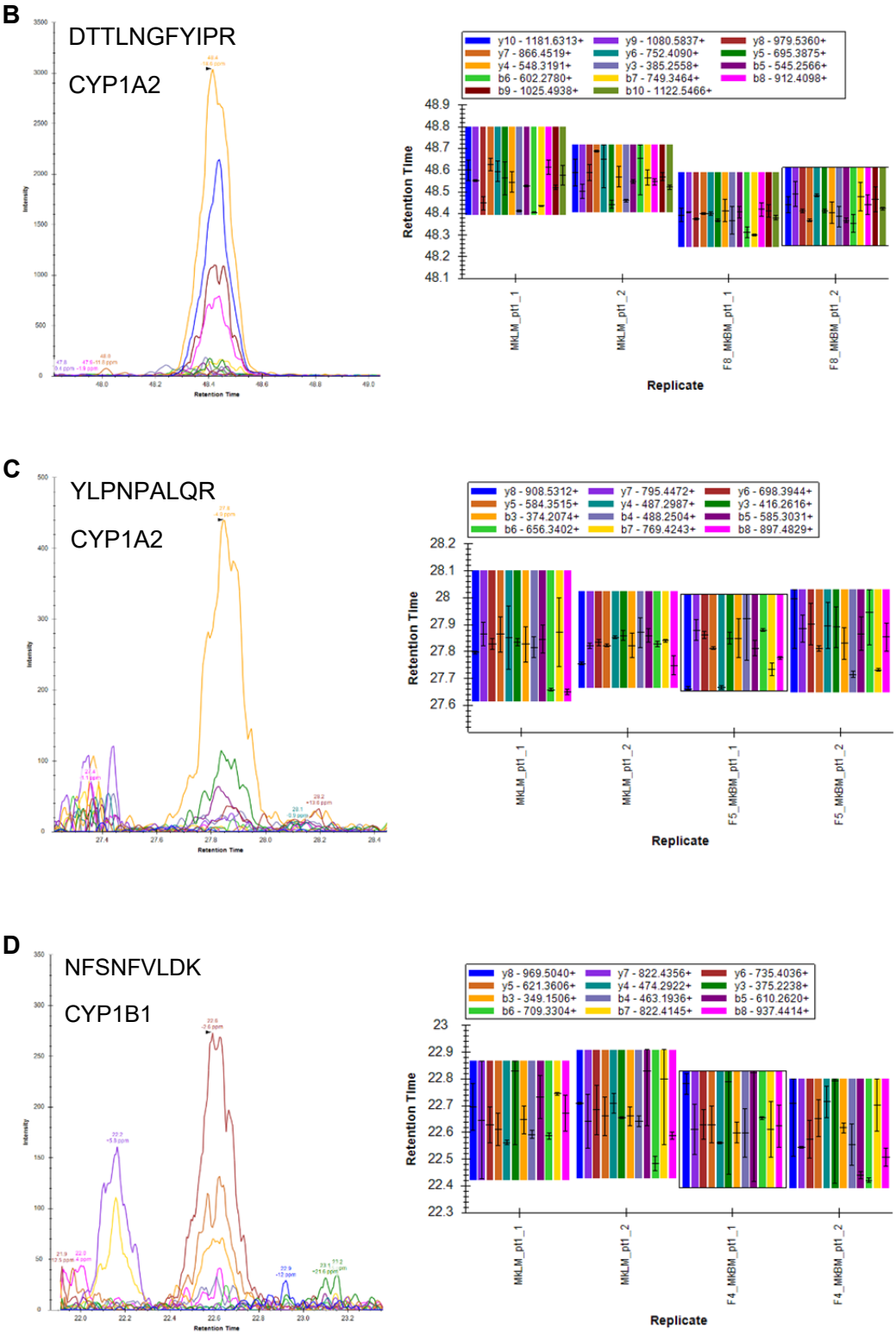
B
DTTLNGFYIPR
CYP1A2
y10 - 1181.6313+
y9 - 1080.5837+
y8 - 979.5360+
y7 - 866.4519+
y6 - 752.4090+
y5 - 695.3875+
y4 - 548.3191+
y3 - 385.2558+
b5 - 545.2566+
b6 - 602.2780+
b7 - 749.3464+
b8 - 912.4098+
b9 - 1025.4938+
b10 - 1122.5466+
Retention Time
Replicate
MKLM_pt1_1
MKLM_pt1_2
F8_MKBM_pt1_1
F8_MKBM_pt1_2
C
YLPNPALQR
CYP1A2
y8 - 908.5312+
y7 - 795.4472+
y6 - 698.3944+
y5 - 584.3515+
y4 - 487.2987+
y3 - 416.2616+
b3 - 374.2074+
b4 - 488.2504+
b5 - 585.3031+
b6 - 656.3402+
b7 - 769.4243+
b8 - 897.4829+
Retention Time
Replicate
MKLM_pt1_1
MKLM_pt1_2
F5_MKBM_pt1_1
F5_MKBM_pt1_2
D
NFSNFVLDK
CYP1B1
y8 - 969.5040+
y7 - 822.4356+
y6 - 735.4036+
y5 - 621.3606+
y4 - 474.2922+
y3 - 375.2238+
b3 - 349.1506+
b4 - 463.1936+
b5 - 610.2620+
b6 - 709.3304+
b7 - 822.4145+
b8 - 937.4414+
Retention Time
Replicate
MKLM_pt1_1
MKLM_pt1_2
F4_MKBM_pt1_1
F4_MKBM_pt1_2

E

GTTVIVPTLDSVLYDNQEFPDPEK

CYP2E1

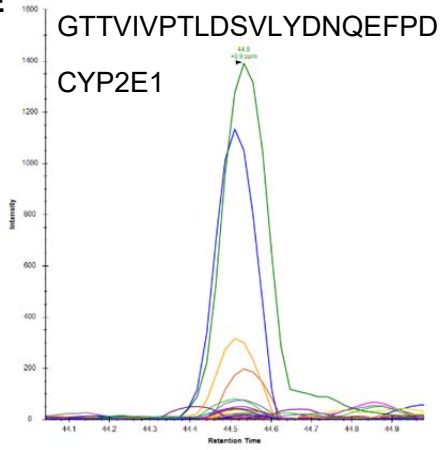

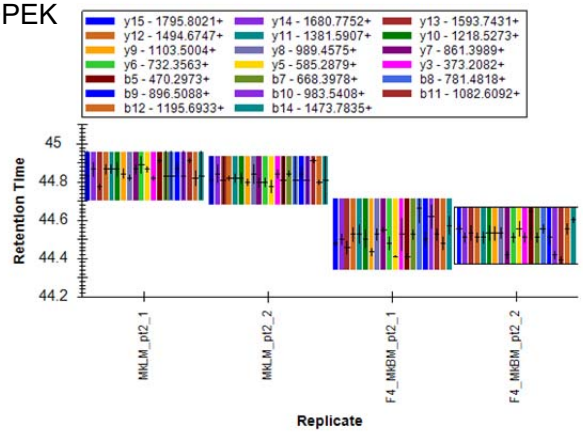

F

ILEEGSFLLAELR

CYP2F1

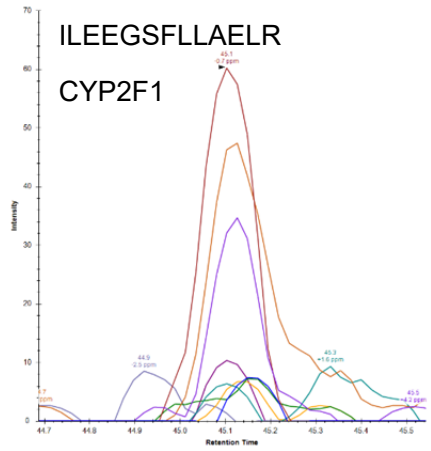

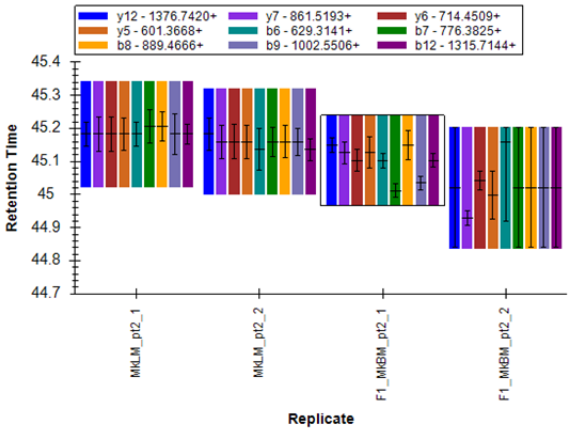

G

GTTVITNLYSVHFDEK

CYP2R1

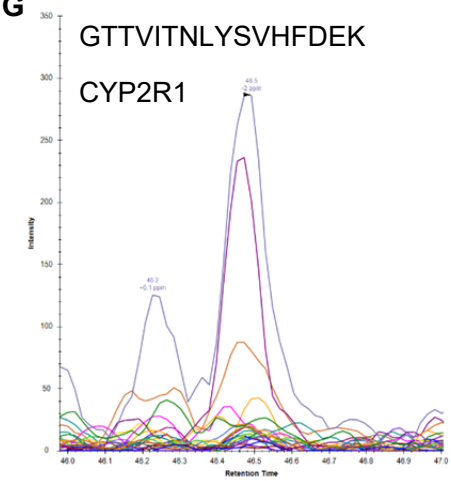

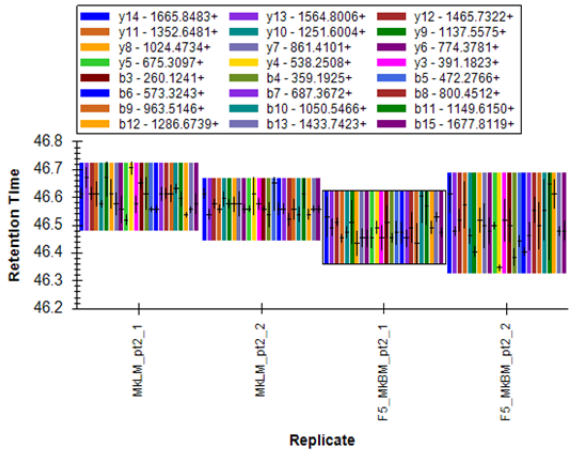

H

EALVQQAEVFSDRPR

CYP2U1

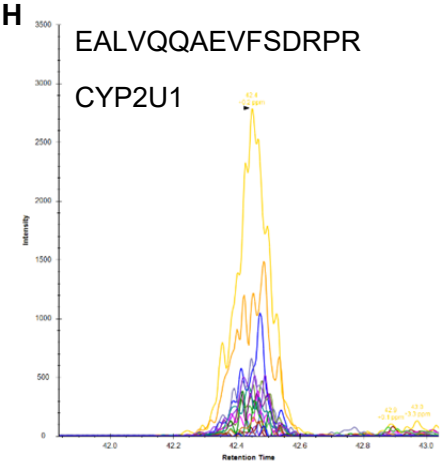

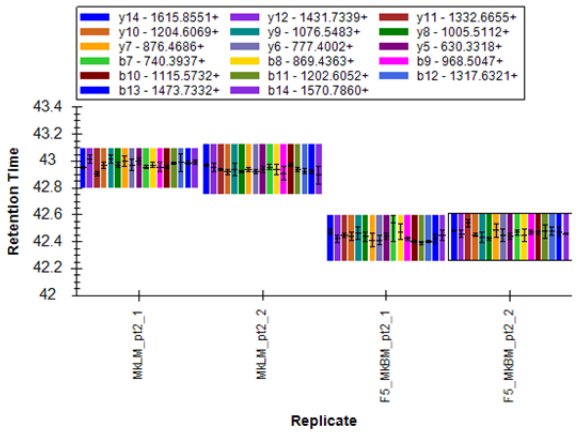

I

GGGIFFSSFAR

CYP2W1

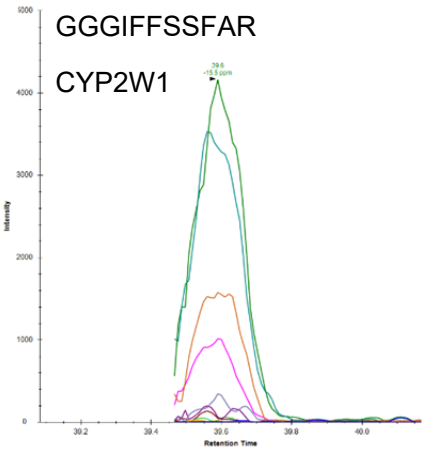

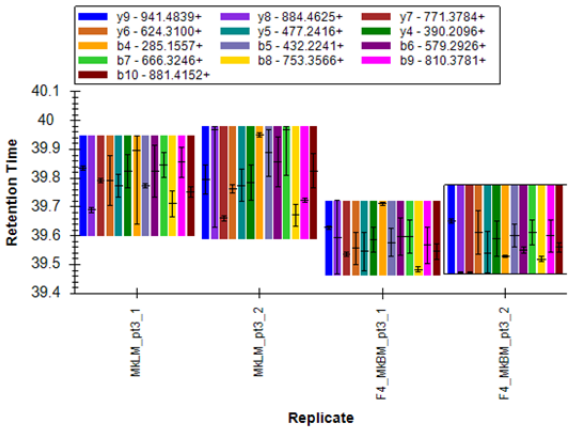

J

SITNASSAIAPK

CYP4F12

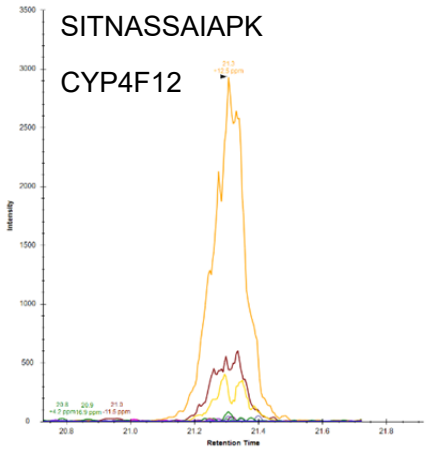

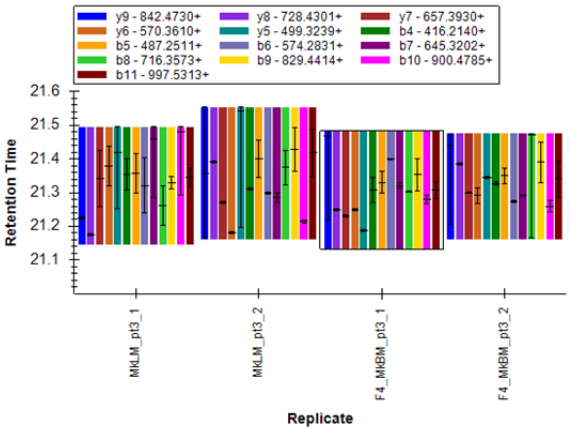

K

SPLAYVPFSAGPR

CYP4F22

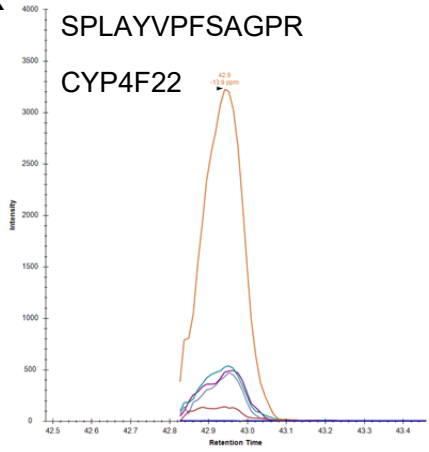

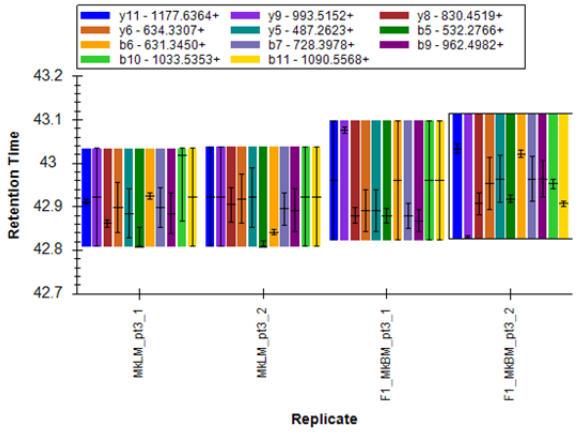

L

EQGYEHLHLEVHQTFQELGOIFR

CYP11B2

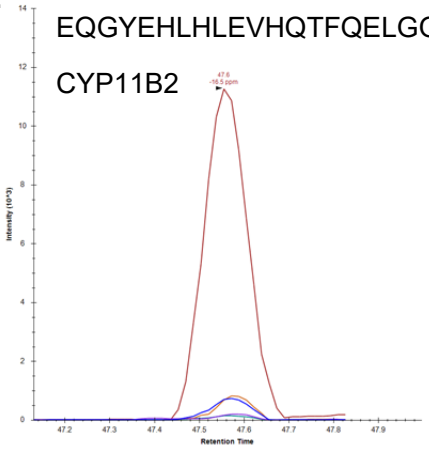

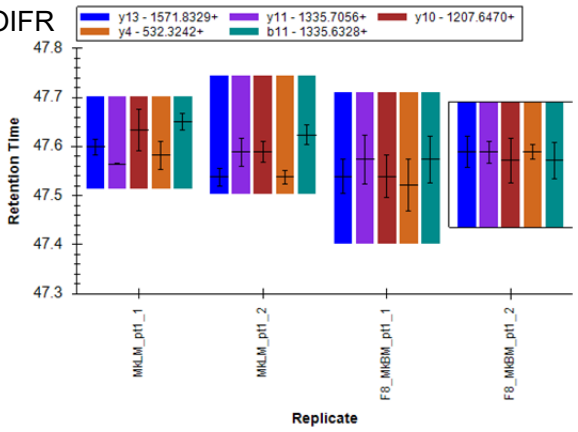

M

EEAWITVSK

CYP20A1

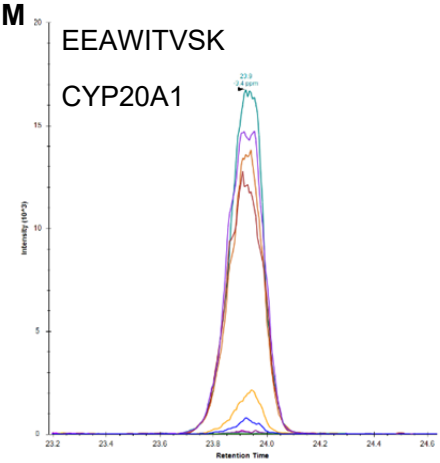

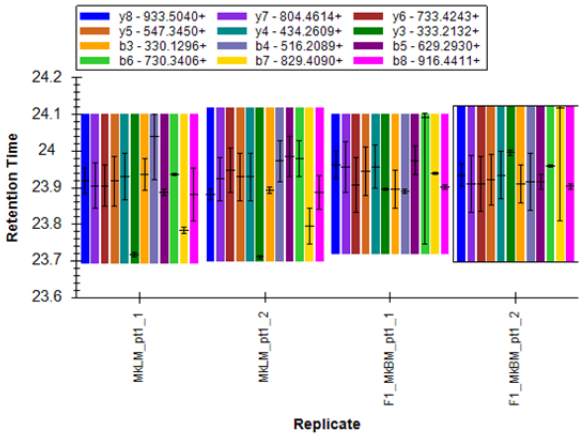

N

LYEEINQVFGNGPVTPEK

CYP20A1

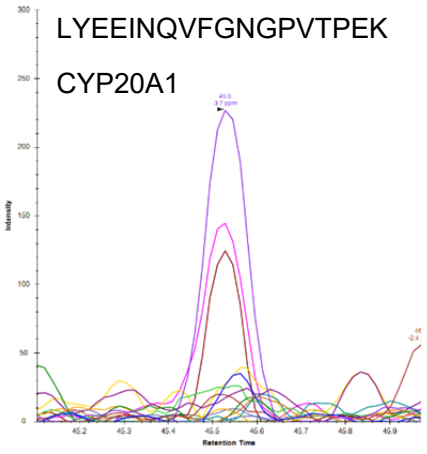

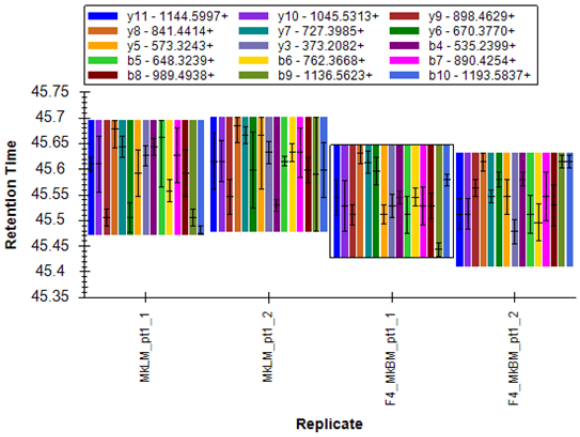

O

TFSSLGFSGTR

CYP20A1

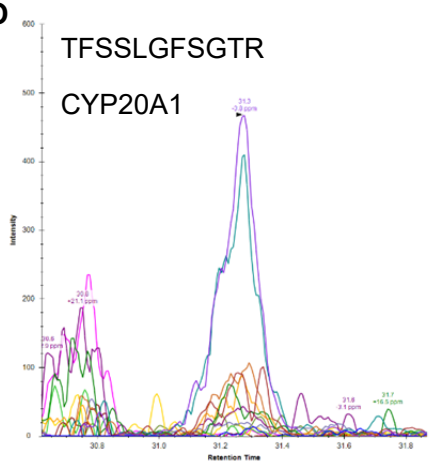

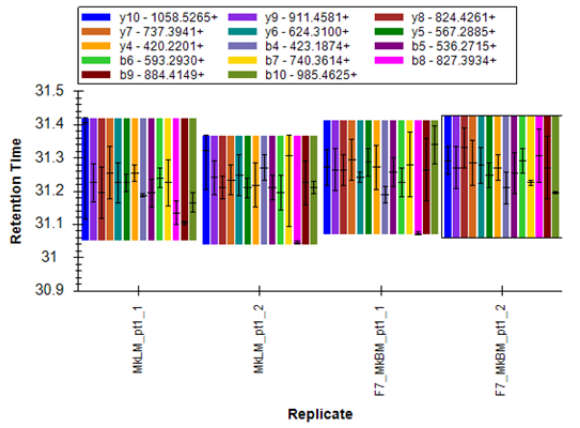

P

WADFAGRPEPLTYK

CYP21A2

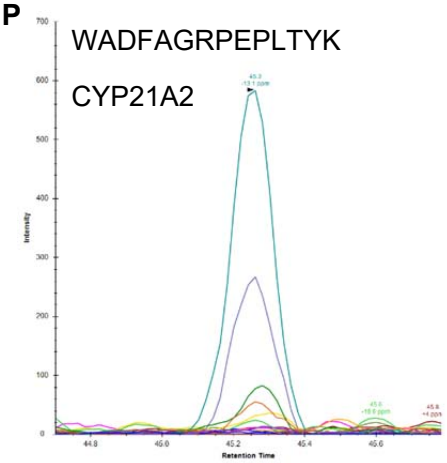

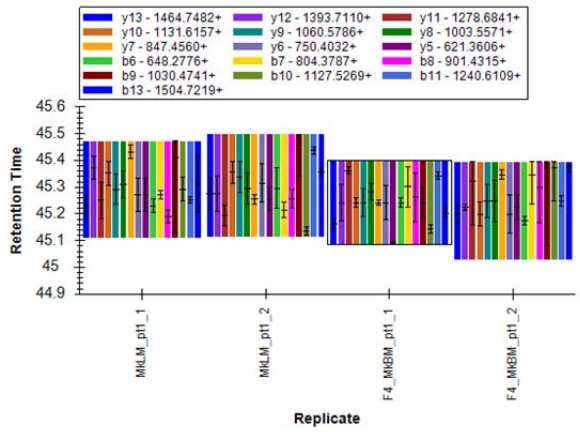

Q

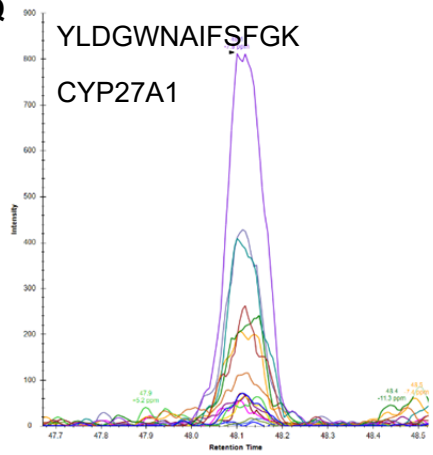
YLDGWNAIFSFGK
CYP27A1
Intensity
Retention Time

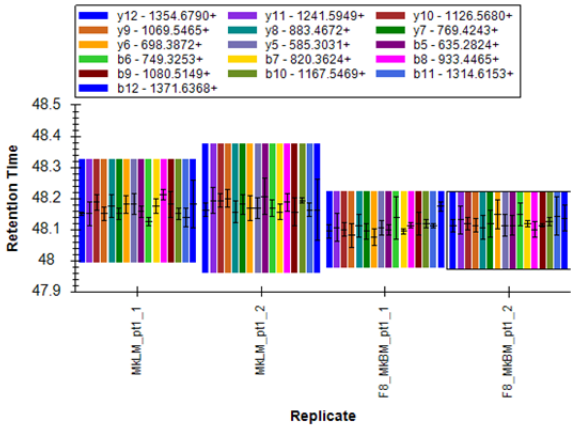
y12 - 1354.6790+
y11 - 1241.5949+
y10 - 1126.5680+
y9 - 1069.5465+
y8 - 883.4672+
y7 - 769.4243+
y6 - 698.3872+
y5 - 585.3031+
b5 - 635.2824+
b6 - 749.3253+
b7 - 820.3624+
b8 - 933.4465+
b9 - 1080.5149+
b10 - 1167.5469+
b11 - 1314.6153+
b12 - 1371.6368+
Retention Time
MKLM_pt1_1
MKLM_pt1_2
F8_MKBM_pt1_1
F8_MKBM_pt1_2
Replicate

R

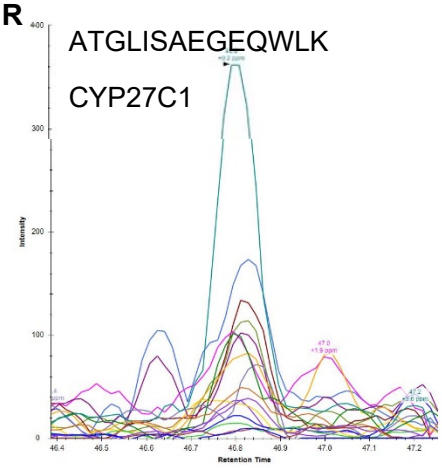
ATGLISAEGEQWLK
CYP27C1
Intensity
Retention Time

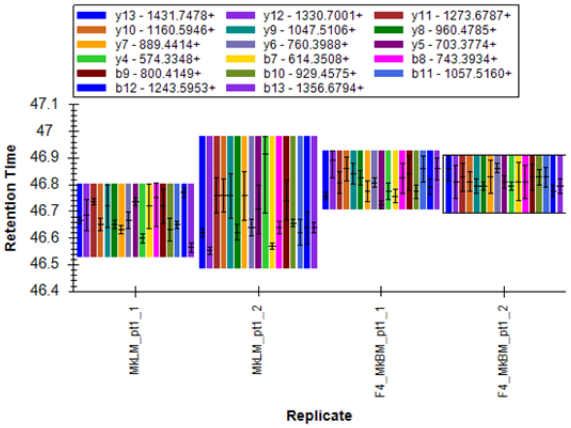
y13 - 1431.7478+
y12 - 1330.7001+
y11 - 1273.6787+
y10 - 1160.5946+
y9 - 1047.5106+
y8 - 960.4785+
y7 - 889.4414+
y6 - 760.3988+
y5 - 703.3774+
y4 - 574.3348+
b7 - 614.3508+
b8 - 743.3934+
b9 - 800.4149+
b10 - 929.4575+
b11 - 1057.5160+
b12 - 1243.5953+
b13 - 1356.6794+
Retention Time
MKLM_pt1_1
MKLM_pt1_2
F4_MKBM_pt1_1
F4_MKBM_pt1_2
Replicate

Biotransformation of efavirenz and proteomic analysis of P450s and UGTs in mouse, macaque, and human brain-derived *in vitro* systems

Abigail M. Wheeler, Benjamin C. Orsburn, and Namandjé N. Bumpus

Drug Metabolism and Disposition

DMD-AR-2022-001195R1

Supplemental Figure 4. Identification of 4 UGTs in the cynomolgus macaque brain microsomes using a targeted proteomics approach. Cynomolgus macaque brain microsomes (MkBM) were digested and resulting peptides were fractionated before using targeted proteomics to show the presence of UGT1A9 (A), UGT1A10 (B), UGT2B9 (C), and UGT2B20 (D). Protein identifications were made using chromatograms (left) and confirmation of consistent retention times and fragment ions (right) with cynomolgus macaque liver microsomes (MkLM). Samples were analyzed in technical triplicate.

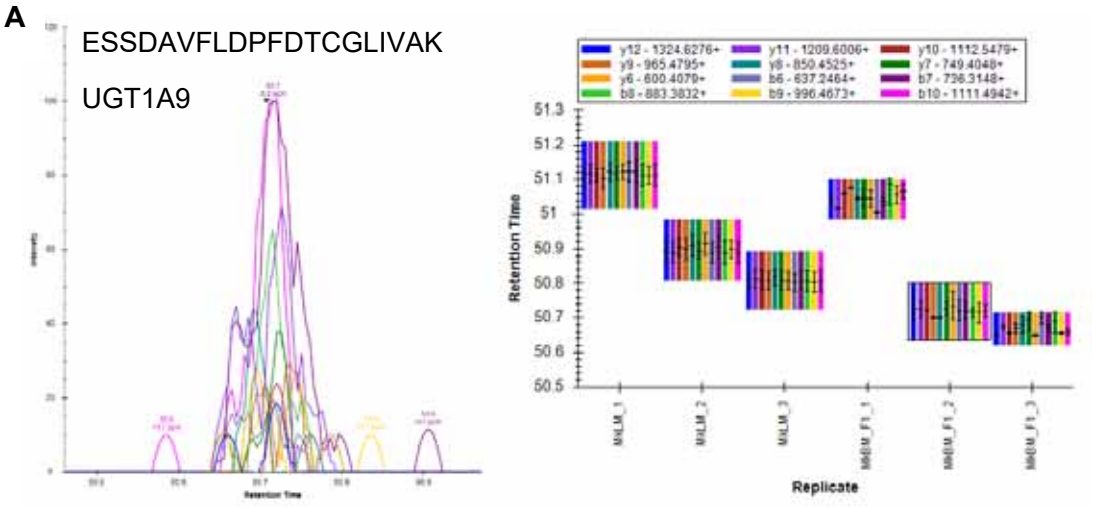

B

TYATSYTLEDLDR

UGT1A10

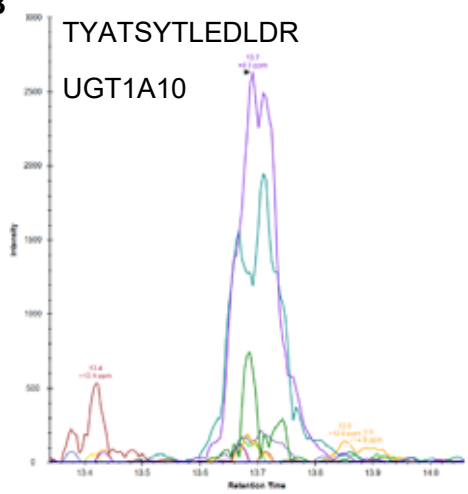

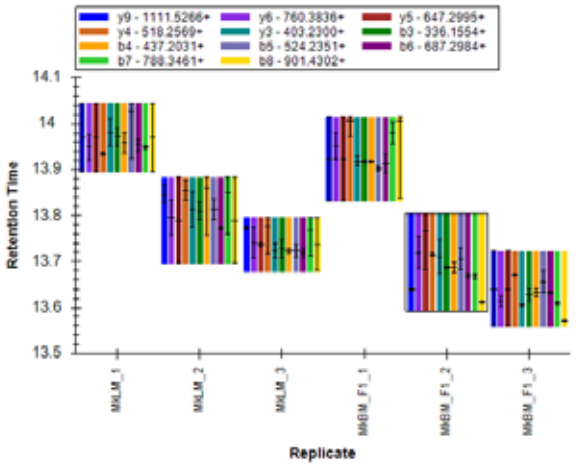

C

DTFWLYFSQMQEIMWR

UGT2B9

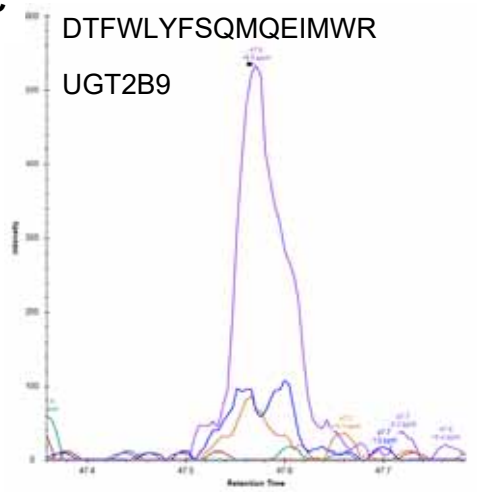

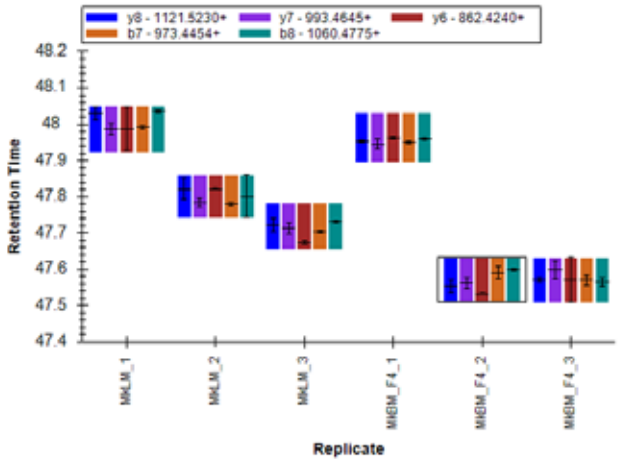

D

FTVGYTFEK

UGT2B20

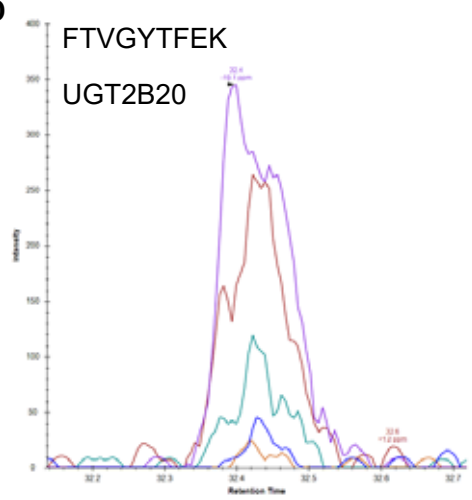

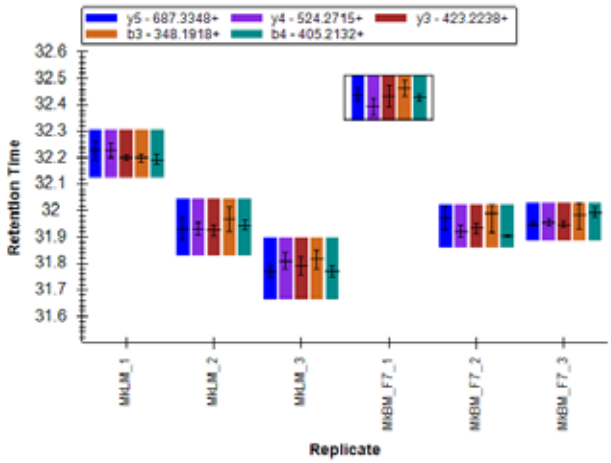

Biotransformation of efavirenz and proteomic analysis of P450s and UGTs in mouse, macaque, and human brain-derived *in vitro* systems

Abigail M. Wheeler, Benjamin C. Orsburn, and Namandjé N. Bumpus

Drug Metabolism and Disposition

DMD-AR-2022-001195R1

Supplemental Figure 5. Identification of 11 P450s in the human brain microsomes using a targeted proteomics approach. Human brain microsomes (HBM) were digested and resulting peptides were fractionated before using targeted proteomics to show the presence of CYP1A2 (A), CYP2A6 (B), CYP2B6 (C), CYP2D6 (D), CYP2E1 (E-F), CYP2J2 (G), CYP3A4 (H-J), CYP4A11 (K), CYP4F3 (L), CYP4F12 (M), and CYP20A1 (N-O). Protein identifications were made using chromatograms (left) and confirmation of consistent retention times and fragment ions (right) with human liver microsomes (HLM). Samples were analyzed in technical duplicates or triplicates.

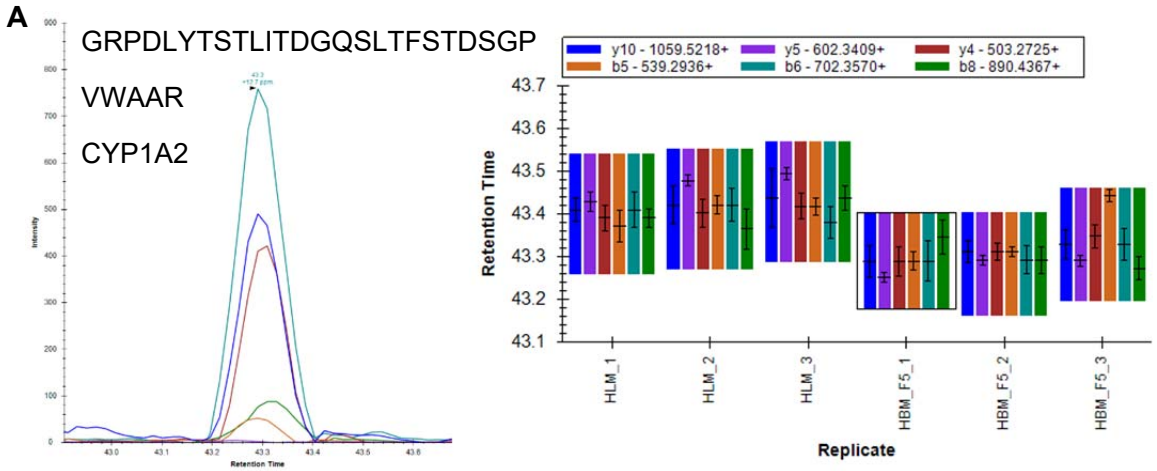

B

MELFLFFTTVMQNFR

CYP2A6

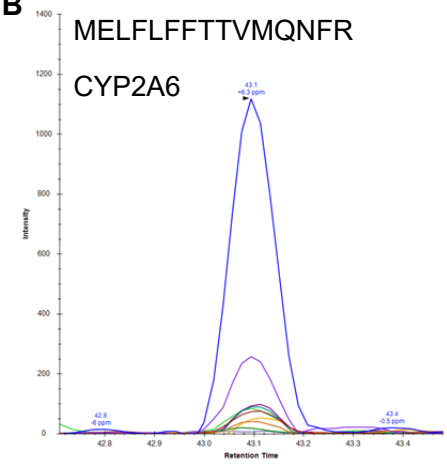

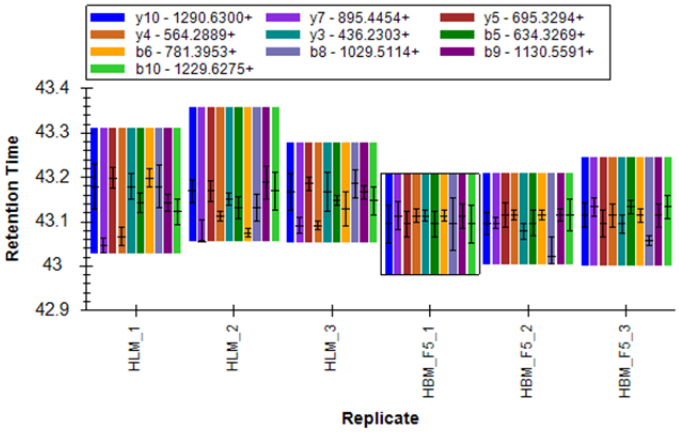

C

DLIDTYLLHMEK

CYP2B6

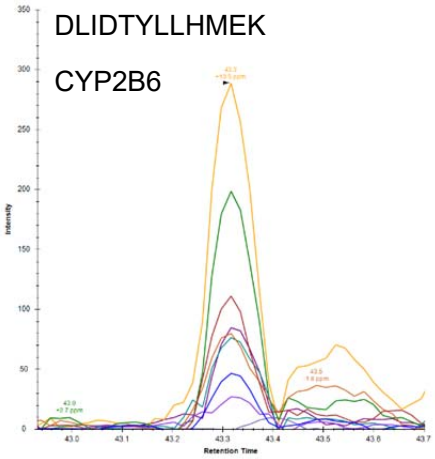

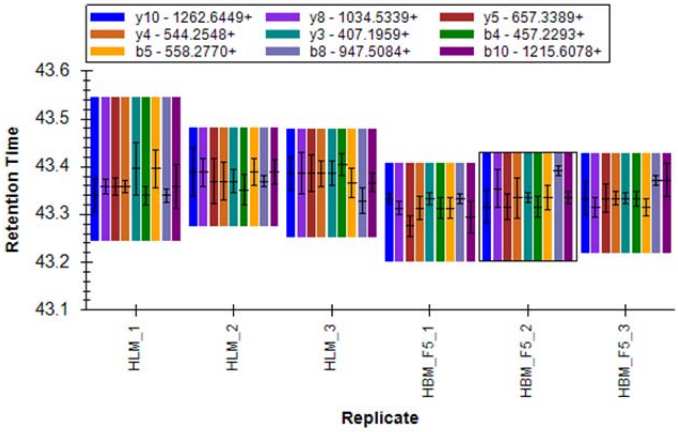

D

AFLTQLDELLTEHR

CYP2D6

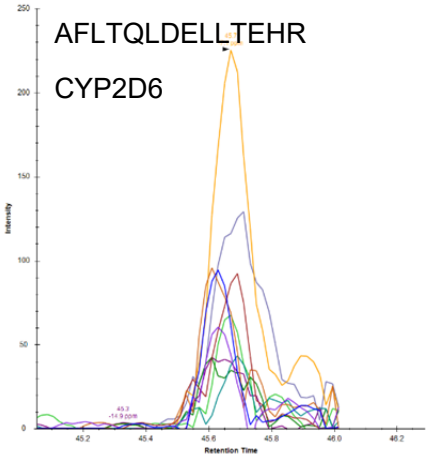

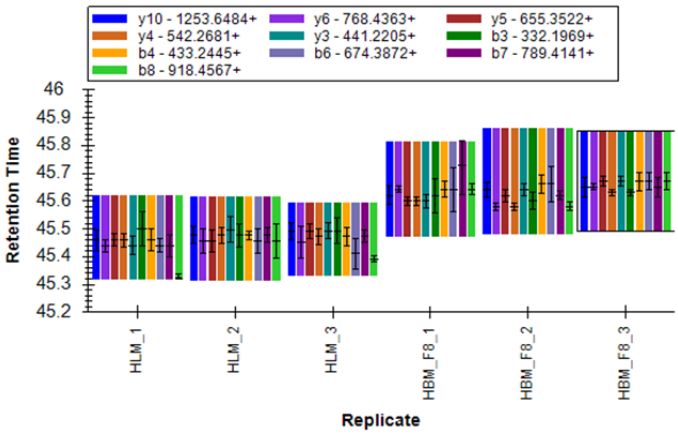

E

EHHQSLDPNCPR

CYP2E1

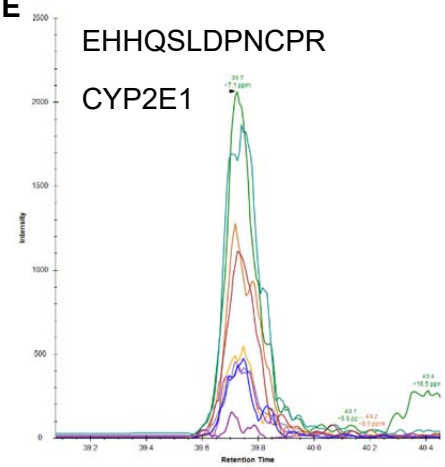

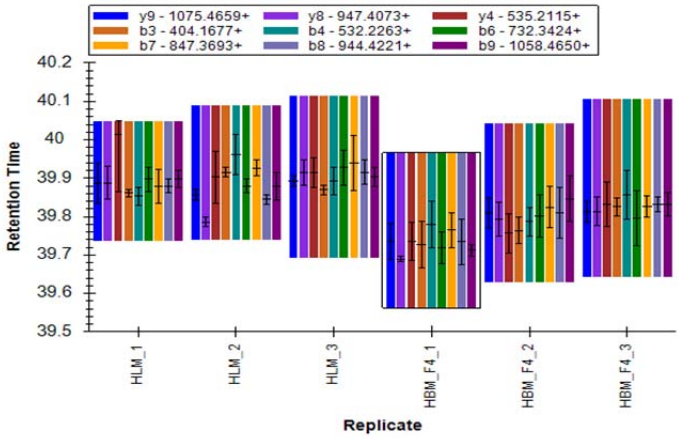

F

LYTMDGITVTVADLFFAGTETTSTT

LR

CYP2E1

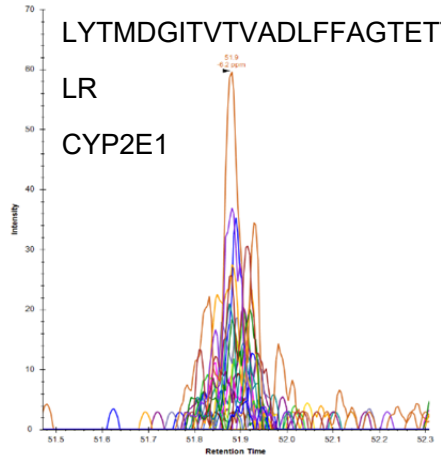

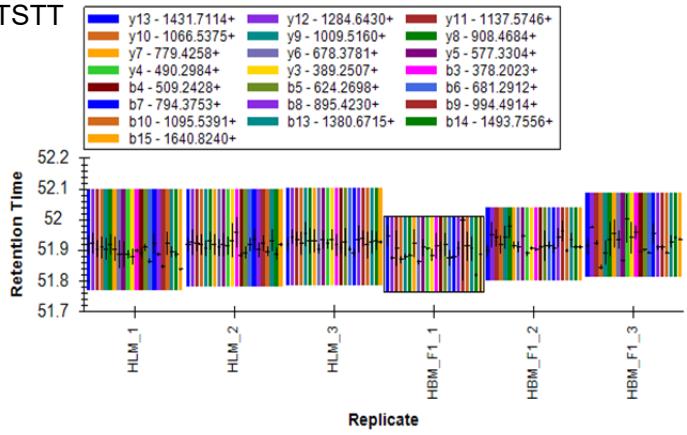

G

EVTVDTTLAGYHLPK

CYP2J2

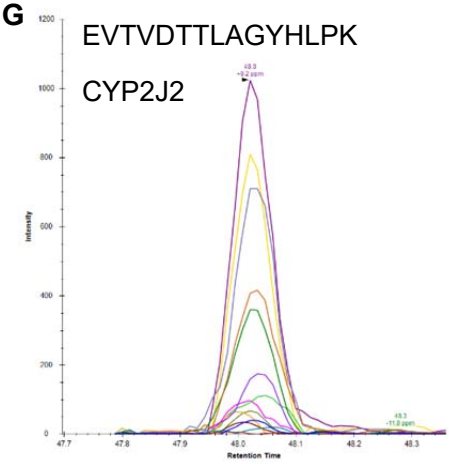

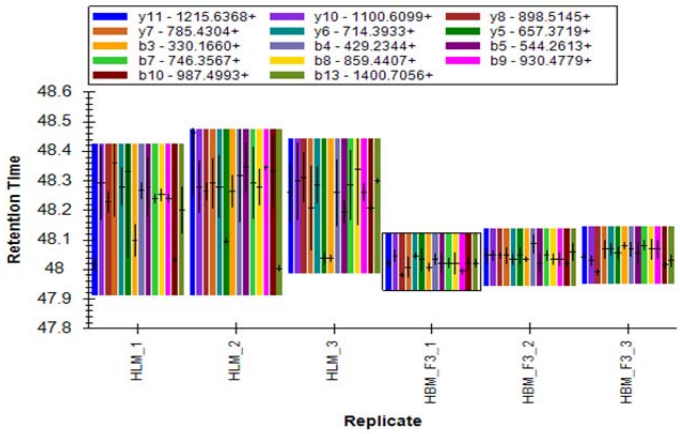

H

APPTYDTVLQMEYLDMVVNETLR

CYP3A4

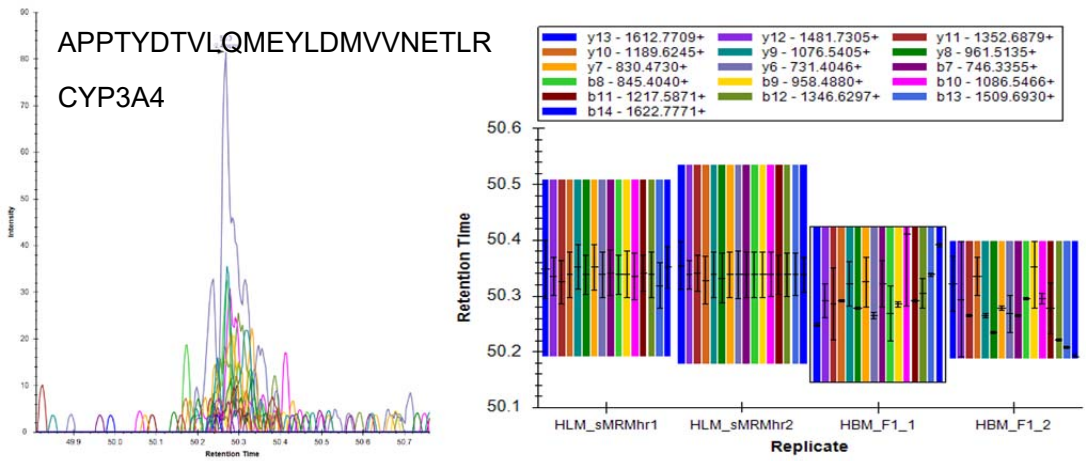

I

FDFLDPFFLSITVFPFLIPILEVLNICV

FPR

CYP3A4

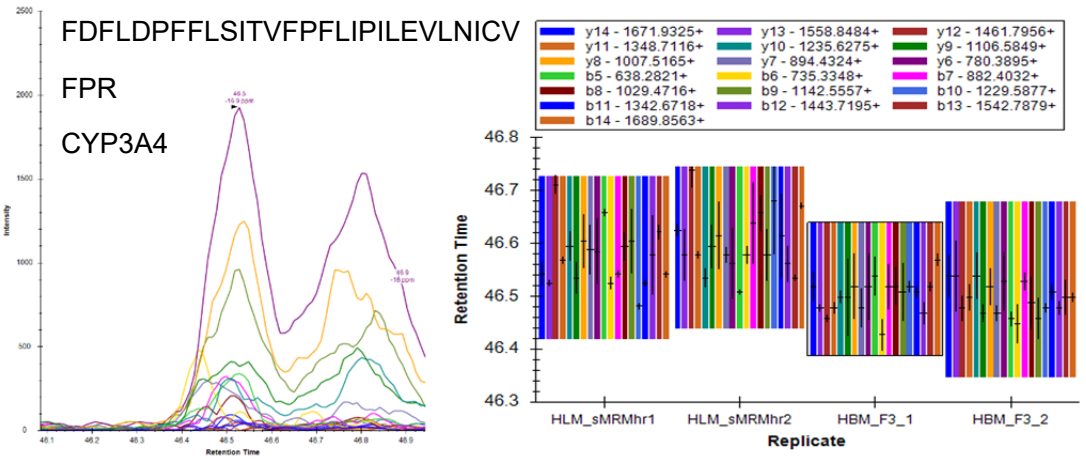

J

VWGFYDGQQPVLAITDPDMIK

CYP3A4

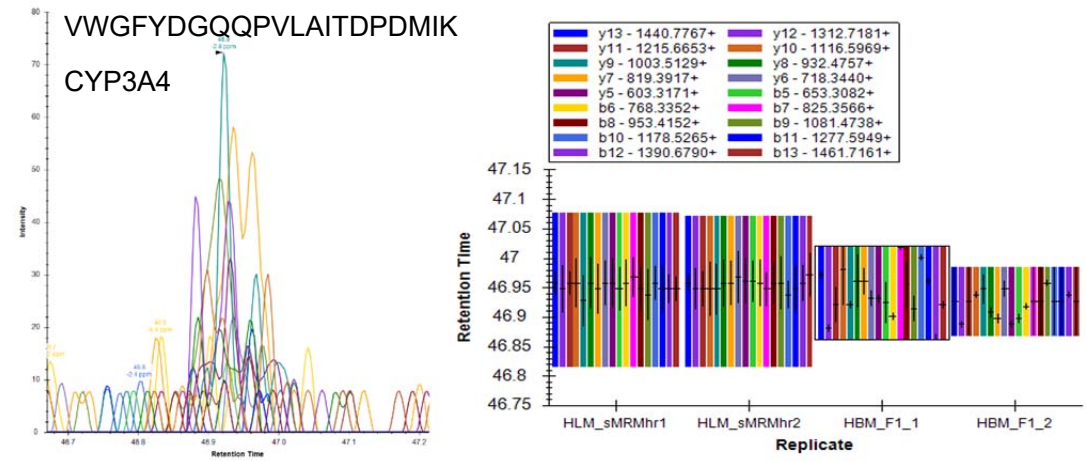

K

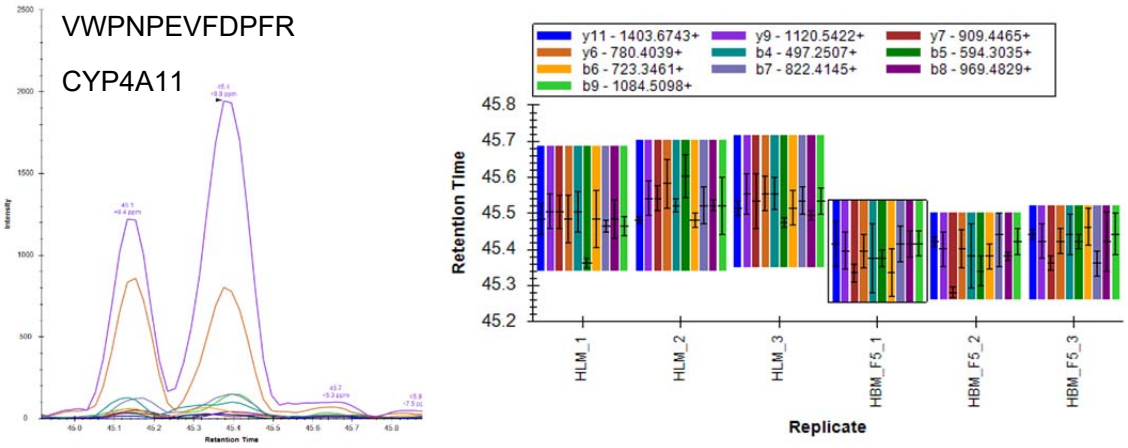
VWPNPEVFDPFR
CYP4A11
y11 - 1403.6743+
y9 - 1120.5422+
y7 - 909.4465+
y6 - 780.4039+
b4 - 497.2507+
b5 - 594.3035+
b6 - 723.3461+
b7 - 822.4145+
b8 - 969.4829+
b9 - 1084.5098+
Retention Time
Intensity
Replicate
HLM_1
HLM_2
HLM_3
HBM_F5_1
HBM_F5_2
HBM_F5_3

L

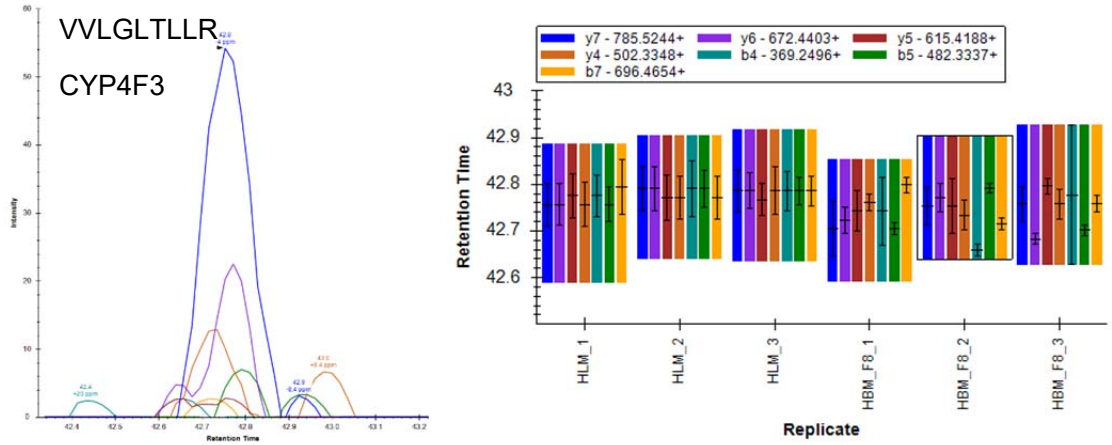
VVLGLTLLR
CYP4F3
y7 - 785.5244+
y6 - 672.4403+
y5 - 615.4188+
y4 - 502.3348+
b4 - 369.2496+
b5 - 482.3337+
b7 - 696.4654+
Retention Time
Intensity
Replicate
HLM_1
HLM_2
HLM_3
HBM_F8_1
HBM_F8_2
HBM_F8_3

M

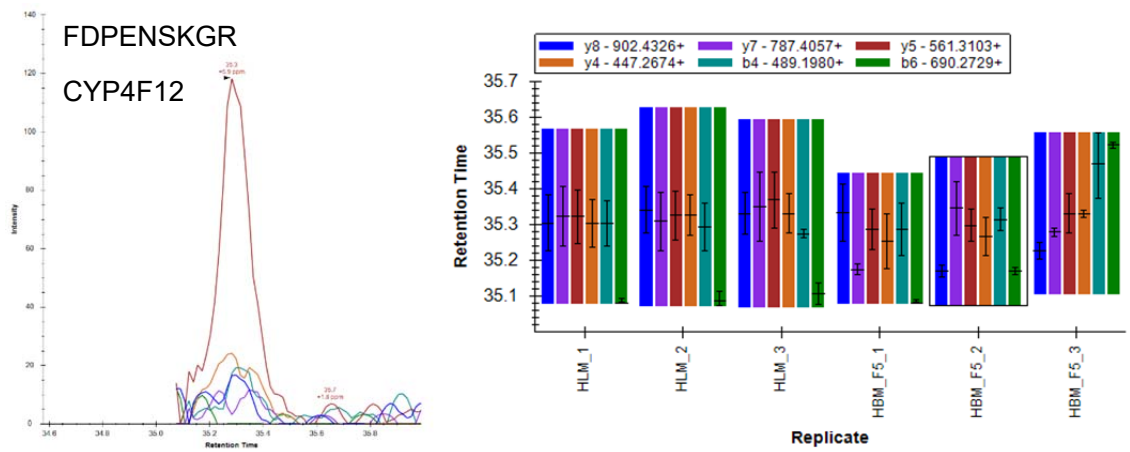
FDPENSKGR
CYP4F12
y8 - 902.4326+
y7 - 787.4057+
y5 - 561.3103+
y4 - 447.2674+
b4 - 489.1980+
b6 - 690.2729+
Retention Time
Intensity
Replicate
HLM_1
HLM_2
HLM_3
HBM_F5_1
HBM_F5_2
HBM_F5_3

N

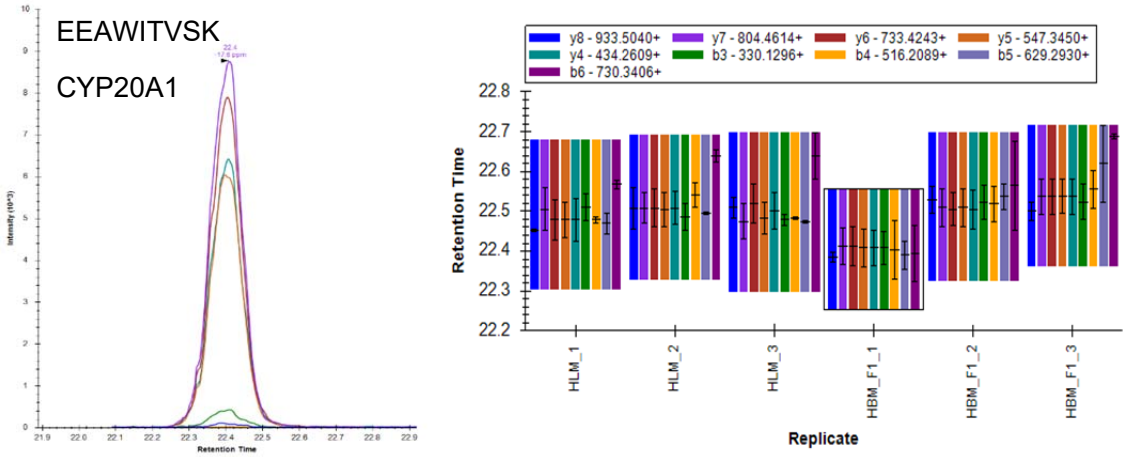
EEAWITVSK
CYP20A1
Intensity (10^3)
Retention Time
y8 - 933.5040+
y7 - 804.4614+
y6 - 733.4243+
y5 - 547.3450+
y4 - 434.2609+
b3 - 330.1296+
b4 - 516.2089+
b5 - 629.2930+
b6 - 730.3406+
Retention Time
HLM_1
HLM_2
HLM_3
HBM_F1_1
HBM_F1_2
HBM_F1_3
Replicate

O

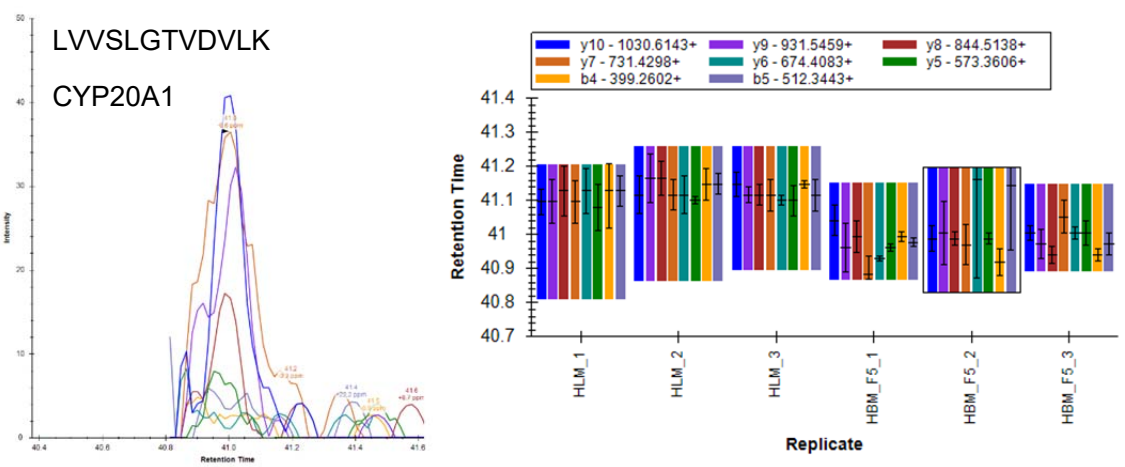
LVVSLGTVDVLK
CYP20A1
Intensity
Retention Time
y10 - 1030.6143+
y9 - 931.5459+
y8 - 844.5138+
y7 - 731.4298+
y6 - 674.4083+
y5 - 573.3606+
b4 - 399.2602+
b5 - 512.3443+
Retention Time
HLM_1
HLM_2
HLM_3
HBM_F5_1
HBM_F5_2
HBM_F5_3
Replicate

and retention time graph (right) are representative of unique fragment ions.

Biotransformation of efavirenz and proteomic analysis of P450s and UGTs in mouse, macaque, and human brain-derived *in vitro* systems

Abigail M. Wheeler, Benjamin C. Orsburn, and Namandjé N. Bumpus

Drug Metabolism and Disposition

DMD-AR-2022-001195R1

Supplemental Figure 6. Identification of 11 UGTs in the human brain microsomes using a targeted proteomics approach. Human brain microsomes (HBM) were digested and resulting peptides were fractionated before using a targeted proteomics approach to show the presence of UGT1A1 (A-B), UGT1A4 (C), UGT1A5 (D), UGT1A6 (E-F), UGT1A8 (G), UGT2A1(H), UGT2A2 (I), UGT2B4 (J-K), UGT2B7 (L), UGT2B17 (M), and UGT2B28 (N). Protein identifications were made using chromatograms (left) and confirmation of consistent retention times and fragment ions (right) with human liver microsomes (HLM). Samples were analyzed in technical duplicate or triplicate.

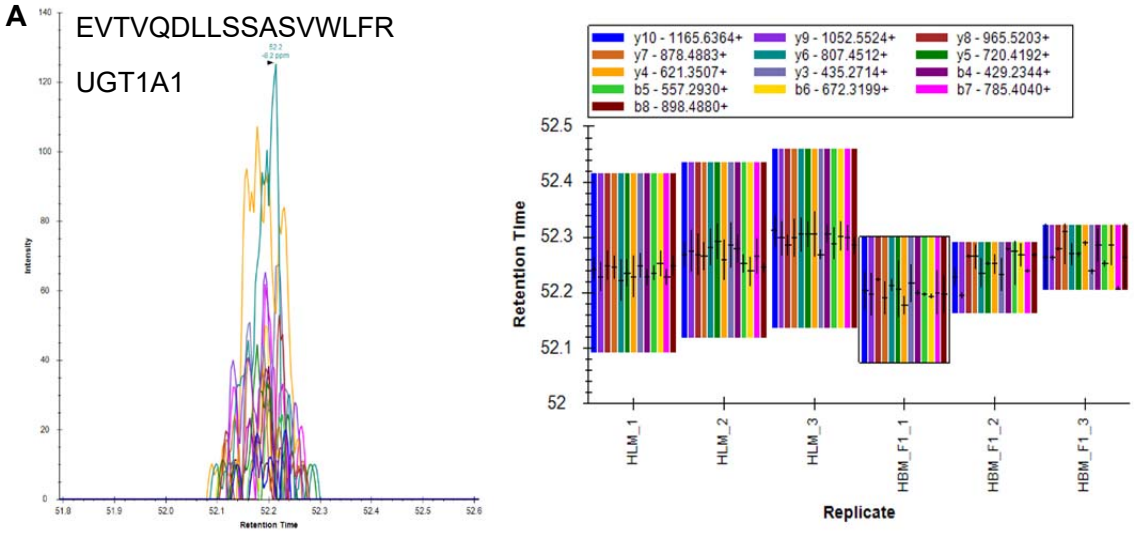

B

ILLIPVDGSHWLSMGAIQQLQQR

UGT1A1

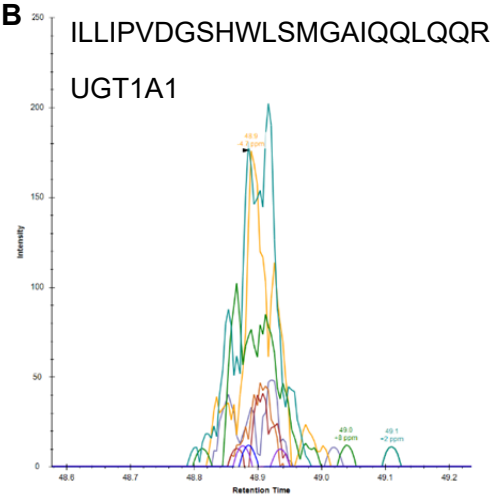

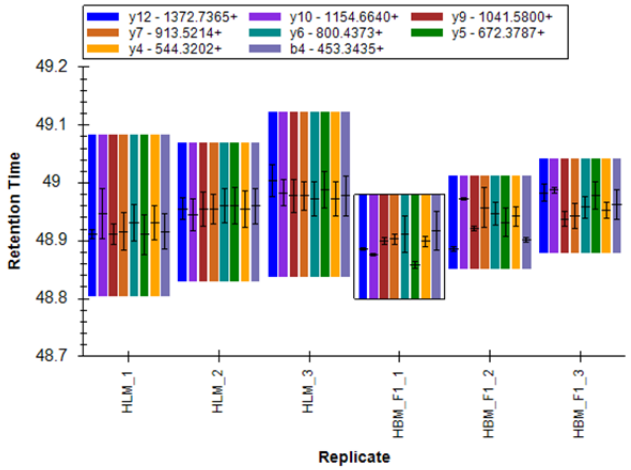

C

EVSVVDLVSYASVWLFR

UGT1A4

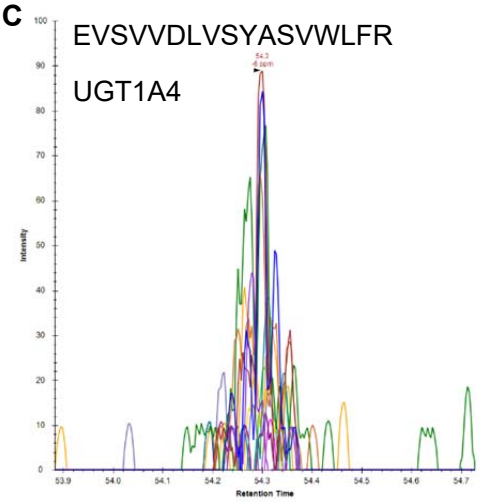

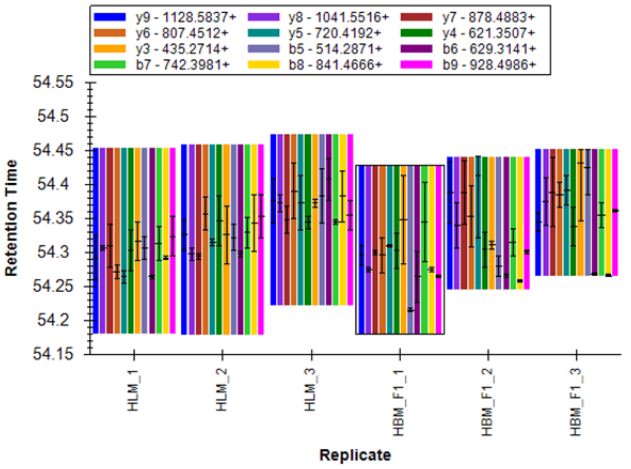

D

EVSVVDLVSHASVWLFR

UGT1A5

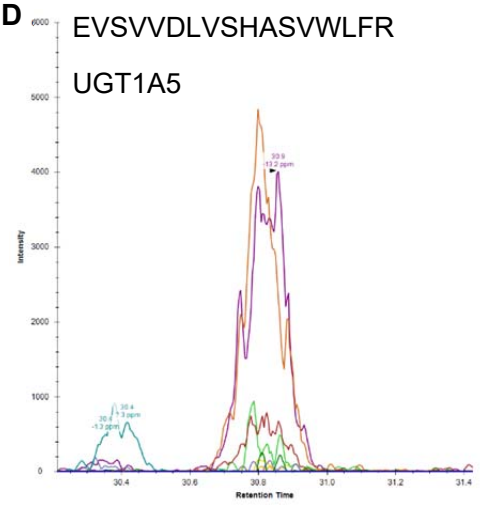

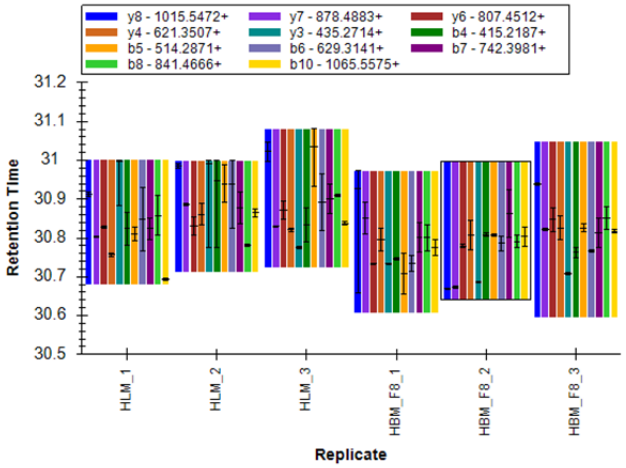

E

DIVEVLSDR

UGT1A6

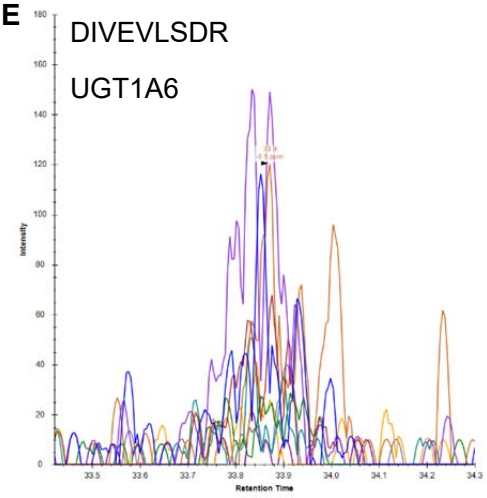

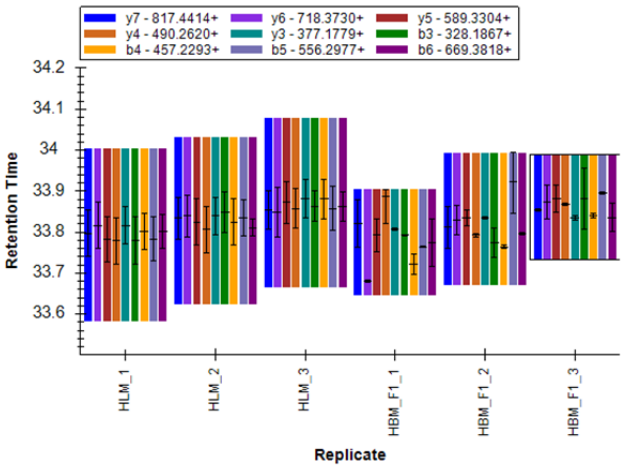

F

NNMIVIGLYFINCSLLQDR

UGT1A6

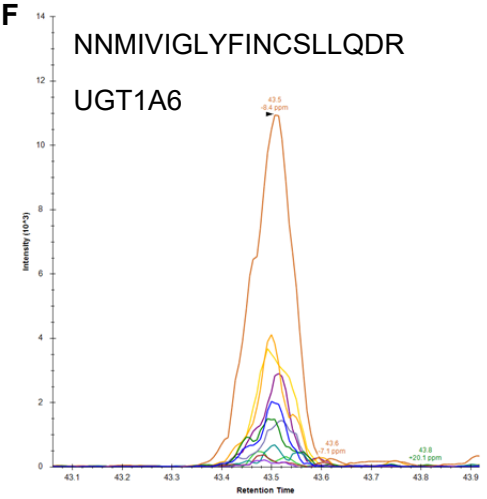

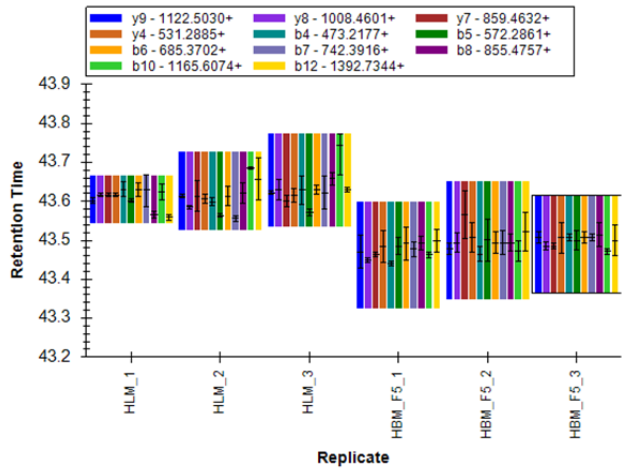

G

ESSFDAVFLDPFDACGLIVAK

UGT1A8

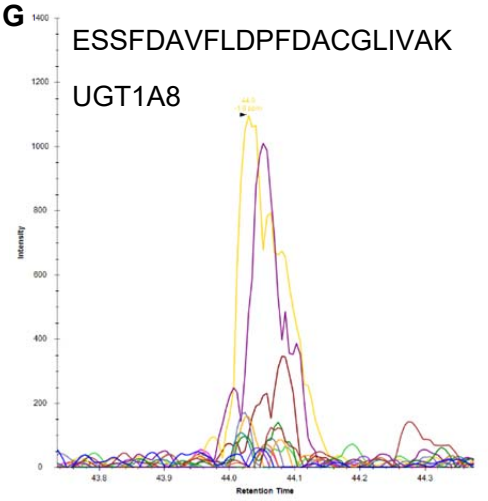

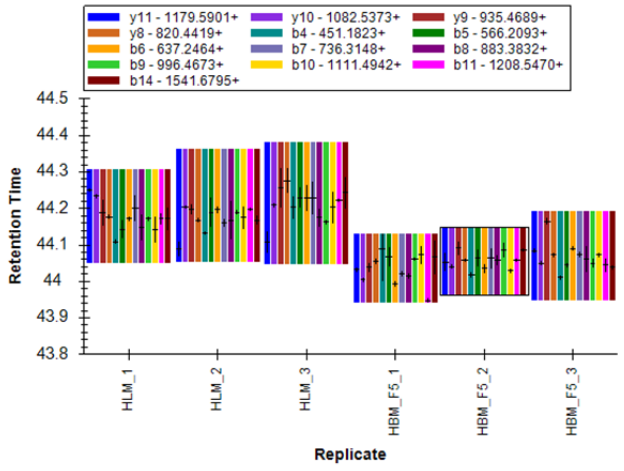

H

DFVLTWLENRPSPSTIWR

UGT2A1

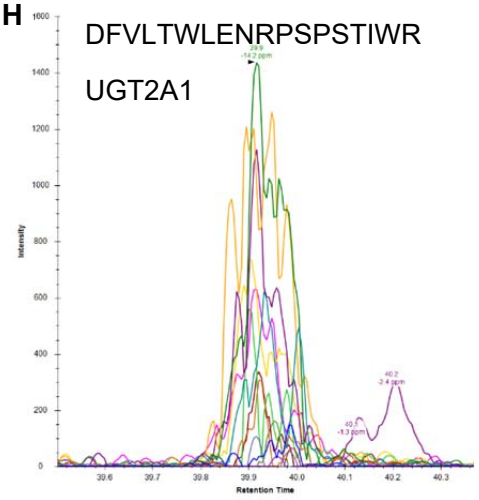

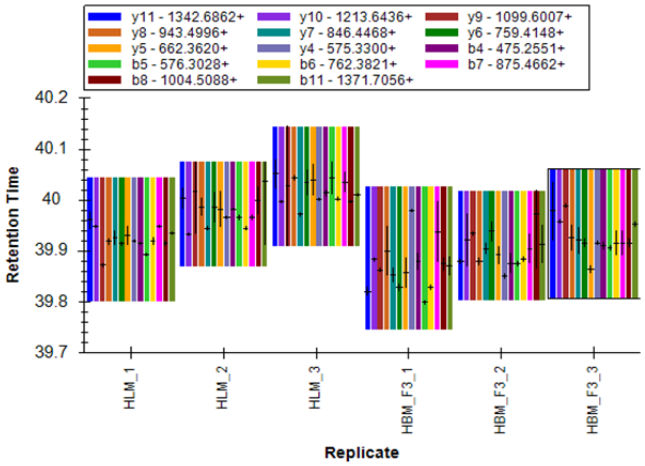

I

FSPASTVER

UGT2A2

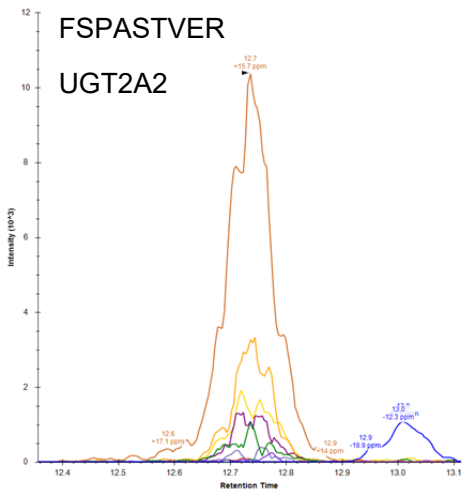

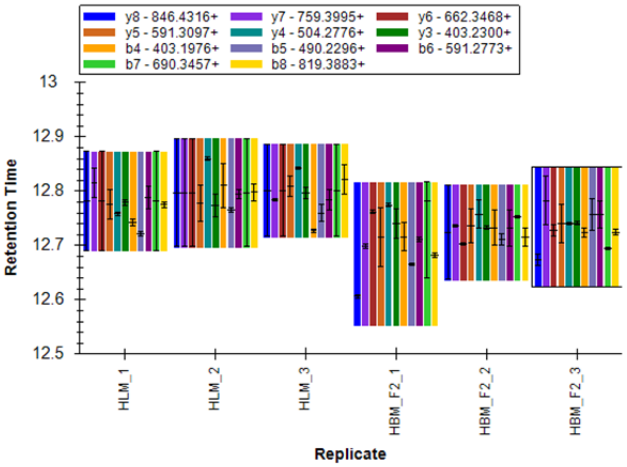

J

FDVVLADAVFPFGELLAELLK

UGT2B4

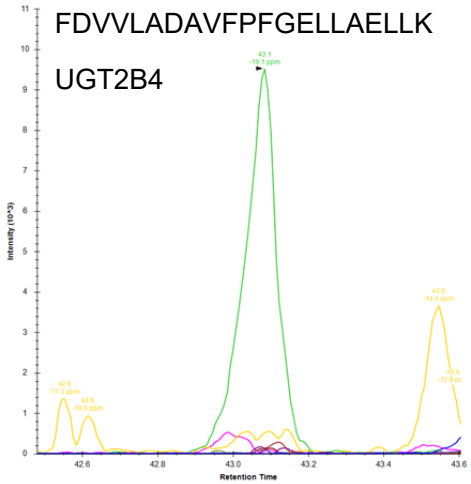

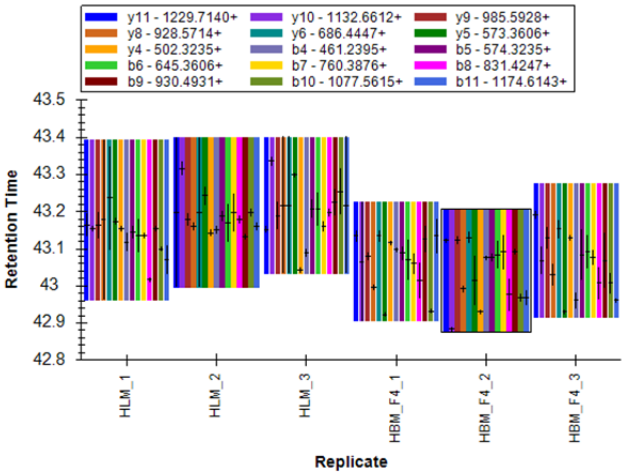

K

TILDELVQR

UGT2B4

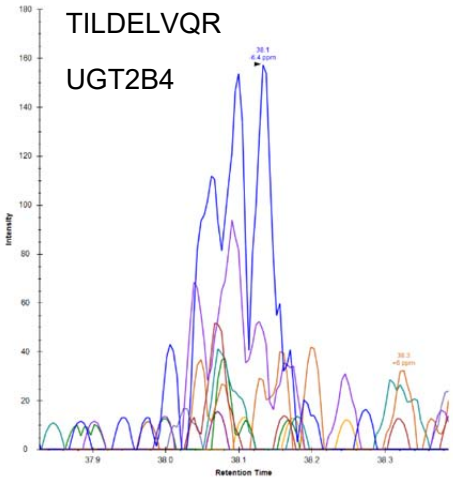

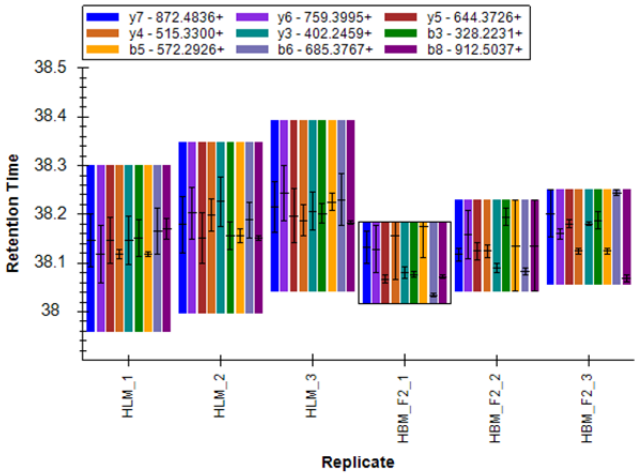

L

HSGGFIFPPSYVPVVMSELTDQMTFMER

UGT2B7

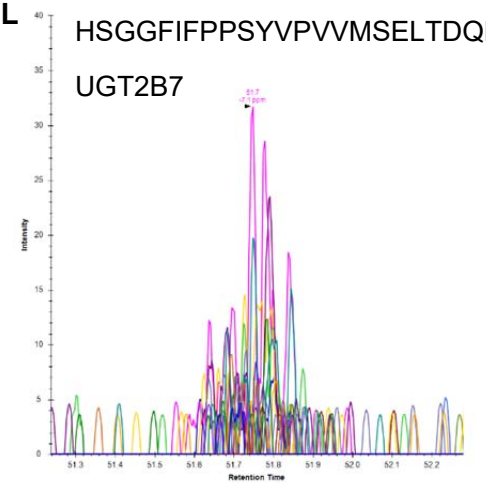

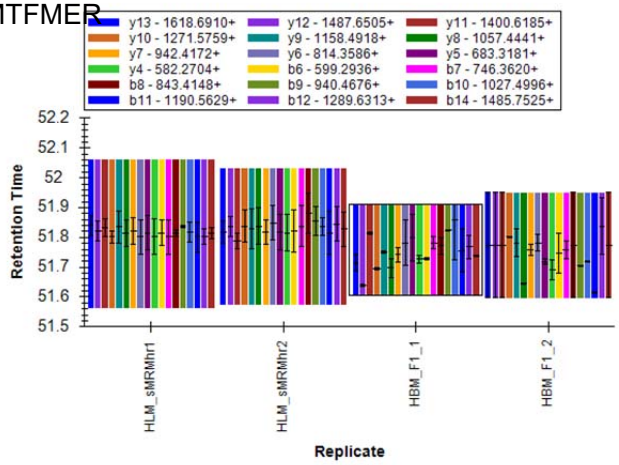

M

GHEVIVLTSSASILVNASK

UGT2B17

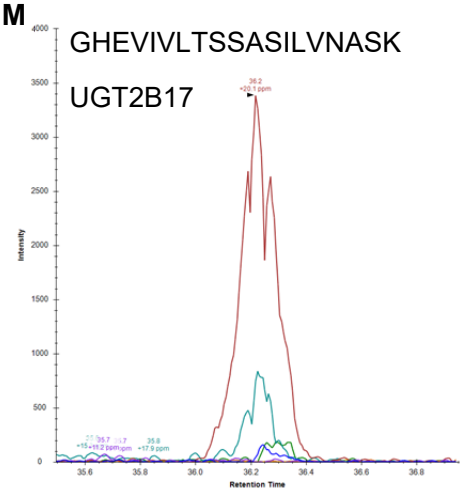

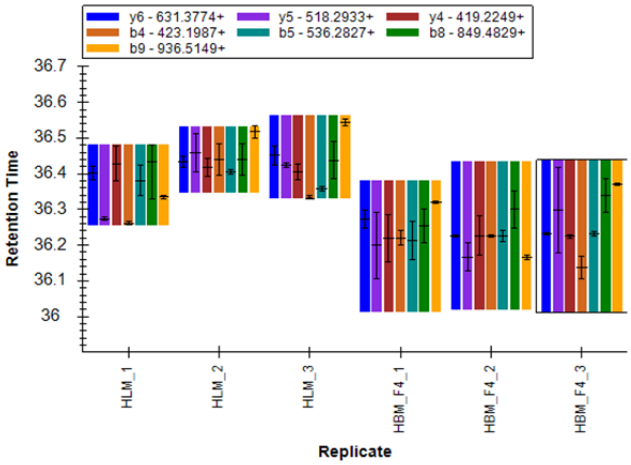

N

LSIIQHDQPVKPLHR

UGT2B28

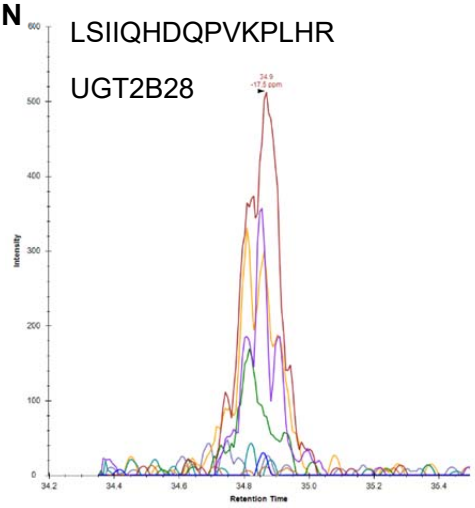

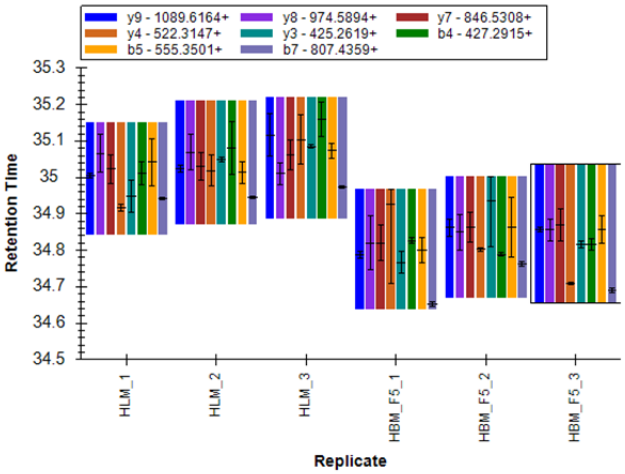

Biotransformation of efavirenz and proteomic analysis of P450s and UGTs in mouse, macaque, and human brain-derived *in vitro* systems

Abigail M. Wheeler, Benjamin C. Orsburn, and Namandjé N. Bumpus

Drug Metabolism and Disposition

DMD-AR-2022-001195R1

Supplemental Table 1. Target peptide list for mouse P450s

Peptide Sequence	Protein	Precursor m/z	CE	RT
VMAEVGHFDPYK	Cyp1a1	696.83	33	25.60
VMAEVGHFDPYK	Cyp1a1	464.89	20	25.60
SEVFLFLAILLQQIEFK	Cyp1a1	510.30	24	37.69
CIYINQWQVNHDEK	Cyp1a2	612.61	27	32.59
DFVENVTSGNAVDFFPVLR	Cyp1a2	1063.53	51	46.91
DNGGLIPEEK	Cyp1a2	536.27	25	23.02
DTSLNGFHIPK	Cyp1a2	614.82	29	30.81
EANHLVSK	Cyp1a2	449.24	21	8.09
FLTNNNSAIDK	Cyp1a2	618.81	29	21.50
GRPDLYSFTLITNGK	Cyp1a2	561.30	25	38.51
IGSTPVVVLSGLNTIK	Cyp1a2	533.32	24	42.00
IHEELDTVVGR	Cyp1a2	634.34	30	23.56
LSQQYGDVLQIR	Cyp1a2	710.38	34	33.39
NSIQDITSALFK	Cyp1a2	668.86	32	44.77
SFSIASDPTSASSCYLEEHVSK	Cyp1a2	797.69	36	36.00
SMTFNPDSGPVWAAR	Cyp1a2	818.38	39	36.63
TFNDNFVLFLQK	Cyp1a2	743.39	35	44.78
TVQEHYQDFNK	Cyp1a2	470.22	21	17.21
VDLTPNYGLTMKPGTCEHVQAWPR	Cyp1a2	690.58	33	38.06
VMLFGLGK	Cyp1a2	432.75	20	39.32
YTSFVPFTIPHSTTR	Cyp1a2	877.45	42	38.69
YLPNPALK	Cyp1a2	458.27	22	24.55
DFIDSFLIHMQK	Cyp2a12	498.59	22	45.85
DVYSSITQLQEHYGPCFTIHLGPR	Cyp2a12	690.11	32	45.14
EALDHAEEFSGR	Cyp2a12	730.34	35	24.47
FAASPTGQLYDMFHSVMK	Cyp2a12	677.32	31	44.96
FCLGDSLAK	Cyp2a12	500.24	24	34.49
FSIATLR	Cyp2a12	404.24	19	32.16
FSNFAPLGIPR	Cyp2a12	609.84	29	38.43

GEQATFNTLFK	Cyp2a12	628.32	30	36.10
GTEVFPILGSLMTDPK	Cyp2a12	852.95	41	46.76
GYGVAFSNGER	Cyp2a12	578.77	27	23.84
IPAFLPFSTGK	Cyp2a12	589.33	28	42.64
IQEEAGCLIK	Cyp2a12	575.29	27	30.56
MLQGTCGAPIDPTIYLSK	Cyp2a12	977.48	47	43.18
MPYTQAVINEIQR	Cyp2a12	781.90	37	36.02
QNQSTLDPNSPR	Cyp2a12	678.83	32	14.36
TASNVISSIVFGDR	Cyp2a12	733.39	35	43.54
VHEEIDR	Cyp2a12	449.22	21	9.54
VVVLYGYDAVK	Cyp2a12	613.34	29	33.43
YGFLLLMK	Cyp2a12	492.78	23	45.06
YVNSEFHMK	Cyp2a12	577.77	27	21.17
DFIDSFLIR	Cyp2a4	563.30	27	45.87
EALVDQAEEFSGR	Cyp2a4	484.23	21	30.48
ELQGLEDFITK	Cyp2a4	646.84	31	39.96
FADLIPMGLAR	Cyp2a4	602.33	29	43.01
FSITTLR	Cyp2a4	419.25	20	32.81
GEQATFDWLFK	Cyp2a4	671.33	32	44.98
IQEEAGFLIDSFR	Cyp2a4	762.89	36	42.83
TNGAFIDPTFYLSR	Cyp2a4	801.40	38	42.83
FADMIPMGLAR	Cyp2a5	611.31	29	40.86
NDAFVPFSIGK	Cyp2a5	597.81	28	39.07
STQAPQDIDVSPR	Cyp2a5	707.35	34	21.00
ATLDPSVPR	Cyp2b10	478.26	22	21.44
DIDLTPK	Cyp2b10	401.22	19	22.88
EALVGQAEAFSGR	Cyp2b10	667.84	32	28.78
EIDQVIGSHR	Cyp2b10	577.30	27	19.24
EYGVIFANGER	Cyp2b10	627.81	30	30.49
FSDLIPIGVPHR	Cyp2b10	450.92	20	37.20
FSLATMR	Cyp2b10	413.22	19	30.22
GTVAVVEPTFK	Cyp2b10	574.32	27	28.70
ICLGESIAR	Cyp2b10	504.25	24	30.40
IPPTYQICFLAR	Cyp2b10	734.38	35	45.17
IQEEAQCLVEELR	Cyp2b10	803.38	38	40.34
LPTLDDR	Cyp2b10	415.22	19	22.71
MPYTDAVIHEIQR	Cyp2b19	524.93	23	33.36
NLQEILDYIGHSVEK	Cyp2b19	586.64	26	46.60
DYIDTYLLR	Cyp2b9	586.30	28	39.63
EALVDHAEAFSGR	Cyp2b9	467.90	21	25.13
FSDLVPIGLPHK	Cyp2b9	441.59	19	36.59

IPPAHQIYFLAR	Cyp2b9	475.94	21	33.01
QQELLDYIAHSVEK	Cyp2b9	558.29	25	41.33
AYGPVFTLYLGSKPTVILHGYEAVK	Cyp2c29	908.50	42	43.66
DFIDYYLIK	Cyp2c29	595.31	28	43.39
EFLILMDK	Cyp2c29	504.78	24	41.34
EFPNPEMFDPGHFLNGNGNFK	Cyp2c29	803.36	37	44.26
ESLDVTNPR	Cyp2c29	515.76	24	18.87
FIDLLPTSLPHAVTCDIK	Cyp2c29	1015.03	49	45.37
FTLMTLR	Cyp2c29	441.25	21	37.40
GFGVVFSNGNR	Cyp2c29	577.29	27	31.57
GSFPMAEK	Cyp2c29	433.71	20	21.20
GTTVITSLSSVLHDSK	Cyp2c29	548.96	24	39.01
ICAGEGLAR	Cyp2c29	468.23	22	23.53
LPPGPTPLPIIGNFLQIDVK	Cyp2c29	710.42	32	49.32
NISQSFTNFSK	Cyp2c29	636.81	30	29.71
SDYFMPFSTGK	Cyp2c29	640.29	30	38.30
SHMPYTDAMIHEVQR	Cyp2c29	605.62	27	27.83
SHMPYTDAMIHEVQR	Cyp2c29	454.46	21	27.83
SPCMQDR	Cyp2c29	441.67	21	15.75
YALLLLLK	Cyp2c29	473.82	22	45.64
ATNGMGLAFSK	Cyp2c37	548.78	26	27.90
DFIDYFLINGGQEDGNQPLQNR	Cyp2c37	851.74	39	45.50
DICQSFTNLSK	Cyp2c37	651.30	31	41.45
EALVDHGEEFAGR	Cyp2c37	477.23	21	22.71
FDPGHFLDENGK	Cyp2c37	459.21	20	32.04
KPTVVLHGYEAVK	Cyp2c37	480.95	21	21.30
LEHLAITVTDLFSAGTETTSTTLR	Cyp2c37	859.79	39	44.54
VQEEIEHVIGK	Cyp2c37	640.85	30	24.12
VYGPVYTLYLGR	Cyp2c37	467.59	20	41.19
NFNQSLTNFSK	Cyp2c38	650.32	31	29.23
VCAGEGLAR	Cyp2c38	461.22	22	20.87
YALLLLMK	Cyp2c38	482.80	23	44.28
EALIDHGEEFSDR	Cyp2c39	506.57	22	24.21
FINLVPNNIPR	Cyp2c39	648.87	31	38.38
INNGLGIVFSNGNR	Cyp2c39	737.89	35	35.13
NHMPYTDAMIHEVQR	Cyp2c39	461.22	21	27.55
SDHFMPFSAGK	Cyp2c39	408.52	18	28.62
VQEEIDHVIGR	Cyp2c39	647.84	31	23.95
DFIDYFLIQR	Cyp2c40	665.35	32	46.50
DIDMTPK	Cyp2c40	410.20	19	18.67
DIGQCLTNFSK	Cyp2c40	636.29	30	40.67

EHEESLDVTNPR	Cyp2c40	475.89	21	17.88
FALLLLMK	Cyp2c40	474.80	22	46.48
GIGFSHGNVWK	Cyp2c40	401.21	17	27.89
GNLPPGPTPLPIIGNYHLIDMK	Cyp2c40	590.07	28	44.20
GTQVMTSLTSVLHDSTEFPNPEVFDPGHFLDDNGNFK	Cyp2c40	1023.98	49	46.66
ICVGESLAR	Cyp2c40	497.25	23	27.57
IPPNFQMCFIPVE	Cyp2c40	790.87	38	49.13
NHMPYTNAMVHEVQR	Cyp2c40	457.47	21	23.43
SDYFVPFSAGK	Cyp2c40	609.30	29	36.19
VFTVNTLR	Cyp2c40	475.28	22	28.63
VQEEAQWLMK	Cyp2c40	631.32	30	31.80
VQEEIDNVIGR	Cyp2c40	636.33	30	27.64
YIDLGPNGVVHEVTCDTK	Cyp2c40	669.32	30	36.90
DLDIKPVTTGLFNLPPPYK	Cyp2c44	710.06	32	43.77
EALLNQGDEFLGR	Cyp2c44	731.37	35	35.32
GPLPIIEDSQK	Cyp2c44	598.83	28	30.74
TDYFVPFSLGK	Cyp2c44	637.33	30	43.07
YITLLPSSLPHAVVQDTK	Cyp2c44	661.37	30	40.07
ATNGMGIIFSK	Cyp2c50	569.80	27	34.09
GTNVITSLSSVLR	Cyp2c50	673.89	32	43.69
LPPGPTPLPIIGNILQINVK	Cyp2c50	698.76	32	48.88
ATNGMGIGFSNGSVWK	Cyp2c54	542.60	24	36.82
DICQSFTNLSR	Cyp2c54	665.30	32	41.92
EALVDHGDVFAGR	Cyp2c54	693.34	33	26.44
FIDLVPNNLPHEVTCDIK	Cyp2c54	529.02	25	43.60
GAQEDDNHPLK	Cyp2c54	408.53	18	8.81
GTTVITSLSSVLR	Cyp2c54	445.26	19	42.37
SHMPYTNAMIHEVQR	Cyp2c54	454.22	21	27.94
FDPGHFLDEK	Cyp2c70	402.19	17	32.52
IQEEIAHVIGR	Cyp2c70	632.85	30	26.71
IQEEILYMLDALR	Cyp2c70	536.29	24	47.90
LPPGPTPLPIVGNILQVDVK	Cyp2c70	689.75	31	47.04
NHMPYTDAVLHEIQR	Cyp2c70	456.73	21	31.46
NHMPYTDAVLHEIQR	Cyp2c70	608.63	27	31.46
SDYFVAFSAGR	Cyp2c70	610.29	29	35.95
SLDLSNPQDFIDYFLIK	Cyp2c70	676.68	31	49.77
SLDLSNPQDFIDYFLIK	Cyp2c70	1014.52	49	49.77
TSQGLGIVFSNGETWK	Cyp2c70	862.44	41	40.09
TTQDVEFR	Cyp2c70	498.24	23	18.53
YGLLLLLK	Cyp2c70	466.81	22	45.46
YPEVTAK	Cyp2c70	404.22	19	16.32

DETVWEKPLR	Cyp2c70	424.89	18	26.81
DIEVQDFLIPK	Cyp2c70	658.86	31	43.62
FEYEDPYLIR	Cyp2d10	672.83	32	36.58
FGDIAPLNLPR	Cyp2d10	404.90	17	38.51
FSVSTLR	Cyp2d10	405.23	19	26.46
GSILIPNMSSVLK	Cyp2d10	679.89	32	42.92
HPEMADQAR	Cyp2d10	527.74	25	8.95
MPYTNAVIHEVQR	Cyp2d10	519.93	23	28.31
NLGVFPFPVAPYPYQLCAVMR	Cyp2d10	810.07	37	50.93
NLTDAFLAEIEK	Cyp2d10	455.24	20	44.30
NTWDPDQPPR	Cyp2d10	409.19	18	21.71
SCLGEPLAR	Cyp2d10	496.24	23	29.16
SLEDWVTK	Cyp2d10	489.25	23	31.66
SLLAIVENLLTENR	Cyp2d10	792.95	38	51.46
VQQEIDAVIGQVR	Cyp2d10	727.90	35	33.59
VQQEIDAVIGQVR	Cyp2d10	485.60	21	33.59
GNPESSFNDENLR	Cyp2d11	493.56	22	23.48
SCLGEALAR	Cyp2d11	483.23	23	31.57
AVSNVIASLIYAR	Cyp2d26	459.60	20	45.30
DLTDAFLAEVEK	Cyp2d26	450.90	20	43.73
EAEHPFNPSPLLSK	Cyp2d26	522.60	23	29.73
FQDFFIPK	Cyp2d26	521.27	25	38.97
FYPEHFLDAQGHFVK	Cyp2d26	459.48	21	34.22
GNPESSFNDK	Cyp2d26	547.74	26	14.86
GVILAPYGPEWR	Cyp2d26	679.37	32	39.23
HEAFMPFSAGR	Cyp2d26	417.20	18	30.61
LNSFIALVNK	Cyp2d26	559.83	26	37.83
MLIEHDLTWDPAQPPR	Cyp2d26	640.32	29	36.42
YGNVFSLQMAWKPVVVVNGLK	Cyp2d26	783.76	36	45.22
DESVWEKPLR	Cyp2d9	629.82	30	27.18
EANHLCDAFTAQAGQPINPNPMLNK	Cyp2d9	914.09	42	40.47
FEYEDPFLIR	Cyp2d9	664.83	32	43.11
FGDIVPVNLPR	Cyp2d9	409.57	18	38.54
GNPESSFNDENLLMVVR	Cyp2d9	640.98	29	42.32
GTILLPNMSSMLK	Cyp2d9	702.88	33	43.64
HPEMADQAHMPYTNAVIHEVQR	Cyp2d9	644.30	30	28.77
SFIAILDNLLTENR	Cyp2d9	809.94	39	50.16
STCNVIASLIFAR	Cyp2d9	720.87	34	48.84
TTWDPVQAPR	Cyp2d9	585.80	28	27.81
VQQEIDEVIGQVR	Cyp2d9	756.90	22	33.26
VQQEIDEVIGQVR	Cyp2d9	504.94	22	33.70

DIDLSPVTIGFGSIPR	Cyp2e1	843.96	40	44.87
DVTDCLLIEMEK	Cyp2e1	485.56	21	45.12
FGPVFTLHLGQR	Cyp2e1	457.92	20	39.54
FINLVPSNLPHEATR	Cyp2e1	427.73	19	35.71
FSLSILR	Cyp2e1	418.26	20	39.54
GDIPVFQEYK	Cyp2e1	598.30	28	33.22
GIIFNNGPTWK	Cyp2e1	623.83	30	36.00
IVVLHGYK	Cyp2e1	464.78	22	21.68
MNMPYMDAVVHEIQR	Cyp2e1	611.95	27	40.30
SLDINCPR	Cyp2e1	482.22	23	30.83
SLDINCPR	Cyp2e1	482.22	23	30.83
VCVGEGLAR	Cyp2e1	475.23	22	24.93
YGLLILMK	Cyp2e1	475.79	22	43.79
YPEIEEK	Cyp2e1	454.22	21	19.23
YSDYFK	Cyp2e1	411.69	19	22.77
DFIDCFLTK	Cyp2f2	574.26	27	46.51
EHQDSLDPNSPR	Cyp2f2	465.55	20	13.19
FADVIPMNLPHR	Cyp2f2	470.58	21	36.06
FSVQILR	Cyp2f2	431.76	20	34.10
GAYPVFFNFTR	Cyp2f2	659.83	31	43.90
GNGIAFSDGER	Cyp2f2	561.76	27	22.02
GQLPPGPKPLPILGNLLQLR	Cyp2f2	707.77	32	46.85
GTDVITLLNTVHYDSDQFK	Cyp2f2	1083.54	52	43.58
HAFLILMK	Cyp2f2	486.79	23	35.63
ILEEGSFLLEVLR	Cyp2f2	759.43	36	47.50
LCLGEPLAR	Cyp2f2	509.26	24	34.52
LLTIIHFINDNFK	Cyp2f2	529.97	23	44.78
MEGKPFDPVFILSR	Cyp2f2	545.96	24	42.39
MPTLEDR	Cyp2f2	431.21	20	21.26
SPAFMPFSAGR	Cyp2f2	584.28	28	35.85
SQDLLTSLTK	Cyp2f2	553.31	26	34.22
TPQEFNPEHFLDDNHSFK	Cyp2f2	551.25	26	36.83
TSMPYTDAVIHEVQR	Cyp2f2	582.95	26	32.04
ACLGEQLAK	Cyp2j5	489.74	23	26.38
EEGGQPFNPHLK	Cyp2j5	451.56	20	21.48
EMFTHLDQNFVNR	Cyp2j5	550.93	24	32.59
ESFLPFSMGK	Cyp2j5	571.78	27	41.96
EWATPEVFNPEHFLENGQFK	Cyp2j5	807.05	37	44.90
FNGFHLPK	Cyp2j5	480.26	22	29.65
LPFVGNFFQIDTK	Cyp2j5	509.27	22	46.50
MGLILSPASYR	Cyp2j5	604.33	29	37.50

MGNIVPLNSSR	Cyp2j5	594.31	28	26.87
NGLVVSNGQTWK	Cyp2j5	651.84	31	26.82
TTSFNEENLISTTLDLFGGTETTSSTLR	Cyp2j5	1050.02	48	52.09
ALLSPTFTSGK	Cyp3a11	561.31	27	30.81
DFGPVGIMSK	Cyp3a11	525.77	25	33.91
DSIEFFK	Cyp3a11	443.22	21	34.12
DVELNGVYIPK	Cyp3a11	623.84	30	34.00
ECFSVFTNR	Cyp3a11	574.75	27	38.05
EMFPVIEQYGDILVK	Cyp3a11	890.96	43	45.78
FALMNMK	Cyp3a11	427.72	20	33.42
GSIDPYVYLPFGNGPR	Cyp3a11	584.63	26	44.04
GSTVMIPSYALHHDPQHWSEPEEFQPER	Cyp3a11	826.88	39	34.46
IMQNFSFQPCK	Cyp3a11	694.81	33	39.25
LQDEIDEALPNK	Cyp3a11	692.85	33	27.27
QGIPGPKPLPFLGTVLNYYK	Cyp3a11	734.75	33	46.11
QGLLQPEKPIVLK	Cyp3a11	731.95	35	31.41
TWGLFDGQTPLLAVTDPETIK	Cyp3a11	768.07	35	47.20
VDFLQLMMNSHNNSK	Cyp3a11	593.28	27	43.17
ALLSPTFTSGR	Cyp3a13	575.32	27	31.36
ECYSTFTNR	Cyp3a13	583.73	28	26.08
FGPVGILK	Cyp3a13	415.76	19	34.25
GTVVMIPTFALHK	Cyp3a13	471.94	21	39.80
TDVEINGLFIPK	Cyp3a13	673.37	32	39.98
VDFLQLMINSQNYK	Cyp3a13	856.94	41	46.23
DSMNFFK	Cyp3a25	444.70	21	32.40
DVEINGVFIPK	Cyp3a25	615.84	29	36.65
EPIFQPEKPIILK	Cyp3a25	517.98	23	34.90
FFGPVGFMK	Cyp3a25	515.26	24	41.77
GNIDPYIYMPFGNGPR	Cyp3a25	905.93	43	43.40
GTVVMIPIYPLHR	Cyp3a25	499.29	22	40.68
LYPIAIR	Cyp3a25	423.27	20	31.42
NPEYWPEPQEFCPER	Cyp3a25	983.91	47	43.07
TLLSPTFTSGK	Cyp3a25	576.32	27	30.88
VDFLQLMMNTQNSK	Cyp3a25	556.94	25	45.47
EFGPVGIMSK	Cyp3a41	532.78	25	33.17
FDMECYEK	Cyp3a41	555.70	26	31.53
GSIDPYLYMPFGIGPR	Cyp3a41	594.97	27	46.13
VMQNFSFQPCQETQIPLK	Cyp3a41	728.68	33	43.08
AYLTVYDPDYMK	Cyp4a10	739.85	35	35.78
ELSTSVTFPDGR	Cyp4a10	654.83	31	29.14
FELLPDPTR	Cyp4a10	544.29	26	36.11

GSVQVDGNYR	Cyp4a10	547.76	26	16.35
HSHSFLPFSGGAR	Cyp4a10	467.23	20	28.49
TYLQAIGDLNNLFHSR	Cyp4a10	621.32	28	46.90
CAFSHEGSVQLDR	Cyp4a12a	498.89	22	26.32
DQDLQDILTR	Cyp4a12a	608.81	29	34.05
ELSSPVTFPDGR	Cyp4a12a	652.83	31	31.22
FLAPWIGR	Cyp4a12a	480.28	23	40.55
IQVYDPDYMK	Cyp4a12a	636.30	30	29.67
MLTPAFHYDILKPYTEIMADSVR	Cyp4a12a	678.59	32	44.73
NFPSACPQWLWGSK	Cyp4a12a	556.26	25	45.71
NIFHQNDIIYR	Cyp4a12a	478.25	21	29.59
SYIQAVEDLNDLVFSR	Cyp4a12a	934.97	45	47.34
VAVALTLLR	Cyp4a12a	478.32	22	39.29
GLLLLDGQTWFQHR	Cyp4a12b	561.97	25	44.41
AVEDLNNLTFFR	Cyp4a14	719.87	34	42.01
SQLQNEEELQK	Cyp4a14	673.33	32	17.60
VLLYDPDYVK	Cyp4a14	612.83	29	34.50
YNIIYNMSSDGR	Cyp4a14	716.83	34	32.22
AENVEVILTSSK	Cyp4v2	645.35	31	30.80
CLHTFTNNVIAER	Cyp4v2	521.92	23	29.06
FAVMEEK	Cyp4v2	427.21	20	22.53
HPYAYVPFSAGPR	Cyp4v2	487.91	21	30.37
MSDMIYR	Cyp4v2	458.21	22	23.73
NIGAQSNNDSEYVR	Cyp4v2	783.86	37	18.83
SLSEDCEVGGYK	Cyp4v2	666.78	32	29.39
VFPSVPLFAR	Cyp4v2	566.83	27	43.11
YLDCVIK	Cyp4v2	450.22	21	35.60
AGLGILPPLNDIEFK	Cyp7a1	798.95	38	45.84
FGSNPLEFLR	Cyp7a1	590.31	28	43.23
EVQEDMNLSLESK	Cyp7b1	761.36	36	28.20
MFLGIQHPDSAVSFR	Cyp7b1	568.96	25	36.15
VAQMQGQSK	Cyp7b1	488.75	23	7.08

Supplemental Table 10. Summary of proteins identified in mouse brain microsomes in present study and those previously noted in mouse brains in the literature

Mouse		
Proteins Identified	Previously Identified (mRNA or protein)	Reference(s)
Cyp1a1	mRNA	Yamaori et al., 2017
Cyp2c39	mRNA	Graves et al., 2017; Yamaori et al., 2017
Cyp2d10	mRNA	Yamaori et al., 2017
Cyp2d11		
Cyp2d26	mRNA	Yamaori et al., 2017
Cyp4a10	mRNA	Yamaori et al., 2017
Cyp7b1	mRNA	Stapleton et al., 1995
Ugt1a1	mRNA	Heydel et al., 2010
Ugt1a2	mRNA	Buckley and Klaassen, 2006; Heydel et al., 2010
Ugt1a5	mRNA	Buckley and Klaassen, 2006; Heydel et al., 2010
Ugt1a7	mRNA	Heydel et al., 2010
Ugt1a8	mRNA	Buckley and Klaassen, 2006
Ugt1a9		
Ugt1a10	mRNA	Buckley and Klaassen, 2006
Ugt2a1	mRNA	Buckley and Klaassen, 2006; Heydel et al., 2010
Ugt2a2	mRNA	Heydel et al., 2010
Ugt2a3	mRNA	Heydel et al., 2010
Ugt2b1	mRNA	Heydel et al., 2010
Ugt2b17		
Ugt2b34	mRNA	Heydel et al., 2010
Ugt2b35	mRNA	Buckley and Klaassen, 2006; Heydel et al., 2010
Ugt3a1	mRNA	Heydel et al., 2010

Supplemental Table 11. Summary of proteins identified in cynomolgus macaque brain microsomes in present study and those previously noted in cynomolgus macaque brains in the literature

Cynomolgus Macaque		
Proteins Identified	Previously Identified (mRNA or protein)	Reference(s)
CYP1A1	mRNA	Uno and Yamazaki, 2020
CYP1A2		
CYP1B1		
CYP2E1	mRNA	Uno and Yamazaki, 2020
CYP2F1		
CYP2R1		
CYP2U1		
CYP2W1		
CYP4F12		
CYP4F22		
CYP11B2		
CYP20A1		
CYP21A2		
CYP27A1		
CYP27C1		
UGT1A9	mRNA	Uno and Yamazaki, 2020
UGT1A10	mRNA	Uno and Yamazaki, 2020
UGT2B9	mRNA	Uno and Yamazaki, 2020
UGT2B20		

Supplemental Table 12. Summary of proteins identified in human brain microsomes in present study and those previously noted in human brains in the literature

Human		
Proteins Identified	Previously Identified (mRNA or protein)	Reference(s)
CYP1A2	mRNA	McFadyen et al., 1998
CYP2A6		
CYP2B6	protein	Gervot et al., 1999
CYP2C9	protein	Booth Depaz et al., 2015
CYP2E1	mRNA, protein	McFadyen et al. 1998; Upadhya et al., 2000
CYP2J2	mRNA	Dutheil et al., 2009
CYP3A4	mRNA	McFadyen et al., 1998
CYP4A11		
CYP4F3		
CYP4F12		
CYP20A1	mRNA	Stark et al., 2008
UGT1A1	mRNA	Court et al., 2012
UGT1A4	mRNA, protein	Court et al., 2012; Ghosh et al., 2010
UGT1A5	mRNA	Ohno and Nakajin, 2009
UGT1A6	mRNA, protein	Court et al., 2012; King et al., 1999
UGT1A8		
UGT2A1	mRNA	Jedlitschky et al., 1999
UGT2A2		
UGT2B4		
UGT2B7	protein	King et al., 1999
UGT2B17	mRNA	Ohno et al., 2009
UGT2B28		

Biotransformation of efavirenz and proteomic analysis of P450s and UGTs in mouse, macaque, and human brain-derived *in vitro* systems

Abigail M. Wheeler, Benjamin C. Orsburn, and Namandjé N. Bumpus

Drug Metabolism and Disposition

DMD-AR-2022-001195R1

Supplemental Table 2. Target peptide list for cynomolgus macaque P450s

Peptide	Protein	Precursor m/z	CE	RT
NFLPLLDAVSR	CYP11A1	415.57	18	44.12
AGSGNFSGDISDDLFR	CYP11A1	553.25	25	26.44
NFLPLLDAVSR	CYP11A1	622.85	30	44.1
LGNVESVYVIDPEDVALLFK	CYP11A1	1110.59	53	46.96
APSTVLPFEAIPQRPGNR	CYP11B2	488.27	22	28.28
LNPDVLSPK	CYP11B2	491.78	23	20.04
LNPDVLSPR	CYP11B2	505.79	24	39.97
NPALFPRPER	CYP11B2	598.83	28	44.75
LYPVGLFLER	CYP11B2	603.85	29	47.36
LQQVDSLHPHR	CYP11B2	665.35	32	45.02
QESLAAAASISEHPQK	CYP11B2	833.92	40	47.27
EQGYEHLHLEVHQTFQELGPIFR	CYP11B2	936.47	43	47.08
EFPNPEVFDPGHFLDESGNFK	CYP17A1	606.28	28	29.58
LYEEIDQNVGFSR	CYP17A1	785.38	38	30.86
FLNPAGTQLISPSLSYLPFGAGPR	CYP17A1	835.12	38	46.09
GTNIVPSLTSVLYDDK	CYP17A1	861.45	41	45.69
GTHVIINLWALHHNEK	CYP17A1	941.51	45	43.53
DFSGRPQVTTLDILSNNR	CYP17A1	1017.02	49	47.35
FDLEVPDDGQLPSLEGNPK	CYP17A1	1035.50	50	43.23
VWISGEETLIISK	CYP19A1	492.28	22	24.98
EIQTVVGER	CYP19A1	515.78	24	22.73
YFQPFGFGPR	CYP19A1	608.30	29	37.56
GIIFNNNPDLWK	CYP19A1	715.87	34	34.64
IQGYFDAWQALLIKPDIFFK	CYP19A1	805.10	37	44.21
VILFGLGK	CYP1A1	423.78	20	38.86
YGDVLQIR	CYP1A1	482.27	23	29.06
QLDENANIQLSDEK	CYP1A1	539.60	24	36.44
IQEELDTVIGR	CYP1A1	636.84	30	44.76
YLPNPALQR	CYP1A2	536.30	25	27.77

IGSTPVLVLSGLDTIR	CYP1A2	547.66	24	45.87
IGSTPVLVLSSLDTIR	CYP1A2	557.66	25	35.22
LSDRPQLPYLEAFILETFR	CYP1A2	577.81	27	23.46
NSHEFVESASSGNPVDFFPILR	CYP1A2	613.05	29	44.67
DTTLNGFYIPR	CYP1A2	648.83	31	48.43
DTTLNGFYIPR	CYP1A2	648.83	31	48.45
IGSTPVLVLSGLDTIR	CYP1A2	820.98	39	45.87
WEVFLFLAILLQQLEFSVPPGVK	CYP1A2	891.84	41	46.42
NFSNFVLDK	CYP1B1	542.28	26	22.66
WPNPENFDPAR	CYP1B1	671.81	32	41.43
AIHQALVQQGSAFADRPSFASFR	CYP1B1	835.43	38	43.44
ILPYTEAFISEVFR	CYP1D1	421.98	19	33.38
YLPLQIINAPR	CYP1D1	433.26	19	40.24
YDHSDEEFLK	CYP1D1	641.78	30	45.95
YLPLQIINAPR	CYP1D1	649.38	31	40.23
ALNGFIALHVQDHLATYDK	CYP1D1	709.37	32	29.22
SLSFSVNYGESWK	CYP1D1	752.36	36	39
NEIFIFITAVLQQLK	CYP1D1	889.02	43	46.09
EEAWITVSK	CYP20A1	531.78	25	23.94
TFSSLGFSGTR	CYP20A1	580.29	27	31.2
LYEEINQVFGNGPVTPEK	CYP20A1	678.68	31	45.6
QAAGIPGITPTEEK	CYP20A1	706.38	34	42.8
LYEEINQVFGNGPVTPEK	CYP20A1	1017.51	49	46.83
TWSHWSIQIVDVIPFLR	CYP21A2	699.71	32	44.49
WADFAGRPEPLTYK	CYP21A2	825.92	40	45.24
NYPDLSLGDYSLLWK	CYP21A2	892.45	43	46.47
LQEELDHELGPGASISR	CYP21A2	925.97	44	45.82
QHDTLVEYHK	CYP24A1	635.31	30	43.52
GHIEDLYSELNK	CYP24A1	709.35	34	29.37
EIQSVLPENQVPR	CYP24A1	754.91	36	46.08
NLFSLPIDVPFSGLYR	CYP26A1	613.33	27	47.5
IFSHEALESYLPK	CYP26B1	767.40	37	39.87
TVLQTFELDGFQIPK	CYP26B1	868.47	42	41.83
YLDGWNAIFSFGK	CYP27A1	759.37	36	48.14
DPEIQEALHEEVVGVVPAGQVPQHK	CYP27A1	902.47	41	45.19
VDNFGSIPFGHGVR	CYP27C1	751.38	36	49.72
ATGLISAEGEQWLK	CYP27C1	751.90	36	46.54
HVGFATIPPNYTMSFLPR	CYP2A13	683.35	31	42.64
GYGVVFSNGER	CYP2A23	592.79	28	26.58
IVVLCGYDAVK	CYP2A23	613.32	29	39.99
GEQATFDWLFK	CYP2A23	671.33	32	44.7

IQEEAGFLIEALR	CYP2A23	744.91	36	43.82
TVSNVISSIVFGDR	CYP2A23	747.40	36	45.19
DTQGANIDPTFFLSR	CYP2A23	841.41	40	41.27
NPNTEFYLK	CYP2A24	563.28	27	30.48
DTHGANIDPTFFLSR	CYP2A24	564.28	25	38.99
VSQGVVFSNGER	CYP2A24	639.83	30	41.95
GEQATFDWVFK	CYP2A24	664.32	32	42.56
FFSIPQDFNPQHFLDEK	CYP2A24	703.67	32	41.63
IQEEADFLIK	CYP2A26	603.32	29	33.49
HLPGPQQQAFK	CYP2A26	625.84	30	19.6
ELQGLEDFIAK	CYP2A26	631.83	30	39.27
GEQATFNWVFK	CYP2A26	663.83	32	41.53
YGPVFTIHLGPR	CYP2A26	678.87	32	37.3
FFSNPQDFNPQHFLDEK	CYP2A26	703.99	32	41.67
EALVDNAEAFSGR	CYP2B6	689.83	33	28.34
LPPGPCPLPLLGNLLQMDR	CYP2B6	697.37	32	51.47
IAITDPVFQGYGVVFANGNR	CYP2B6	713.37	32	43.85
ETLDPSAPQDLIDSYLLQMEK	CYP2B6	802.73	37	47.31
NLIINTLSLFFAGTETTSTTLR	CYP2B6	805.10	37	42.45
NLQEINAYIGHSVEK	CYP2B6	857.94	41	32.81
HRETLDPSAPQDLIDSYLLQMEK	CYP2B6	900.45	41	44.87
IAITDPVFQGYGVVFANGNR	CYP2B6	1069.56	51	43.89
YIDLIPTNLPHAVTCDVK	CYP2C18	686.68	31	44.81
LPSGPTPLPIIGNILQLDVK	CYP2C18	695.75	31	50.33
DIDITSIANAFGR	CYP2C18	696.86	33	44.6
VYGPVFTVYFGLKPIVVLHGYEAVK	CYP2C18	699.64	33	44.49
VPPLYHLCFIPV	CYP2C18	722.38	34	49.86
YIDLIPTNLPHAVTCDVK	CYP2C18	1029.52	49	43.49
ITNGLGIISSNGK	CYP2C20	637.36	30	28.45
YIDLVPTGVPHAVTTDIK	CYP2C20	647.02	29	37.65
VQEEIDHVIGR	CYP2C20	647.84	31	23.68
EHQATLDVNNPR	CYP2C20	697.34	33	45.26
LPPGPTPLPIIGNILQIDVK	CYP2C20	699.09	32	48.86
DFIDCFLMK	CYP2C75	589.26	28	47.76
VMEKLNENVK	CYP2C75	602.32	29	32.81
FDYKDQQFLK	CYP2C75	666.34	32	45.05
HNQQSEFTIENLENTAVDLFGAGTETTSTTLR	CYP2C75	881.92	42	47.42
HNQQSEFTIENLENTAVDLFGAGTETTSTTLR	CYP2C75	1175.56	54	48.75
GTTILTDLTSVLYDDKEFPNPEK	CYP2C76	649.83	31	46.49
GTTILTDLTSVLYDDKEFPNPEK	CYP2C76	866.11	40	46.53
GTTILTDLTSVLYDDK	CYP2C76	877.96	42	47.38

MELFLILTTILQNFTLKPLVDPK	CYP2C76	896.52	41	58.33
SRMPYTDAVVHEIQR	CYP2C76	901.45	43	45.27
GFGTIPPFYELCFIPV	CYP2C76	923.45	44	55.59
DNKEFPNPEMFDPR	CYP2C9	579.26	26	35.4
EHQESMDMNNPR	CYP2C9	744.30	36	35.75
ILSSPWIQIYNNFSPIIDYFPGTHNK	CYP2C9	766.89	36	50.59
LPPGPTPLPVIGNILK	CYP2C9	813.50	39	46.94
GKLPPGPTPLPVIGNILK	CYP2C9	906.06	43	44.78
ILSSPWIQIYNNFSPIIDYFPGTHNK	CYP2C9	1022.19	47	50.59
YPPGPLPLPGLGNLLHVDFK	CYP2D17	536.80	25	47.02
AVSNVIASLTYGR	CYP2D17	675.87	32	38.89
GTTLFTNLSSVLK	CYP2D17	690.89	33	44.19
YPPGPLPLPGLGNLLHVDFK	CYP2D17	715.40	32	47.07
GNPESSFNEENLR	CYP2D17	746.84	36	23.76
VQQEIDDVIGQVR	CYP2D17	749.90	36	31.17
AFLTQLDELLTEHR	CYP2D17	843.45	40	45.46
FVKPEAFLPFSAGR	CYP2D44	522.62	23	40.4
LLNLAQEGLK	CYP2D44	549.83	26	43.84
EVLNAVPLLLR	CYP2D44	618.89	29	43.66
DIEVQGFLIPK	CYP2D44	629.86	30	45.73
VQQEIDNVIGQVR	CYP2D44	749.40	36	31.19
IPGWAWWLTPVIPALWEAEAGGSPK	CYP2D8	683.86	32	40.08
SQGVFLAHGPAWR	CYP2D8	713.37	34	43.88
FKPEHFLDESGK	CYP2E1	478.57	21	23.93
FGPVFTLYVGSR	CYP2E1	671.86	32	43.03
GIIFNNRPTWK	CYP2E1	673.37	32	41.09
FKPEHFLDESGK	CYP2E1	717.36	34	46.57
FITLVPSNLPHEATR	CYP2E1	847.96	41	35.29
GTVIVPTLDSVLYDNQEFPDPEK	CYP2E1	859.43	39	44.55
GTVIVPTLDSVLYHNQEFPDPEK	CYP2E1	866.77	40	46.52
GDYPVFFNFTK	CYP2F1	667.82	32	35.97
ILEEGSFLLAELR	CYP2F1	745.42	36	45.14
YPEAFYPQHFLDEQGR	CYP2G2	499.99	23	36.24
YPEAFYPQHFLDEQGR	CYP2G2	666.31	30	36.24
EALVDQADEFSGR	CYP2G2	718.84	34	40.85
NFQGHGVALANGER	CYP2G2	735.37	35	43.44
YGNLFSLELGDISAVLITGLPLIK	CYP2J2	637.37	30	43.67
EATVDTTLAGYHLPK	CYP2J2	808.42	39	32.87
TCQLYNIFPWLMK	CYP2J2	851.91	41	51.19
FLPGPHQTLFSNWEK	CYP2J2	900.96	43	45.23
DPTEWATPDTFNPEHFLENGQFK	CYP2J2	907.41	42	45.46

ENLIFSVGELIIAGTETTTNVLR	CYP2R1	623.34	29	33.57
LWGGEEGAAALGGALFLLLFALGVR	CYP2R1	626.10	29	43.38
GTTVITNLYSVHFDEK	CYP2R1	912.46	44	46.52
EELTQELGSGQAPSLGDR	CYP2S1	629.64	28	35.3
EALGGQAEEFSGR	CYP2S1	675.82	32	39.48
QRPDHVLSGAAAAPAEDPPWPAR	CYP2U1	803.74	37	42.32
EALVQQAEVFSDRPR	CYP2U1	872.95	42	42.88
GGGIFFSSGAR	CYP2W1	528.27	25	40.21
QEAFLPFSAGR	CYP2W1	611.81	29	34.84
APLEFIEK	CYP39A1	473.77	22	30.85
YFPEPELFKPER	CYP39A1	517.93	23	35.97
HLLYPVTVNTLFNK	CYP39A1	553.65	25	40.48
LGIPGPTPLPFLGTILFYLR	CYP3A43	547.08	25	28.94
TLLSPAFTSVK	CYP3A43	582.34	28	26.59
RQGIPGPTPLPFLGNILSYR	CYP3A5	549.81	26	23.2
APATYDAMVQMEYLDMVVNETLR	CYP3A5	665.82	31	44.89
QGIPGPTPLPFLGNILSYR	CYP3A5	680.71	31	48.31
TQDGQLPVLTITDPDMIK	CYP3A5	993.02	48	42.45
GFWTFDMECYK	CYP3A8	736.79	35	45.49
LGGLLQTEKPIVLK	CYP3A8	754.97	36	33.5
NAISIAEDEEWKR	CYP3A8	780.89	37	28.77
GFWTFDMECYKK	CYP3A8	800.84	38	42.83
VWGFYDGRQPVLAITDPNMIK	CYP3A8	807.42	37	43.62
GVVVMIPSYALHHDPK	CYP3A8	881.97	42	32.4
LGIPGPTPLPLLGNILSYR	CYP3A8	996.09	48	49.27
NNDNIDPYIYTPFGSGPR	CYP3A8	1020.48	49	40.09
YLDFEDLGR	CYP46A1	564.27	27	36.05
LYPPAWGTFR	CYP46A1	604.32	29	30.24
AEQLVEILEAK	CYP46A1	621.85	30	33.63
TSVIITSPESVK	CYP46A1	630.86	30	30.42
LQAEVDEVIGSK	CYP46A1	644.34	31	31.77
LLEEETLIDGVR	CYP46A1	693.88	33	44.89
LLEEETLIDGVR	CYP46A1	693.88	33	44.89
NVFHQNDTIYSLTSTGR	CYP4A11	651.65	29	31.47
DSQSYIQAISDLNNLVFSR	CYP4A11	724.03	33	47.49
QEFQQDQELQR	CYP4A11	724.84	35	31.77
FLAPWIGYGLLLLNGQTWFQHR	CYP4A11	877.47	40	36.5
NAFHQNDTIYSLTSTGR	CYP4A11	962.96	46	29.48
QLSKPVTFVDGR	CYP4B1	673.87	32	32.97
HLDFLDILLGAR	CYP4B1	691.89	33	30.7
LVSFHYHNDFIYWLTPHGR	CYP4B1	801.40	37	40.69

TQGIDNFLK	CYP4F11	518.28	24	33.07
NQHVLVYPDFLYHLTPDGQR	CYP4F11	603.81	28	41.83
VTQLVATYPQGFK	CYP4F11	726.40	35	32.84
NQHVLVYPDFLYHLTPDGQR	CYP4F11	804.74	37	43.3
SITNASAAIAPK	CYP4F12	572.32	27	20.98
FLKPWLGEGILLSGGDK	CYP4F12	610.68	27	43.29
SPLAYVPFSAGPR	CYP4F22	454.58	20	44.87
VVVALTLLR	CYP4F22	492.33	23	27.51
LHHYLDFIYYR	CYP4F22	513.93	23	32.2
QQGAEAWLK	CYP4F22	515.77	24	26.76
FDPDNPQQR	CYP4F22	558.76	26	26.38
SPLAYVPFSAGPR	CYP4F22	681.36	32	43.56
TLDFIDVLLLSK	CYP4F45	459.61	20	48.74
VLTQLVATYPQGFR	CYP4F45	531.63	24	37.48
SPLAFIPFSAGPR	CYP4F45	680.37	32	43.56
TLDFIDVLLLSK	CYP4F45	688.91	33	48.75
TLPSQGVEDFLQAK	CYP4F45	766.90	37	38.3
LVHDFTDAVIQER	CYP4F45	771.90	37	29.51
VLTQLVATYPQGFR	CYP4F45	796.94	38	37.48
VLAWTYTFYDNSR	CYP4F45	818.39	39	44.13
HQQFLLHIDFLYYLTPDGQR	CYP4F45	835.43	38	42.09
FLEPWLGDGLLLSAGDK	CYP4F45	915.99	44	46.82
LHPPASFISR	CYP4F57	562.81	27	45.62
SITNASAATAPK	CYP4F57	566.30	27	36.71
FLKPWLGEGIILSNGDK	CYP4F57	629.68	28	33.37
EFFQQIIEYTEEYR	CYP4V2	632.30	28	48.01
ILHAFTNNVIAER	CYP4V2	749.41	36	31.24
EELGLEGQLILRPTNGIWIK	CYP4V2	760.43	35	38.23
NIGAQSNDDSEYVR	CYP4V2	784.35	37	19.12
LLLWGAASAVSLAGASLVLSLLQR	CYP4V2	803.81	37	45.22
AFLDLLLSVTDDEGNR	CYP4V2	889.45	43	46.09
LWVGPVPMVALYNAENVEVILTSSK	CYP4V2	910.49	42	52.19
LYSFLYHSDIIFK	CYP4X1	412.22	19	29.2
LLTPGFHFNILK	CYP4X1	467.27	20	46.5
VAIALILLHFR	CYP4X1	633.41	30	36.26
LLTPGFHFNILK	CYP4X1	700.41	33	29.69
YQDFLDIVLSAK	CYP4X1	706.38	34	40.01
QHVSIIEKETK	CYP51A1	656.37	31	38.55
LAAGHLVQLPAGAK	CYP51A1	673.40	32	30.27
NEDLNAEDVYSR	CYP51A1	712.82	34	23.18
SPVEFLENAYEK	CYP51A1	713.35	34	43.79

CIGENFAYVQIK	CYP51A1	715.84	34	37.5
AHILNNLDNFK	CYP7A1	649.85	31	46.5
GDGLKDLNETMLDSLSFVMLK	CYP8B1	582.30	27	48.15
MASGQEYLFR	CYP8B1	601.29	29	30.17
GTVPWLGYAMAFR	CYP8B1	734.87	35	46.07

Supplemental Table 3. Target peptide list for human P450s

Peptide Sequence	Protein	Precursor m/z	CE	RT
HSSFLPFTIPHSTTR	CYP1A2	432.73	20	35.36
DITGALFK	CYP1A2	432.74	20	34.25
CEHVQAR	CYP1A2	444.69	21	7.91
ELDTVIGR	CYP1A2	451.75	21	24.04
MMLFGMGK	CYP1A2	457.72	21	38.71
YGDVLQIR	CYP1A2	482.27	23	29.53
FLWFLQK	CYP1A2	491.28	23	45.31
YLPNPALQR	CYP1A2	536.30	25	24.89
IGSTPVLVLSR	CYP1A2	571.35	27	32.96
DTTLNGFYIPK	CYP1A2	634.83	30	36.3
VDLTPIYGLTMK	CYP1A2	675.87	32	41.71
FLTADGTAINKPLSEK	CYP1A2	852.96	41	27.38
LAQNALNTFSIASDPASSSSCYLEEHVSK	CYP1A2	1039.15	48	40.93
GRPDLYTSTLITDGQSLTFSTDSGPVWAAR	CYP1A2	1071.53	49	43.59
NTHEFVETASSGNPLDFFPILR	CYP1A2	1246.12	60	46.85
EEAWITVSK	CYP20A1	531.78	25	22.84
LVVSLGTVDVLK	CYP20A1	621.89	30	41.55
LTPVSAQLQDIEGK	CYP20A1	749.91	36	34.82
ETLVLYALGVVLQDPNTWPSPHK	CYP20A1	859.80	39	49.35
TLDPNSPR	CYP2A6	450.23	21	12.48
NCFGEGLAR	CYP2A6	506.72	24	30.24
NPNTEFYLK	CYP2A6	563.28	27	28.12
DFIDSFLIR	CYP2A6	563.30	27	45.82
NYTMSFLPR	CYP2A6	564.78	27	36.67
SDAFVPFSIGK	CYP2A6	584.31	28	39.18
GYGVVFSNGER	CYP2A6	592.79	28	26.97
FGDVIPMSLAR	CYP2A6	603.32	29	38.9
GEQATFDWVFK	CYP2A6	664.32	32	42.85
YGPVFTIHLGPR	CYP2A6	678.87	32	37.78

GTEVYPMLGSVLR	CYP2A6	711.38	34	41.64
EALVDQAEEFSGR	CYP2A6	725.84	35	30.4
IQEEAGFLIDALR	CYP2A6	737.90	35	43.79
TVSNVISSIVFGDR	CYP2A6	747.40	36	45.42
GTGGANIDPTFFLSR	CYP2A6	776.89	37	41.21
MPYMEAVIHEIQR	CYP2A6	808.90	39	41.64
MELFLFFTTVMQNFR	CYP2A6	962.48	46	43.35
LPPGPTPLPFIGNYLQLNTEQMYNSLMK	CYP2A6	1059.54	49	50.3
DPSFFSNPQDFNPQHFLNEK	CYP2A6	1204.55	58	43.52
FSVTTMR	CYP2B6	421.22	20	25.98
IAMVDPFFR	CYP2B6	548.29	26	42.77
GYGVIFANGNR	CYP2B6	584.30	28	29.91
TEAFIPFSLGK	CYP2B6	605.33	29	42.43
FHYQDQEFLK	CYP2B6	677.82	32	34.33
DLIDTYLLHMEK	CYP2B6	745.88	36	43.63
MPYTEAVIYEIQR	CYP2B6	806.91	39	40.2
NLQEINAYIGHSVEK	CYP2B6	857.94	41	33.16
LPPGPRPLPLLGNLLQMDR	CYP2B6	699.74	32	47.41
FSDLLPMGVPHIVTQHTSFR	CYP2B6	571.30	27	41.99
SNAHSEFSHQNLNLNTLSLFFAGTETTSTTLR	CYP2B6	885.44	42	45.97
IAENFAYIK	CYP2C18	534.79	25	30.08
DIDITPIANAFGR	CYP2C18	701.87	33	42.26
HFLDEGGNFK	CYP2C19	582.28	28	24.34
SNYFMPFSAGK	CYP2C19	624.79	30	37.55
NLAFMESDILEK	CYP2C19	705.35	34	41.15
IYGPVFTLYFGLER	CYP2C19	837.95	40	47.93
FNENFR	CYP2C8	413.70	19	20.32
GNSPISQR	CYP2C8	429.73	20	10.88
ICAGEGLAR	CYP2C8	468.23	22	23.58
GLGIISSNGK	CYP2C8	473.27	22	24.18
NLNTTAVTK	CYP2C8	481.27	23	15.08
DQNFLTLMK	CYP2C8	555.29	26	39.71
VQEEIDHVIGR	CYP2C8	647.84	31	23.92
EHQASLDVNNPR	CYP2C8	690.34	33	15.25
EALIDNGEEFSGR	CYP2C8	718.84	34	27.52
VQEEAHCLVEELR	CYP2C8	800.88	38	33.44
GIVSLPPSYQICFIPV	CYP2C8	889.96	43	46.31
VYGPVFTVYFGMNPIVVFHGYEAVK	CYP2C8	945.15	43	48.62
SEFNIENLVGTVADLFVAGTETTSTTLR	CYP2C8	995.84	46	56.43
GIFPLAER	CYP2C9	451.76	21	34.77
EHQESMDMNNPQDFIDCFLMK	CYP2C9	873.35	40	47.52

NLDTTPVVNGFASVPPFYQLCFIPV	CYP2C9	928.80	43	54.56
ILSSPWIQICNNFSPIIDYFPGTHNK	CYP2C9	1017.50	47	50.87
LPPGPTPLPVIGNILQIGIK	CYP2C9	1019.13	49	49.06
YIDLLPTSLPHAVTCDIK	CYP2C9	1023.03	49	44.52
HNQPSEFTIESLENTAVDLFGAGTETTSTTLR	CYP2C9	1156.23	54	48.03
LLDLAQEGLK	CYP2D6	550.32	26	33.29
MTWDPAQPPR	CYP2D6	599.79	28	27.97
AVSNVIASLTCGR	CYP2D6	668.84	32	42.3
DLTEAFLAEMEK	CYP2D6	698.84	33	44.7
GNPESSFNDENLR	CYP2D6	739.83	35	23.51
VQQEIDDVIGQVR	CYP2D6	749.90	36	32.78
FGDIVPLGVTHMTSR	CYP2D6	815.42	39	36.46
AFLTQLDELLTEHR	CYP2D6	843.45	40	45.3
EVLNAVPVLLHIPALAGK	CYP2D6	927.56	45	45.64
EALLDYK	CYP2E1	426.23	20	25.63
YPEIEEK	CYP2E1	454.22	21	19.25
LHEEIDR	CYP2E1	456.23	21	12.1
VCAGEGLAR	CYP2E1	461.22	22	20.78
YGLLILMK	CYP2E1	475.79	22	43.76
MVVMHGYK	CYP2E1	482.74	23	18.57
HFDYNDEK	CYP2E1	534.23	25	13.63
GDLPAFHAHR	CYP2E1	560.79	27	19.25
EAHFLLEALR	CYP2E1	599.83	28	36.72
GIIFNNGPTWK	CYP2E1	623.83	30	35.92
YSDYFKPFSTGK	CYP2E1	720.35	34	31.22
DLTDCLLVEMEK	CYP2E1	727.83	35	46.13
FGPVFTLYVGSQR	CYP2E1	735.89	35	42.98
EHHQSLDPNCPR	CYP2E1	739.82	35	40.32
FITLVPSNLPHEATR	CYP2E1	847.96	41	35.75
GTVVVPTLDSVLYDNQEFPDPEK	CYP2E1	854.76	39	44.34
LYTMDGITVTVADLFFAGTETTSTTLR	CYP2E1	975.49	45	51.91
MGNIIPLNVPR	CYP2J2	612.35	29	37.21
LLDEVTYLEASK	CYP2J2	690.87	33	35.17
EVTVDTTLAGYHLPK	CYP2J2	822.44	39	48.53
LFPIAMR	CYP3A4	424.25	20	35.52
EVTNFLR	CYP3A4	439.74	21	27.6
LQEEIDAVLPNK	CYP3A4	684.87	33	31.18
GFCMFDMECHK	CYP3A4	720.24	34	43.35
GVVVMIPSYALHR	CYP3A4	721.40	34	36.54
LSLGGLLQPEKPVVLK	CYP3A4	846.03	41	41.13
APPTYDTVLQMEYLDMVVNETLR	CYP3A4	900.11	41	49.22

LGIPGPTPLPFLGNILSYHK	CYP3A4	712.07	32	48.58
VWGFYDGQQPVLAITDPDMIK	CYP3A4	1197.10	58	45.9
FDFLDPFFLSITVFPFLIPILEVLNICVFPR	CYP3A4	930.25	44	46.57
SLGPVGFMK	CYP3A5	468.25	22	33.19
DTINFLSK	CYP3A5	469.25	22	31.36
DVEINGVFIPK	CYP3A5	615.84	29	36.63
LDTQGLLQPEKPIVLK	CYP3A5	896.53	43	49.73
DSIDPYIYTPFGTGPR	CYP3A5	899.94	43	42.25
LGIPGPTPLPLLGNVLSYR	CYP3A5	989.08	48	48.29
MWGTYEGQLPVLAITDPDVIR	CYP3A5	1187.61	57	46.92
VLQNFSFKPCK	CYP3A7	678.84	32	34.09
FNPLDPFVLSIK	CYP3A7	695.39	33	45.15
VATALTLLR	CYP4A11	479.31	23	35.71
LYPPVPGIGR	CYP4A11	534.81	25	32.31
FELLPDPTR	CYP4A11	544.29	26	36.05
VQLYDPDYMK	CYP4A11	636.30	30	31.03
ACQLAHQHTDQVIQLR	CYP4A11	636.32	29	27.29
ELSTPVTFPDGR	CYP4A11	659.84	31	31.2
HLDFLDILLLAK	CYP4A11	705.92	34	48.64
VWPNPEVFDPFR	CYP4A11	751.87	36	45.58
MLTPAFHYDILKPYVGLMADSVR	CYP4A11	879.79	40	44.9
NAFHQNDTIYSLTSAGR	CYP4A11	947.96	45	49.88
NSQSYIQAISDLNNLVFSR	CYP4A11	1085.05	52	47.19
SVNIMHDK	CYP4F11	472.24	22	14.95
FDQENIKER	CYP4F11	589.79	28	31.04
TLTQLVTTYPQGFK	CYP4F11	798.94	38	37.59
AEGGLWLRVEPLGANSQ	CYP4F11	898.97	43	45.5
ALSDEDIR	CYP4F12	459.73	22	37.68
FDPENSKGR	CYP4F12	525.25	25	35.81
SITNASAAIAPK	CYP4F12	572.32	27	21.26
VVLALTLLR	CYP4F2	499.34	24	44.24
SVINASAAIAPK	CYP4F2	571.33	27	25.32
HVTQDIVLPDGR	CYP4F2	675.36	32	24.75
NCIGQTFAMAEMK	CYP4F2	745.32	36	41.43
VLTQLVATYPQGFK	CYP4F2	782.94	37	37.43
VWMGPISPLLSLCHPDIIR	CYP4F2	1097.07	53	37.77
VVLGLTLLR	CYP4F3	492.33	23	43.06
LVHDFTDAVIQER	CYP4F3	771.90	37	29.35
LDMFEHISLMTLDSLQK	CYP4F3	1011.01	49	45.86
AFLDLLLSVTDDEGNR	CYP4V2	889.45	43	46.29
EFFQQIIEYTEEYR	CYP4V2	947.95	45	49.92

Supplemental Table 4. Target peptide list for mouse UGTs

Peptide Sequence	Protein	Precursor m/z	CE	RT
DYPRPIMPNMVFIGGINCLQK	Ugt1a1	818.0718	37.3	47.62
EGSFYTLR	Ugt1a1	486.7429	22.9	28.76
EVTVQDLLSPASIWLMR	Ugt1a1	979.5244	47	50.66
EVTVQDLLSPASIWLMR	Ugt1a1	653.352	29.4	50.47
KFPVPFQK	Ugt1a1	495.7922	23.3	29.49
LLVFPMDGSHWLSMLGVIQQLQQK	Ugt1a1	923.4924	42.3	51.09
LPCSLDSEATQCPVPLSYVPK	Ugt1a1	780.3645	35.5	46.43
MNFLQR	Ugt1a1	404.7103	18.8	28.05
SLSFNSDR	Ugt1a1	463.2223	21.7	21.06
TAFNQDSFLLR	Ugt1a1	656.3382	31.2	38.38
VVYSPYGSLATEILQK	Ugt1a1	884.48	42.3	44
VVYSPYGSLATEILQK	Ugt1a1	589.9891	26.3	43.91
SFDAVFLDPFDVCGLIVAK	Ugt1a10	701.3494	31.7	54.74
TPEQSIR	Ugt1a10	415.722	19.4	25.07
TYSVSHTLEDLDR	Ugt1a10	512.5827	22.6	44.17
TYSVSHTLEDLDREFK	Ugt1a10	647.3181	29.1	37.78
DVVRELHAR	Ugt1a2	547.8069	25.8	29.52
EEYQQEILSDIEK	Ugt1a2	812.3911	38.8	40.54
ELHARGHQTVVLASEVTVHIK	Ugt1a2	775.4326	35.2	44.68
GHQTVVLASEVTVHIK	Ugt1a2	573.3247	25.5	46.54
TQHFVKAFFETTASIR	Ugt1a2	941.9941	45.2	55.96
EEDFFTFKVYAVPYTR	Ugt1a5	1006.494	48.3	42.48
EEDFFTFKVYAVPYTR	Ugt1a5	671.3315	30.2	42.73
ELHAQGHQTVVLAPEVNMR	Ugt1a5	710.3689	32.1	28.22
IKEEDFFTFK	Ugt1a5	652.3321	31	33.33
QELEEMMENLK	Ugt1a5	465.2161	20.3	38.52
VYAVPYTR	Ugt1a5	484.7636	22.8	24.86
DSATLSFLR	Ugt1a6	505.2693	23.8	36.24

DVSLPSLHQNSLWLLR	Ugt1a6	626.6793	28.1	44.85
EIVEHLSER	Ugt1a6	556.2907	26.3	18.84
FSDHMTFPQR	Ugt1a6	422.5292	18.3	26.15
GFPCSLEHMLGQSPSPVSYVPR	Ugt1a6	812.0499	37	45.62
GHDIMVLVPEVNLLLGESK	Ugt1a6	688.3784	31	47.4
IFSVTYSLEELQTR	Ugt1a6	843.4409	40.3	44
LLVVPQDGSHWLSMK	Ugt1a6	570.6396	25.4	39.7
YEIIASDLLK	Ugt1a6	582.8292	27.6	39.97
EFKIFIDAQWK	Ugt1a7	712.8823	33.9	35.09
EFKIFIDAQWK	Ugt1a7	475.5906	20.8	34.95
SQQEGGILPLLDSPAK	Ugt1a7	826.9463	39.5	43.48
TYAVSHTQEDLNR	Ugt1a7	767.3682	36.6	28.45
TYAVSHTQEDLNREFK	Ugt1a7	646.6499	29	41.6
YFSLPSVVFSR	Ugt1a7	651.3481	30.9	46.91
GFFQVLFSHCR	Ugt1a8	693.8259	33	44.29
GHEVVVVIPEVSWHLGK	Ugt1a8	629.0159	28.2	24.18
HSGKGFFQVLFSHCR	Ugt1a8	898.4296	43	46.98
QRSFDAVFLDPFDVCGLTIAK	Ugt1a8	796.7291	36.2	42.96
GFFELTFSHCR	Ugt1a9	463.8741	20.3	43.95
GHEVVVVIPEVSWQLGK	Ugt1a9	626.0158	28	43.26
LLVVPMDGSHWFTMQMVVEK	Ugt1a9	783.0598	35.6	46.66
SFLTGSAR	Ugt1a9	419.7245	19.6	23.02
TPEHSIR	Ugt1a9	420.2221	19.6	8.03
TYSISHTLEDLDR	Ugt1a9	517.2546	22.8	34.29
YFSLPSVIFAR	Ugt1a9	650.3584	30.9	46.92
YLSYTQWK	Ugt1a9	544.7742	25.7	31.16
YTDTMTFK	Ugt1a9	503.7311	23.7	24.83
ALGRPTTLCETMGK	Ugt2a1	508.5841	22.4	30.33
EKIESVIK	Ugt2a1	473.2844	22.2	31.68
EMAKVIEEFHLVSR	Ugt2a1	563.2994	25	41.14
FSPASTVEK	Ugt2a1	483.2506	22.7	29.12
GICDGVLK	Ugt2a1	425.7117	19.9	34.45
LGIPFIYSLR	Ugt2a1	589.8502	27.9	38.72
ELGNLLATFYTTNK	Ugt2a2	528.9471	23.4	33.17
FSPAFTVER	Ugt2a2	527.2718	24.8	36.99
IPAPISYVPAALSELTDQMSFGER	Ugt2a2	864.772	39.5	43.61
LDAFINFEEIPVSYTKSK	Ugt2a2	701.0333	31.6	36.57
NHSVTVLAPSETLFINSR	Ugt2a2	993.0262	47.7	42.25
VKNIISYSLQDYIFK	Ugt2a2	916.0036	43.9	43.86
ANLIASVLAQIPQK	Ugt2a3	733.4405	34.9	46.86
ANLIASVLAQIPQK	Ugt2a3	489.2961	21.5	46.86

AVINEPSYK	Ugt2a3	510.7717	24	21.14
AVINEPSYKENAMR	Ugt2a3	541.2716	24	22.17
FSMGYYMEK	Ugt2a3	578.2461	27.3	33.6
GHEVTVLK	Ugt2a3	441.7558	20.6	15.6
KPATLGSNTR	Ugt2a3	522.7935	24.6	8.9
LFNWIPQNDLLGHPK	Ugt2a3	597.9895	26.7	43.69
TILEELGAR	Ugt2a3	501.2849	23.6	34.93
VSISTMTSTDLLSAVR	Ugt2a3	840.9455	40.2	43.1
VSISTMTSTDLLSAVR	Ugt2a3	560.9661	24.9	42.92
ADIWLVR	Ugt2b1	436.7531	20.4	36.61
DDLEYAFEK	Ugt2b1	565.256	26.7	31.25
FDGKKPDTLGSNTR	Ugt2b1	512.5986	22.6	14.39
ISSEYSDMIESFCK	Ugt2b1	842.8488	40.3	47.04
ISSEYSDMIESFCK	Ugt2b1	562.235	25	46.87
SWNQFYSDVLGRPTTLTEMMGK	Ugt2b1	854.4103	39	45.93
TPLVYSLR	Ugt2b1	474.7793	22.3	31.24
TVINDPSYKENAMR	Ugt2b1	546.6032	24.2	21.12
DNLENFFIK	Ugt2b17	570.2902	26.9	42.31
FETFPTSVSK	Ugt2b17	571.79	27	28.47
FETFPTSVSKDNLENFFIK	Ugt2b17	755.0476	34.2	44.94
FSPGYQIEK	Ugt2b17	534.7717	25.2	24.68
FVDVWTYEMPR	Ugt2b17	721.8423	34.4	43.34
GAAVALNIR	Ugt2b17	442.7693	20.7	26.5
SDVLNALEEVIENPFYK	Ugt2b17	660.6702	29.7	50.76
TPATLGHNTR	Ugt2b17	534.2833	25.2	10.37
ANVIAAGLAQIPQK	Ugt2b34	697.4117	33.2	36.03
ANVIAAGLAQIPQK	Ugt2b34	465.2769	20.3	36.03
FEGKKPETLGSNTR	Ugt2b34	521.9424	23.1	13.79
SRFDVILADPFIPCGDLLAEVLK	Ugt2b34	859.7867	39.3	35.62
TVTNDPSYKENAMR	Ugt2b34	542.5911	24	16.37
WIPQNDLLGHSK	Ugt2b34	469.9175	20.6	30.23
YSGGLPLPPSYVPVVMSELSDR	Ugt2b34	788.4032	35.8	47.87
AEMWFIR	Ugt2b35	476.7391	22.4	41.1
ANAISWALAQIPQK	Ugt2b35	755.9225	36	45.16
DYLETFLTK	Ugt2b35	565.2924	26.7	42.31
FDGKTPASLGPNTR	Ugt2b35	487.5879	21.4	20.98
FSPGYQVEK	Ugt2b35	527.7638	24.9	21.76
GTAVALNIR	Ugt2b35	457.7745	21.4	26.24
LSDYSLSLCKEAVSNK	Ugt2b35	901.9368	43.2	46.98
LVDEWTFEVPR	Ugt2b35	695.8537	33.1	42.32
SDLLNALEEVINNPSYK	Ugt2b35	959.9915	46	49.01

TPASLGPNTR	Ugt2b35	507.2724	23.9	16.37
FETFPTSVTK	Ugt2b37	578.7979	27.4	24.35
QLMTKLQESK	Ugt2b37	603.3316	28.6	33.69
AESFLLTMK	Ugt3a1	520.2783	24.5	37.55
EVIEDQR	Ugt3a1	444.7247	20.8	12.68
LIDEYAYGR	Ugt3a1	550.2746	26	25.82
LPEDQQK	Ugt3a1	429.2218	20	9.11
SKYHTLLK	Ugt3a1	495.2926	23.3	21.77
WHRLIDEYAYGR	Ugt3a1	526.9319	23.3	36.73
YKTAAMASK	Ugt3a1	485.755	22.8	37.42
AESFALTMK	Ugt3a2	499.2548	23.5	30.81
EILSQYDSTIQEHFVEGSQPVLSDLLLK	Ugt3a2	1063.55	49.1	46.9
HRLTEEITYGR	Ugt3a2	458.909	20	20.38
IMDWLPQTDLLAHPSIR	Ugt3a2	669.3558	30.1	44.71
LLYESANIPDFR	Ugt3a2	719.3723	34.2	38.34
LLYESANIPDFRK	Ugt3a2	522.6156	23.1	33.71
LTEEITYGR	Ugt3a2	541.2798	25.5	23.3

Biotransformation of efavirenz and proteomic analysis of P450s and UGTs in mouse, macaque, and human brain-derived *in vitro* systems

Abigail M. Wheeler, Benjamin C. Orsburn, and Namandjé N. Bumpus

Drug Metabolism and Disposition

DMD-AR-2022-001195R1

Supplemental Table 5. Target peptide list for cynomolgus macaque UGTs

Peptide Sequence	Protein	Precursor m/z	CE	RT
AMAIADALGK	UGT1A1	480.76	23	29.75
ESFVSLGHNVFENDSFLQR	UGT1A1	742.36	34	42.39
ESFVSLGHNVFENDSFLR	UGT1A1	699.67	32	43.05
EVTVQNLLSSASVWLLR	UGT1A1	639.03	29	50.91
GHEIVVLAPDASLYIGEGAFYTLK	UGT1A1	855.12	39	45.2
GHEIVVLAPDASLYIR	UGT1A1	876.99	42	39.42
TYPVPFQR	UGT1A1	504.27	24	28.47
ELLGFSDAMTFK	UGT1A10	679.84	32	42.96
TYATSYTLEDLDR	UGT1A10	516.58	23	13.84
GIFCHYLEEGAQCPAPLSYVPR	UGT1A10	848.05	39	45.54
GIFCHYLEEGAQCPAPLSYVPR	UGT1A10	636.29	30	45.58
LMLGHAQLYFETEHFLK	UGT1A2	520.02	24	41.03
VLVVPIDGSHWLSMR	UGT1A2	570.31	25	42.78
HLNATSFDVVLIDPIYLCGVVLAK	UGT1A2	662.36	31	46.46
GHQVVVLTPEVNMHIK	UGT1A5b	900.99	43	49.29
EVSVVDLFSHASVWLFR	UGT1A5b	664.35	30	42.59
MLVVPADGGHWLSMR	UGT1A5c	834.92	40	42.42
DIVEVLSDR	UGT1A6	523.28	25	34.08
DVDVITLYQK	UGT1A6	597.32	28	33.75
FSDHMTFPQR	UGT1A6	422.53	18	25.61
GHDIVVVVPEVNLLLK	UGT1A6	582.02	26	44.59
LLVIPQDGSHWLSMK	UGT1A6	575.31	26	40.71
SFLTAPQTEYR	UGT1A6	438.22	19	29.9
SPNPVSYIPR	UGT1A6	565.30	27	30.65
VSVWLLR	UGT1A6	436.77	20	39.65
YDELASAVLK	UGT1A6	554.80	26	31.51
YQLFGNNHFAER	UGT1A6	499.24	22	30.74
LLVVPMDGSHWFTMR	UGT1A7	596.97	27	34.77

LLVVPMDGSHWFTMQSVVEK	UGT1A8	768.39	35	44.54
EFMTFAHAQWK	UGT1A8	465.89	20	26.71
AFAQAQWK	UGT1A9	475.25	22	23.96
GHEVVVVMPK	UGT1A9	547.80	26	23.49
ILLGFSDAMTFK	UGT1A9	671.86	32	44.12
LLVVPVDGSHWLSMR	UGT1A9	570.31	25	42.75
NHIMHLEER	UGT1A9	589.79	28	15.47
YLSLPSVVFAR	UGT1A9	626.36	30	43.67
ESSFDAVFLDPFDTCGLIVAK	UGT1A9	1160.55	56	51.06
ESSFDAVFLDPFDTCGLIVAK	UGT1A9	774.03	35	50.98
VPYPPSYVPAVLSELTDQMSFTDR	UGT2A1	678.84	32	45.79
NFISYHLQDYMFETLWK	UGT2A1	559.52	26	26.75
ELGNLLDTFFQINMQICDGVLNNPK	UGT2A2	577.28	27	34.15
ANLIASALAQIPQK	UGT2A2	719.42	34	42.78
ANLIASALAQIPQK	UGT2A2	479.95	21	42.87
AFITHGGMNGVYEAIYHGVPMVGVPIFGDQPDNIAHMK	UGT2A3	817.40	39	45.42
ANIIASALAQIPQK	UGT2A3	719.42	34	42.86
FEVVHMPQDK	UGT2A3	410.54	18	25.77
GAAVEINFK	UGT2A3	474.76	22	28.29
GHEVTVLTHSK	UGT2A3	403.22	17	13.32
IHHDQSVKPLDR	UGT2A3	482.26	21	10.95
LNDFFVEIR	UGT2A3	576.81	27	41.17
LPAPLSYVPVPMTR	UGT2A3	514.29	23	43.37
LYDWIPQNDLLGHPQTK	UGT2A3	510.27	24	40.23
TSLGGNMER	UGT2A3	482.73	23	15.97
VILEELIVR	UGT2A3	542.34	26	41.53
SFLIDYR	UGT2A3	457.24	21	34.06
NSMLSVFFHFWIQDYDYDFWK	UGT2A3	930.09	43	45.48
TMTSEDLLR	UGT2A3	533.27	25	27.15
AFITHGGSNGIYEAIYHGVPMVGIPLFADQPDNIAHMK	UGT2B18	817.01	39	45.42
EMEEFVQSSGENGVVVFSLGSMVTNMK	UGT2B18	979.12	45	46.46
LDFDTMSSTDLVNALK	UGT2B18	885.43	42	43.66
WDQFYSEVLGRPTTLSETMGK	UGT2B18	815.73	37	41.45
FTPGYNFEK	UGT2B18	551.76	26	27.08
AFITHGGANGIYEAIYHGIPMVGVPLFADQPDNIAHMK	UGT2B19	813.81	39	45.81
DQMTFMER	UGT2B19	529.23	25	27.31
GHEVTVLAYSTSILPDPNNPSPLK	UGT2B19	850.45	39	41.62
HGGGFLFPPSYVPVTMSELR	UGT2B19	731.04	33	44.37
LDFDTMSSTDLLNALK	UGT2B19	595.30	27	45.47
TVINDPIYK	UGT2B19	531.80	25	27.94
VLGRPTTLFEIMAK	UGT2B19	525.97	23	41.65

VQNMIYMVYFDFWFQVWDVK	UGT2B19	665.32	31	42.86
ANMIASALAQIPQK	UGT2B20	485.94	21	41.01
FEVYPTSLTK	UGT2B20	592.81	28	31.94
GAALSVDIR	UGT2B20	451.26	21	26.58
IHHDQPMKPLDR	UGT2B20	496.26	22	13
KPNTLGSNTR	UGT2B20	544.30	26	7.88
NDMEDSLMK	UGT2B20	541.73	26	24.78
NGGGFLFPPSYVPVVMSELSDQMTFTER	UGT2B20	1035.83	48	50.81
SVINEPIYK	UGT2B20	531.80	25	25.82
TILEELVR	UGT2B20	486.79	23	39.03
VLVWPTEYSHWINMK	UGT2B20	634.99	29	43.78
WDQFYSEVLGRPTTLFETMR	UGT2B20	826.07	38	45.31
LLDIWTYSISNSTFLSYFSK	UGT2B20	597.06	28	33.21
FTVGYTFEK	UGT2B20	546.27	26	32.08
DQPVKPLDR	UGT2B23	534.30	25	14.64
EMEEFVQSSGENGVVVFTLGSMITNMK	UGT2B23	988.47	45	48.47
HTTLSEIMGK	UGT2B23	558.79	26	26.12
IEVFPTSLPKPEFENIVTQEIK	UGT2B23	853.46	39	44.26
WDQFYSEVLGR	UGT2B23	700.34	33	39.66
AFITHGGANGIYEAIYHGIPMVGVPLFADQLDNIAHMK	UGT2B30	817.02	39	47.87
DTFWLYFSQIQEIMWR	UGT2B33	721.68	33	40.75
EMEEFVQSSGENGVVVFSLGSMVTNMEEER	UGT2B9	1117.50	52	47.34
TEFENISMQEVK	UGT2B9	485.57	21	30.52
DTFWLYFSQMQEIMWR	UGT2B9	1091.00	53	47.85
FTPGYIFEK	UGT2B9	551.28	26	35.15
LDFDTMSSTDLANR	UGT2B9	529.24	23	32.45
MHSAFSHLPQGVIWK	UGT3A1	435.23	20	34.31
SAVAAASVILR	UGT3A1	529.32	25	31.6
HFNSYIETALDGR	UGT3A1	508.25	22	34.06
LVKPFVAILPTR	UGT3A1	451.96	20	37.48
SQWDLLSTFDNTIK	UGT3A1	834.42	40	45.61

Biotransformation of efavirenz and proteomic analysis of P450s and UGTs in mouse, macaque, and human brain-derived *in vitro* systems

Abigail M. Wheeler, Benjamin C. Orsburn, and Namandjé N. Bumpus

Drug Metabolism and Disposition

DMD-AR-2022-001195R1

Supplemental Table 6. Target peptide list for human UGTs

Peptide Sequence	Protein	Precursor m/z	CE	RT
DGAFYTLK	UGT1A1	457.73	21	28.57
TYPVPFQR	UGT1A1	504.27	24	28.16
GHEIVVLAPDASLYIR	UGT1A1	584.99	26	39.16
EVTVQDLLSSASVWLFR	UGT1A1	650.68	29	52.32
ILLIPVDGSHWLSMLGAIQQLQQR	UGT1A1	679.88	32	48.98
ESFVSLGHNVFENDSFLQR	UGT1A1	742.36	34	42.2
SMAMLNNMSLVYHR	UGT1A3	556.27	25	36.83
LLTTNSDHMTFMQR	UGT1A3	565.60	25	29.4
VLVVPIDGSHWLSMR	UGT1A3	570.31	25	42.69
EVSVVDILSHASVWLFR	UGT1A3	653.02	29	50.87
YLSIPTVFFLR	UGT1A3	678.39	32	47.79
FFTLTAYAVPWTQK	UGT1A4	558.30	25	45.06
YIPCDLDFK	UGT1A4	580.26	27	42.47
EVSVVDLVSYASVWLFR	UGT1A4	657.02	30	54.35
YLSIPAVFFWR	UGT1A4	699.88	33	48.67
GTQCPNPSSYIPK	UGT1A4	719.33	34	33.84
CCVELLHNEALIR	UGT1A4	802.87	38	41.41
VLVVPTDGSPWLSMR	UGT1A4	828.94	40	43.08
EVSVVDLVSHASVWLFR	UGT1A5	486.52	22	30.9
VLVVPTDGSHWLSMREALR	UGT1A5	542.29	25	44.36
SFLTAPQTEYR	UGT1A6	438.22	19	29.58
DTLNFFK	UGT1A6	442.73	21	35.73
GFPCSLEHTFSR	UGT1A6	476.21	21	38.03
YQSFGNNHFAER	UGT1A6	490.56	22	21.31
DIVEVLSDR	UGT1A6	523.28	25	33.85
SPDPVSYIPR	UGT1A6	565.80	27	30.82
LLVVPQDGSHWLSMK	UGT1A6	570.64	25	38.69
GHEIVVVVPEVNLLLK	UGT1A6	586.69	26	44.41

NNMIVIGLYFINCQSLLQDR	UGT1A6	600.80	28	43.62
FSDHMTFSQR	UGT1A6	628.28	30	22.94
ESSFDAVFLDPFDACGLIVAK	UGT1A8	764.03	35	44.24
GIACHYLEEGAQCPAPLSYVPR	UGT1A8	822.71	38	47.98
NHIMHLEEHLLCHR	UGT1A9	457.72	21	28.2
AFAHAQWK	UGT1A9	479.75	23	18.85
LLVVPMDGSHWFTMR	UGT1A9	596.97	27	43.89
ESSFDAVFLDPFDNCGLIVAK	UGT1A9	778.37	35	49.7
GILCHYLEEGAQCPAPLSYVPR	UGT1A9	836.72	38	45.25
FYQEMAK	UGT2A1	458.72	22	42.83
DFVLTWLENRPSPSTIWR	UGT2A1	739.72	34	40.02
FSPASTVER	UGT2A2	497.25	23	12.74
GGFDVLVADPVTICGDLVALK	UGT2A2	537.78	25	39.01
IPAPVSYVPAALSELTDQMTFGER	UGT2A2	648.83	30	43.45
NGVVVFSLGSMVKNLTEEK	UGT2A2	684.37	31	36.81
ANLIASALAQIPQK	UGT2A2	719.42	34	42.61
FPHPFLPNVDFVGGLHCKPAKPLPK	UGT2B10	561.10	26	41.08
HSGGFIFPPSYVPVVMSK	UGT2B10	650.34	29	42.44
GHEVTVLASSASILFDPNDSSTLK	UGT2B10	830.09	38	42.53
FEVYPTSLTK	UGT2B11	592.81	28	35.58
AVFWIEFVMPHK	UGT2B11	752.39	36	41.78
WIYGVSK	UGT2B15	426.73	20	27.22
IHHDQPMKPLDR	UGT2B15	496.26	22	12.89
SVINDPVYK	UGT2B15	517.78	24	23.66
FSVGYTFEK	UGT2B15	539.27	25	31.75
NYLEDSLLK	UGT2B15	547.79	26	34.44
ENVMKLSRIHHDQPMKPLDR	UGT2B15	815.43	37	49.13
WTYSISK	UGT2B17	442.73	21	25.66
GHEVIVLTSSASILVNASK	UGT2B17	482.02	22	36.2
FSVGYTVEK	UGT2B17	515.27	24	26.27
SVINDPIYK	UGT2B17	524.79	25	26.53
NDLEDFFMK	UGT2B17	579.76	27	42.05
WIPQNDLLGLPK	UGT2B28	465.27	20	45.88
LSIIQHDQPVKPLHR	UGT2B28	594.34	27	35.1
ADIWLIR	UGT2B4	443.76	21	38.75
ANVIASALAK	UGT2B4	479.29	23	28.28
TEFEDIIK	UGT2B4	497.76	23	31.91
IPFVYSLR	UGT2B4	497.79	23	38.02
FSPGYAIEK	UGT2B4	506.26	24	24.59
TILDELVQR	UGT2B4	543.81	26	38.18
FEVYPVSLTK	UGT2B4	591.82	28	35.55

VLVWPTEFSHWMNIK	UGT2B4	629.66	28	45.75
GAAVSLDFHTMSSTDLLNALK	UGT2B4	731.04	33	43.99
FDVVLADAVFPFGELLAELLK	UGT2B4	769.43	35	43.15
GHEVTVLASSASISFDPNSPSTLK	UGT2B4	815.41	37	35.71
ADVWLIR	UGT2B7	436.75	20	37.33
VDFNTMSSTDLLNALK	UGT2B7	442.98	20	25.17
VINDPSYK	UGT2B7	468.25	22	16.07
WIPQNDLLGHPK	UGT2B7	473.26	21	31.45
IQHDQPVKPLDR	UGT2B7	482.60	21	15.09
TELENFIMQQIK	UGT2B7	498.59	22	45.1
FDGNKPDTLGLNTR	UGT2B7	516.60	23	24.54
TILDELIQR	UGT2B7	550.82	26	42.57
IEIYPTSLTK	UGT2B7	582.83	28	32.89
VLVWAAEYSHWMNIK	UGT2B7	616.32	28	44.87
ANVIASALAQIPQK	UGT2B7	712.42	34	41.53
HSGGFIFPPSYVPVVMSELTDQMTFMER	UGT2B7	801.38	38	51.78
GHEVTVLASSASILFDPNNSSALK	UGT2B7	819.76	37	43.84
DTFWLYFSQVQEIMSIFGDITR	UGT2B7	899.44	41	57.37
AFITHGGANGIYEAIYHGIPMVGIPLFADQPDNIAHMK	UGT2B7	1020.51	49	47.52
NYGVSIR	UGT3A1	404.72	19	21.03
SYQVISWLAPEDHQR	UGT3A2	610.30	27	38.68

Supplemental Table 7. Fragment ions detected for each peptide observed in mouse brain microsomes

Mouse Brain Microsomes			
Protein	Peptide	Fragment Ions	Fraction
Cyp1a1	SEVFLFLAILLQQIEFK	y3, y4, b3, b5, b6, b8	5
Cyp2c39	INNGLGIVFSNGNR	y5, y6, y7, y8, y9, y10, y11, y12, y13, b6, b7, b8, b9, b11	4
Cyp2d10	MPYTNAVIHEVQR	y3, y4, y5, y6, y7, y8, y9, y10, b3, b4, b5, b6, b7, b8, b9, b10	3
Cyp2d10	SCLGEPLAR	y3, y4, y5, y6, y7, y8, b3, b4, b5, b7, b8	3
Cyp2d11	GNPESSFNDENLR	y3, y4, y5, y6, y7, y8, y9, y10, b4, b5, b6, b7, b8, b9	1
Cyp2d26	DLTDAFLAEVEK	y3, y4, y5, y6, y7, y8, y9, b3, b4, b5, b6, b7, b8, b9	2
Cyp4a10	TYLQAIGDLNNLFHSR	y3, y4, y5, y6, y7, y8, b4, b5, b8, b9, b10, b11, b12	8
Cyp7b1	EVQEDMNLSLESK	y5, y6, y7, y8, y9, y10, y11, b5, b6, b7	1
Cyp7b1	MFLGIQHPDSAVSFR	y3, y4, y5, y6, y7, y8, y9, b4	6
Cyp7b1	VAQMQGQSK	y3, y4, y5, y6, y7, y8, b3, b4, b5, b7, b8	2
Ugt1a1	DYPRPIMPNMVFIGGINCLQK	y5, y6, y7, y8, y9, y10, y11, y12, b4, b6, b7, b9, b10, b11, b12	1
Ugt1a1	EVTVQDLLSPASIWLMR	y3, y4, y6, y7, y8, y9, b4, b5, b6, b7, b8, b9	1
Ugt1a2	EEYQQEILSDIEK	y3, y4, y5, y6, y7, y8, y9, y10, y11, y12, b3, b4, b5, b6, b7, b8, b9, b10, b11, b12	4
Ugt1a2	ELHARGHQTVVLASEVTVHIK	y3, y4, y5, y6, y7, y8, ,y9, b3, b4, b5, b6, b8, b9, b10, b11, b12	3
Ugt1a5	IKEEDFFTFK	y3, y4, y5, y6, y7, y8, y9, b4, b5, b6, b7, b8, b9	4
Ugt1a7	EFKIFIDAQWK	y4, y5, y6, y7, y8, y10, b4, b5, b6, b7, b8, b9, b10	4
Ugt1a7	SQQEGGILPLLDSPAK	y3, y4, y5, y6, y7, y8, y9, y12, y13, y14, b3, b4, b5, b6, b7, b8, b9, b10, b11, b12, b13, b14, b15	4
Ugt1a7	TYAVSHTQEDLNR	y4, y5, y6, y7, y9, y10, y11, y12, b6, b7, b8, b9, b10, b11, b12,	1

Ugt1a8	QRSFDAVFLDPFDVCGLTIAK	y3, y5, y6, y7, y8, y9, y10, y11, y12, y13, y14, y15, b3, b4, b5, b6, b7, b8, b9, b10, b11, b13	4
Ugt1a9	GHEVVVVIPEVSWQLGK	y3, y4, y5, y6, y7, y8, y9, b5, b6, b7, b8, b10	1
Ugt1a10	TYSVSHTLEDLDR	y3, y4, y5, y6, y7, y9, y11, b4, b5, b6, b7, b8	4
Ugt2a1	ALGRPTTLCETMGK	y3, y4, y5, y6, y7, y9, b4, b5, b6, b9	2
Ugt2a1	EKIESVIK	y3, y4, y5, y6, y7, b3, b4, b5, b6, b7	6
Ugt2a1	EMAKVIEEFHLVSR	y3, y4, y5, y6, y7, b4, b5, b6, b7, b8, b9, b10, b11	4
Ugt2a1	FSPASTVEK	y3, y4, y5, y6, y7, y8, b3, b4, b5, b6, b7, b8	2
Ugt2a1	GICDGLVK	y3, y4, y5, y6, y7, b3, b4, b5, b6, b7	4
Ugt2a1	LGIPFIYSLR	y3, y4, y5, y6, y7, y9, b3, b4, b5, b6, b8, b9	3
Ugt2a2	IPAPISYVPAALSELTDQMSFGER	y3, y4, y5, y6, y7, y8, y9, y10, y11, y12, y13, y15, b7, b8, b9, b10, b11, b12	4
Ugt2a3	VSISTMTSTDLLSAVR	y3, y4, y5, y6, y7, y8, y9, y10, y11, y12, b3, b4, b5, b6, b7, b12	1
Ugt2b1	VDFDTMSTTDLLTALK	y4, y5, y6, y7, y8, y9, y10, y11, y12, y13, y14, b4, b5, b6, b7, b8, b9, b10, b11, b12	1
Ugt2b17	SDVLNALEEVIENPFYK	y3, y4, y5, y6, y7, y8, y9, y10, y11, y12, b5, b6, b7, b8, b9, b10, b11, b12, b13	1
Ugt2b34	LDFLTMSSTDHLTALK	y4, y5, y6, y7, y8, y9, y10, y11, y12, b4, b5, b6, b7, b9	1
Ugt2b34	SRFDVILADPFIPCGDLLAEVLK	y6, y9, y10, y11, y12, b6, b7, b8, b9, b10, b11, b12	4
Ugt2b35	LSDYSLSLCKEAVSNK	y3, y4, y5, y6, y7, y8, y9, y10, y11, y12, y13, y14, y15, b3, b4, b5, b6, b7, b8, b9, b10, b11, b12, b13, b14, b15	3
Ugt3a1	SKYHTLLK	y4, y7, b3, b4, b5, b6, b7	2

Supplemental Table 8. Fragment ions detected in peptides observed in macaque brain microsomes

Macaque Brain Microsomes			
Protein	Peptide	Fragment Ions	Fragment
CYP1A1	YQDVLQIR	y2, y3, y4, y6, y7, b3, b4, b5, b6, b7	1
CYP1A2	DTTLNGFYIPR	y3, y4, y5, y6, y7, y8, y9, y10, b5, b6, b7, b8, b9, b10	8
CYP1A2	YLPNPALQR	y3, y4, y5, y6, y7, y8, b3, b4, b5, b6, b7, b8	5
CYP1B1	NFSNFVLDK	y3, y4, y5, y6, y7, y8, b3, b4, b5, b6, b7, b8	4
CYP2E1	GTTVIVPTLDSVLYDNQEFPDPEK	y3, y5, y6, y7, y8, y9, y10, y11, y12, y13, y14, y15, b5, b7, b8, b9, b10, b11, b12, b14	4
CYP2F1	ILEEGSFLLAELR	y5, y6, y7, y12, b6, b7, b8, b9, b12	1
CYP2R1	GTTVITNLYSVHFDEK	y3, y4, y5, y6, y7, y8, y9, y10, y11, y12, y13, y14, b3, b4, b5, b6, b7, b8, b9, b10, b11, b12, b13, b15	5
CYP2U1	EALVQQAEVFSDRPR	y5, y6, y7, y8, y9, y10, y11, y12, y14, b7, b8, b9, b10, b11, b12, b13, b14	5
CYP2W1	GGGIFFSSFAR	y4, y5, y6, y7, y8, y9, b4, b5, b6, b7, b8, b9, b10	4
CYP4F12	SITNASSAIAPK	y5, y6, y7, y8, y9, b5, b6, b7, b8, b9, b10, b11	4
CYP4F22	SPLAYVPFSAGPR	y5, y6, y8, y9, y11, b5, b6, b7, b9, b10, b11	1
CYP11B2	EQGYEHLHLEVHQTFQELGOIFR	y4, y10, y11, y13, b11	8
CYP20A1	EEAWITVSK	y3, y4, y5, y6, y7, y8, b3, b4, b5, b6, b7, b8	1
CYP20A1	LYEEINQVFGNGPVTPEK	y3, y5, y6, y7, y8, y9, y10, y11, b4, b5, b6, b7, b8, b9, b10	4
CYP20A1	TFSSLGFSGTR	y4, y5, y6, y7, y8, y9, y10, b4, b5, b6, b7, b8, b9, b10	7
CYP21A2	WADFAGRPEPLTYK	y5, y6, y7, y8, y9, y10, y11, y12, y13, b6, b7, b8, b9, b10, b11, b13	4
CYP27A1	YLDGWNAIFSFGK	y5, y6, y7, y8, y9, y10, y11, y12, b5, b6, b7, b8, b9, b10, b11, b12	8
CYP27C1	ATGLISAEGEQWLK	y4, y5, y6, y7, y8, y9, y10, y11, y12, y13, b7, b8, b9, b10, b11, b12, b13	4

UGT1A9	ESSDAVFLDPFDTCGLIVAK	y6, y7, y8, y9, y10, y11, y12, b6, b7, b8, b9, b10, b13	1
UGT1A10	TYATSYTLEDLDR	y3, y4, y5, y6, y9, b3, b4, b5, b6, b7, b8	1
UGT2B9	DTFWLYFSQMQEIMWR	y6, y7, y8, b7, b8	4
UGT2B20	FTVGYTFEK	y3, y4, y5, b3, b4	7

Biotransformation of efavirenz and proteomic analysis of P450s and UGTs in mouse, macaque, and human brain-derived *in vitro* systems

Abigail M. Wheeler, Benjamin C. Orsburn, and Namandjé N. Bumpus

Drug Metabolism and Disposition

DMD-AR-2022-001195R1

Supplemental Table 9. Fragment ions detected in peptides observed in human brain microsomes

Human Brain Microsomes			
Protein	Peptide	Fragment Ions	Fraction
CYP1A2	GRPDLYTSTLITDGQSLTFSTDSGPVWAAR	y4, y5, y10, b5, b6, b8	5
CYP2A6	MELFLFFTTVMQNFR	y3, y4, y5, y7, y10, b5, b6, b8, b9, b10	5
CYP2B6	DLIDTYLLHMEK	y3, y4, y5, y8, y10, b4, b5, b8, b10	5
CYP2D6	AFLTQLDELLTEHR	y3, y4, y5, y6, y10, b3, b4, b6, b7, b8	5
CYP2E1	EHHQSLDPNCPR	y4, y8, y9, b3, b4, b6, b7, b8, b9	4
CYP2E1	LYTMDGITVTVADLFFAGTETTSTTLR	y3, y4, y5, y6, y7, y8, y9, y10, y11, y12, y13, b3, b4, b5, b6, b7, b8, b9, b10, b13, b14, b15	1
CYP2J2	EVTVDTTLAGYHLPK	y5, y6, y7, y8, y10, y11, b3, b4, b5, b7, b8, b9, b10, b13	3
CYP3A4	APPTYDTVLQMEYLDMVVNETLR	y6, y7, y8, y9, y10, y11, y12, y13, b7, b8, b9, b10, b11, b12, b13, b14	1
CYP3A4	FDFLDPFFLSITVFPFLIPILEVLNICVFPR	y6, y7, y8, y9, y10, y11, y12, y13, y14, b5, b6, b7, b8, b9, b10, b11, b12, b13, b14	3
CYP3A4	VWGFYDGQQPVLAITDPDMIK	y5, y6, y7, y8, y9, y10, y11, y12, y13, b5, b6, b7, b8, b9, b10, b11, b12, b13	1
CYP4A11	VWPNPEVFDPFR	y6, y7, y9, y11, b4, b5, b6, b7, b8, b9	5
CYP4F3	VVLGLTLLR	y4, y5, y6, y7, b4, b5, b7	8
CYP4F12	FDPENSKGR	y4, y5, y7, y8, b4, b6	5
CYP20A1	EEAWITVSK	y4, y5, y6, y7, y8, b3, b4, b5, b6	1
CYP20A1	LVVSLGTVDVLK	y5, y6, y7, y8, y9, y10, b4, b5	5
UGT1A1	EVTVQDLLSSASVWLFR	y3, y4, y5, y6, y7, y8, y9, y10, b4, b5, b6, b7, b8	1
UGT1A1	ILLIPVDGSHWLSMGAIQQLQQR	y5, y6, y7, y9, y10, y12, b4	1
UGT1A4	EVSVVDLVSYASVWLFR	y3, y4, y5, y6, y7, y8, y9, b5, b6, b7, b8, b9	1
UGT1A5	EVSVVDLVSHASVWLFR	y3, y4, y6, y7, y8, b4, b5, b6, b7, b8, b10	8
UGT1A6	DIVEVLSDR	y3, y4, y5, y6, y7, b3, b4, b5, b6	1
UGT1A6	NNMIVIGLYFINCSLLQDR	y4, y7, y8, y9, b4, b5, b6, b7, b8, b10, b12	5
UGT1A8	ESSFDAVFLDPFDACGLIVAK	y8, y9, y10 ,y11, b4, b5, b6, b7, b8, b9, b10, b11, b14	5

UGT2A1	DFVLTWLENRPSPSTIWR	y4, y5, y6, y7, y8, y9, y10, y11, b4, b5, b6, b7, b8, b11	3
UGT2A2	FSPASTVER	y3, y4, y5, y6, y7, y8, b4, b5, b6, b7, b8	2
UGT2B4	FDVVLADAVFPFGELLAELLK	y4, y5, y6, y8, y9, y10, y11, b4, b5, b6, b7, b8, b9, b10, b11	4
UGT2B4	TILDELVQR	y3, y4, y5, y6, y7, b3, b5, b6, b8	2
UGT2B7	HSGGFIFPPSYVPVVMSELTDQMTFMER	y4, y5, y6, y7, y8, y9, y10, y11, y12, y13, b6, b7, b8, b9, b10, b11, b12, b14	1
UGT2B17	GHEVIVLTSSASILVNASK	y4, y5, y6, b4, b5, b8, b9	4
UGT2B28	LSIIQHDQPVKPLHR	y3, y4, y7, y8, y9, b4, b5, b7	5